PhD degree in Molecular Medicine

European School of Molecular Medicine (SEMM),

University of Milan and University of Naples "Federico II"

Faculty of Medicine

Settore disciplinare: BIO/10

MOLECULAR BASIS FOR THE DUAL FUNCTION OF EPS8 IN CONTROLLING ACTIN CYTOSKELETON DYNAMICS: BUNDLING AND CAPPING

Milanesi Francesca

IFOM-IEO Campus, Milan

Matricola n. R07388

Supervisor: Dr. Prof. Giorgio Scita

IFOM-IEO Campus, Milan

Added co-Supervisor: Dr. Andrea Musacchio

IFOM-IEO Campus, Milan

Anno accademico 2009-2010

1. TABLE OF CONTENTS

1. TABLE OF CONTENTS **3**

2. LIST OF ABBREVIATIONS **7**

3. FIGURES INDEX **9**

4. ABSTRACT **12**

5. INTRODUCTION **14**

5.1 The cell cytoskeleton **14**

5.2 Actin and cell migration **16**

5.3 Actin cytoskeleton architecture **18**

5.3.1 Crosslinking proteins 19

5.4 Actin dynamics **21**

5.4.1 Actin monomer structure 21

5.4.2 Actin filament structure 23

5.4.3 Actin filament assembly 25

5.5 Actin treadmilling **26**

5.5.1 Nucleating factors 27

5.5.2 Depolymerizing factor 33

5.5.3 Monomeric actin binding proteins 34

5.5.4 Capping proteins 36

5.6 Eps8 ..... **44**

5.6.1 Eps8 structural organization 44

5.6.2 Eps8 functions 45

6. RATIONAL **52**

7. MATERIALS AND METHODS **54**

7.1 Common laboratory Solutions **54**

7.1.1 Phosphate-buffered saline (PBS) 54

7.1.2 Tris HCl (1M) 54

7.1.3 10X Tris EDTA (pH 7.4-8.0) 54

7.1.4 50x TAE (Tris-Acetate-EDTA) 54

7.1.5 Tris-buffered saline (TBS) 55

7.1.6 1.4x JS lysis buffer 55

7.1.7 5x (2x) SDS-PAGE Sample Buffer 55

7.1.8 10x SDS-PAGE Running Buffer 56

7.1.9 10x Western Transfer Buffer 56

7.1.10 Ponceau S 56

7.2 Reagents and antibodies 56

7.3 Cloning techniques 57

7.3.1 Agarose gel electrophoresis 57

7.3.2 Minipreps 57

7.3.3 DNA digestion 57

7.3.4 Large Scale Plasmid Preparation 57

7.3.5 Transformation of competent cells 58

7.3.6 DNA elution from agarose gel 58

7.3.7 PCR (Polymerase Chain Reaction) 58

7.3.8 Site directed mutagenesis 59

7.3.9 Generation of EPS8 constructs 60

7.3.10 Generation of EPS8 point mutants 61

7.4 Cell culture 62

7.4.1 Cells culture 62

7.4.2 Transfection 62

7.4.3 Retroviral infection 63

7.4.4 Cell lysis 63

7.5 Imaging techniques 63

7.5.1 Immunofluorescence 63

7.5.2 Cell Spreading 64

7.5.3 Live cells imaging 64

7.5.4 FRAP experiments 65

7.6 Biochemical procedures 65

7.6.1 SDS polyacrylamide gel electrophoresis (SDS PAGE) 65

7.6.2 Western blot 66

7.6.3 GST-fusion proteins production 66

7.6.4 PPDM cross-linking of Eps8 (648-821) and actin 69

7.6.5 Gel filtration analysis 69

7.6.6 Hydrodynamic analysis 69

7.7 Mass Spectrometry analysis 71

7.8 Biochemical actin-based assays 72

7.8.1 Common buffers 72

7.8.2 Actin purification 73

7.8.3 Pyrenyl-actin labelling 74

7.8.4 NBD-actin labelling 76

7.8.5 Actin polymerization assays 77

7.8.6 *In vitro* actin-based motility assays 78

7.8.7 Actin low speed co-sedimentation assays 80

7.8.8 Fluorescence microscopy of actin bundling 81

7.8.9 NBD-actin and AEDANS -actin binding assays 81

7.8.10 Nucleotide Exchange on G-actin 82

7.9 Electron microscopy 83

7.9.1 grids preparation 83

7.9.2 Image Processing 84

7.9.3 Docking and modelling of EPS8 C-terminal domain bound to F-actin 85

7.10 *C. elegans* techniques 85

7.10.1 *C. elegans* strains and mantainment 85

7.10.2 Cleaning worm cultures 86

7.10.3 Freezing worms 87

7.10.4 Crossing 88

7.10.5 *C. elegans* injection 88

7.10.6 Rescue experiments and phenotypical analysis 89

7.10.7 Single worm PCR 90

7.10.8 C. *elegans* imaging 90

8. RESULTS 92

8.1 Eps8 C-terminal region (aa 648-821) binds monomeric ATP and ADP actin 92

8.2 Eps8 C-terminal region (aa 648-821) and monomeric actin form a 1:1 complex 95

8.3 Eps8 C-terminal region sequesters monomeric actin 97

8.4 The minimal actin binding region of Eps8 C-terminal domain encompasses its amphiphatic H1 helix 99

8.5 The Amphiphatic H1 helix of Eps8 contacts the hydrophobic pocket between subdomain 1 and 3 of the actin monomer 104

8.6 H1 is connected to the H2-H5 globular core via a cleavable linker 110

8.7 The Eps8 actin binding domain wraps around actin filaments 112

8.8 Eps8 capping and bundling activities can be biochemically dissected 114

8.9 Eps8 capping and bundling properties correlate with a specific cellular localization of the protein 125

8.10 Eps8 capping activity mediates the sustaining of actin based motility 130

8.11 Eps8 bundling activity is required for proper intestinal morphogenesis *in vivo* 134

9. DISCUSSION 141

9.1 Eps8 H1 helix is crucial for the capping activity of the protein 143

9.2 The H2-H5 helical globular lobe is responsible for Eps8 bundling activity 145

9.3 The flexible linker between H1-H2 connects the two Eps8 actin binding surfaces 146

9.4 Correlating Eps8 dual functions and actin-binding modes from *in vitro* to *in vivo* 147

9.5 Perspectives 149

10. REFERENCES 151

11. SUPPLEMENTRY MATERIAL 156

2. LIST OF ABBREVIATIONS

EM	Electron Microscopy
ATP	Adenosine triphosphate
ADP	Adenosine diphosphate
ABP	Actin Binding Protein
GTP	Guanosine-5'-triphosphate
GDP	Guanosine-5'-diphosphate
kD	KiloDalton
GEFs	Guanine-nucleotide exchange factors
GAPs	GTPase activating factors
GDIs	Guanine nucleotide dissociation inhibitors
F-actin	Filamentous actin
G-actin	Globular actin
Cc	Critical concentration
WH	Wasp Homology
NPFs	Nucleation Promoting Factors
NMR	Nuclear Magnetic Resonance
C.e.	*Caenorhabditis elegans*
RTK	Receptor Tyrosine Kinase
OSCC	Oral Squamous Cell carcinoma
EGF	Epidermal Growth Factor
CDR	Circular Dorsal Ruffle
PM	Plasma Membrane
3D	Three Dimansional

PI(4,5)K	Phosphatidylinositol 4-5-bisphosphate kinase
PIP2	Phosphatidylinositol bisphosphate
PCR	Polymerase Chain Reaction
MEF	Mouse Embryonic Fibroblast
DMEM	Dulbecco's Modified Eagle Medium
FCS	Foetal bovine Calf Serum
DNA	Deoxyribonucleic acid
GFP	Green Fluorescence Protein
BSA	Bovine Serum Albumin
LB	Lysogeny broth
RT	Room Temperature
GST	Glutathione S-transferase
SEC	Size Exclusion Chromatography
WT	Wild Type
FRAP	Fluorescence Recovery After Photobleaching
Hs	Human
Mm	Mouse

3. FIGURES INDEX

Figure 1: Elements of the cytoskeleton 14

Figure 2: The actin cytoskeleton sustains cellular movement 17

Figure 3: Actin based structures 19

Figure 4: Crosslinkers affect the structural organization of the actin network 21

Figure 5: Monomeric actin structure 23

Figure 6: F-actin structure 24

Figure 7: The three phases of actin polymerization 26

Figure 8: Treadmilling of the actin filaments 27

Figure 9: The Arp2/3 complex structure at branches 29

Figure 10: NPFs mediated Arp2/3 complex activation as an actin nucleator 30

Figure 11: Elongation model of Formins 32

Figure 12: WH2 domain – actin structures 33

Figure 13: Role of Profilin in accelerating the actin treadmilling 35

Figure 14: Regulation of the actin treadmilling by capping proteins: the funneling hypothesis 37

Figure 15: Three dimensional structure of CP 38

Figure 16: Two step binding model for CP interaction with the plus end 39

Figure 17: Gelsolin domain organization and actin binding 40

Figure 18: Comparison between Gelsolin and Twinfilin organization 42

Figure 19: Schematic representation of the domain organization of the mammalian Eps8 family genes 43

Figure 20: Eps8 structure 44

Figure 21: Eps8 C-terminal region (648-821) binds monomeric actin 93

Figure 22: Eps8 (648-821) binding to ADP\ATP actin. 94

Figure 23: Eps8 (648-821) forms a 1:1 complex with monomeric actin 96

Figure 24: Eps8 (648-821) and actin form a 1:1 complex in gel filtration 97

Figure 25: Eps8 (648-821) affects actin growth both at the plus and at the minus end 98

Figure 26: Eps8 C-terminal region (648-821) is highly conserved 99

Figure 27: Eps8 (648-821) possess two monomeric actin binding surfaces: H1-H2 and H5 101

Figure 28: H1-H2 and H5 influence the actin filaments elongation rate with different thermodynamic constants 103

Figure 29: Helical wheel analysis of the predicted helix H1 of Eps8 104

Figure 30: Eps8 (648-821), Thymosin β4, Ciboulot and ADF/Cofilin share common binding surfaces on actin 106

Figure 31: Competition experiments between Eps8 and Thymosin β4 for actin binding . 107

Figure 32: Mapping of the interaction surfaces between Eps8 (648-821) and G-actin by mass spectrometry 109

Figure 33: Modeling Eps8 tertiary structure 110

Figure 34: Limited proteolysis analysis of the C-terminal Eps8 fragment 111

Figure 35: Three-dimensional reconstruction of Eps8 (535-821) bound to actin filaments 113

Figure 36: Dimerization drives Eps8 (648-821) bundling activity 116

Figure 37: Dimerization drives Eps8 (648-821) bundling activity 117

Figure 38: Gel filtration analysis of GST Eps8 (648-821) 117

Figure 39: Glycerol density gradient of GST Eps8 (648-821) 118

Figure 40: Eps8 capping activity requires an intact H1 helix and H1-to-H2 linker region 120

Figure 41: Eps8 bundling activity is mediated by a Villin –like motif in the globular domain 122

Figure 42: The Eps8 Villin-like motif is responsible for Eps8 bundling activity 123

Figure 43: Hydrodynamic analysis of wild type and GST-Eps8 (648-821) mutants 124

Figure 44: Differential requirement of Eps8 actin activities in architecturally diverse actin-based processes 126

Figure 45: Differential requirement of Eps8 activities in architecturally diverse actin-based processes in B16 melanoma cells..... 127

Figure 46: Eps8 dynamics at the cellular leadig edge..... 128

Figure 47: Eps8 dynamics on microspikes 129

Figure 48: The Eps8 capping, but not its bundling activity, is required to reconstitute actin-based motility in biomimetic motility assays..... 131

Figure 49: Requirement of Eps8 capping activity for optimal rocketing velocity of PIP2-rich endomembranes 133

Figure 50: EPS-8 in *C. elegans* 134

Figure 51: Analysis of the capping activity of the nematode EPS-8A mutants..... 135

Figure 52: Analysis of the bundling activity of the nematode EPS-8A mutants 136

Figure 53: Morphological analysis of the intestine of C.e. strains expressing EPS-8A WT or mutant proteins 137

Figure 54: CeEPS8::GFP WT and mutant protein expressed in the intestine display an apical-restricted localization 138

Figure 55: Specific localization of CeEPS8::GFP WT and mutant protein along the brush border 139

Figure 56: A schematic model for the binding modes of Eps8 to actin..... 142

4. ABSTRACT

Actin capping and cross-linking proteins regulate the dynamics and architectures of different cellular protrusions by controlling the number of free actin growing ends and organizing filaments into higher order structures, respectively. Eps8 is the founding member of a unique family of capping proteins capable of side-binding and bundling actin filaments. However, the structural basis through which Eps8 exerts these functions remains elusive.

Here, we combined biochemical, structural and genetic approaches to dissect the molecular mechanism responsible for the distinct Eps8 activities. We show how diverse portions within the C-terminal region of Eps8 contribute to actin binding and mediate Eps8 functions. An N-terminal amphipathic H1 helix, homologous to WH2 domains, is responsible for high affinity interactions with the barbed end unit of filamentous actin and is crucial for the capping activity of the protein. A four helix bundle represents the second interaction surface which mediates contact with the filament side and is crucial for the F-actin bundling activity. Within this context, the two actin binding surfaces are spatially coordinated by a flexible linker that contributes to the high affinity interaction of Eps8 to filaments ends, ensuring a bimodal topological arrangement of Eps8 wrapped around actin filaments. This bimodal way of association to the terminal ends of actin filaments also accounts for the dual modes of organizing F-actin, via capping and cross-linking, respectively. Single-point mutagenesis validated this mode of binding, further permitting us to dissect Eps8 capping from bundling activity *in vitro* and *in vivo*. Thus, Eps8 controls actin-based motility through its capping activity, while, as a bundler, is essential for proper intestinal morphogenesis of developing *Caernorhabditis elegans* strains.

In summary, we provided molecular and structural details of how Eps8 uniquely associates with barbed ends and sides of actin filaments through distinct structural modules. We further showed that the capping and the bundling activities of Eps8 can be

fully dissected *in vivo*, demonstrating the physiological relevance of the identified Eps8 structural/functional module.

5. INTRODUCTION

5.1 The cell cytoskeleton

A living cell constantly needs to dynamically change and modify its shape and internal organization in response to external stimuli. The cytoskeleton is mainly responsible of this dynamic behaviour. The cytoskeleton carries out three main activities: i) it spatially organizes the content of the cell controlling the organization of protein complexes and organelles, also providing paths of communication between them; ii) it provides a connection between the cell and the external environment mediating both short and long timescale changes in the cellular behaviour; iii) it mechanically supports the cell generating coordinate forces that enable a cell to move and change shape thus controlling its physical properties [1]. The cytoskeleton performs this diverse set of functions thanks to its intrinsic dynamic properties, featuring a plastic structural architecture composed by protein polymers that can assemble and disassemble and organize themselves into higher order complex arrays. The dynamic and plasticity of cytoskeletal structures are tightly controlled by several classes of cytoskeletal regulatory proteins. There are three major kinds of protein filaments that make up the cytoskeleton: microtubules, intermediate filaments and actin filaments (Figure 1).

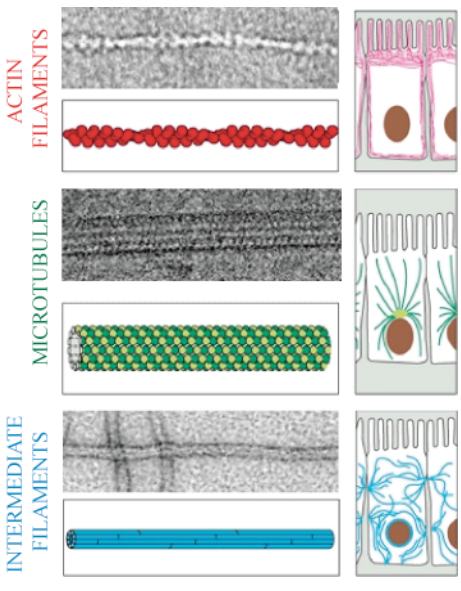

Figure 1: Elements of the cytoskeleton

The cell cytoskeleton is composed by three kinds of filaments: actin filaments, microtubules and intermediate filaments.

Top panel: EM picture and cartoon representation of an actin filament. On the right the position of the actin cortex inside an epithelial cell is shown.

Middle panel: EM picture and cartoon representation of a microtubule. On the right the microtubule organization from the cellular centrosome is shown.

Bottom panel: EM picture and cartoon representation of an intermediate filament. On the left the position of the intermediate filaments in an epithelial cell is shown. (Modified from Molecular biology of the cell, Alberts, 1994).

These polymers differ mainly in their stiffness, dynamic of assembly, and type of molecular motors that can associate with. Because of these differences they mediate distinct functions, being however connected and coordinated to one another.

Microtubules are very stiff polymers with a very complex dynamic of assembly and disassembly. They can switch between two states: stably growing and rapidly shrinking. They are polarized structures, made of dimers of α and β tubulin, with a fast end growth and a slow end growth that is associated with a centrosomal structure. They are mainly involved in the process of cell division, with a key role in controlling the correct chromosomal segregation in mitosis. They are also involved in vesicles and organelles transport through molecular motors such as kinesins and dyneins that move along them.

Intermediate filaments are the least stiff of the three kinds of cytoskeletical polymers. They are not polarized and cannot support directional movement of molecular motors.

Actin filaments are less rigid than microtubules, but they can generate very stiff cellular structures, such as intestinal microvilli and stereocilia of the inner hair thanks to a plethora of crosslinking proteins that can bind and bundle actin filaments together. The actin cytoskeleton forms also very dynamic structures such as lamellipodia and filopodia that have a critical role in controlling changes in cell shape during tissues morphogenesis and cell migration. These structures dynamically assemble and disassemble in a process referred to as actin dynamics. Actin filaments associated molecular motors are myosin proteins. As microtubules, actin filaments are polarized structures, with a net polymerization at one end (called plus or barbed end) and a net depolymerization at the other end (pointed or minus end). ATP bound actin monomers are incorporated at the plus end; as filaments growth ATP is hydrolyzed and ADP actin monomers are released from the minus end. Steady state of the filaments is thus controlled by ATP hydrolysis in a process that is called treadmilling. This process is controlled by several classes of actin

binding proteins (ABPs) that can both modify the rate of the treadmilling and drive the formation of distinct architectural structures.

5.2 Actin and cell migration

Cell migration is a stepwise process that can be generally divided into four phases. In a first step the cell arranges protrusive structures at the leading edge, which is the front of cell migration. The cell starts then to adhere to the substrate via the formation of focal adhesions that anchor it to the extra cellular environment. Next, the nucleus of the cell starts to be moved forward thanks to traction forces generated by the adhesive structures. Finally the rear of the cell retracts and the whole cell is thus moved forward (Figure 2). Actin is involved in every step of the process. Protrusive structures came mainly in the form of lamellipodia and filopodia, both composed of actin filaments arranged in a network or in bundles respectively (see below for further details). Adhesion to the substrate is achieved through the formation of focal adhesion structures that are connected on one end to the extracellular matrix via transmembrane proteins such as integrins, and to the other side to the stress fibers formed by actin filaments. Retraction of the back of the cell finally occurs through actin retraction fibers and acto-myosin contractility [2] (Figure 2).

The actin cytoskeleton rearranges in response to extracellular signals in order to form all these diverse structures. Key signalling regulatory proteins are small Rho GTPases, of which the best characterized are Rac, CDC42 and Rho, that mediate, in response to growth factors stimulation, the formation of lamellipodia, filopodia and stress fibers respectively [3]. Rho-GTPases are small proteins (between 20-30 kD) that can switch between an active (GTP-bound) and an inactive (GDP-bound) state. This switch is regulated by three distinct classes of proteins. Guanine-nucleotide exchange factors (GEFs) promote the GDP\GTP exchange and thus the GTP loading of the protein. GTPase activating factors (GAPs) promote the GTP hydrolysis. Guanine nucleotide dissociation

inhibitors (GDIs) finally inhibit the GDP dissociation from the protein thus acting as negative regulators of the protein activity [4]. Rho GTPases switch capability renders them ideal molecules to control changes in the cytoskeleton dynamics allowing a spactial and timing restricted response to extracellular stimuli.

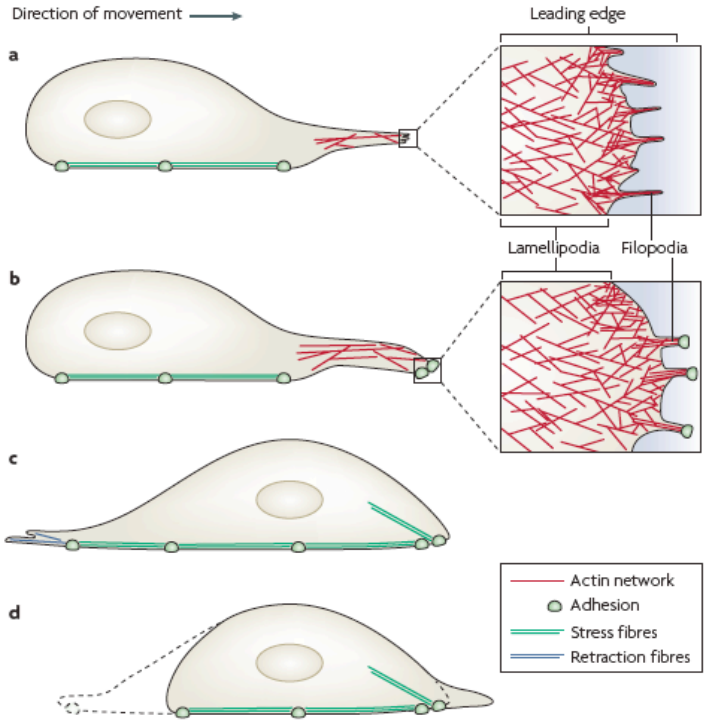

Figure 2: The actin cytoskeleton sustains cellular movement

The different steps of the migratory process and the cytoskeletical structures involved are described.

Cell motility initiates with the formation of actin protrusive structures at the leading edge, such as lamellipodia and filopodia (a). The cell then adheres to the substrate through the formation of focal adhesions that anchor it to the substrate (b). Next, the cell starts to move forward through actomyosin-based contraction forces mediated by stress fibers anchored to focal adhesions (c). Finally retraction fibers pull the rear of the cell and the migratory event is completed by the disassembling of the adhesive structures and the retraction of the protrusions (d). Modified from [2].

Two elements make the actin cytoskeleton the key regulator of cell migration; i) its structural plasticity that enables actin polymers to form specific and distinct architectures with defined stiffness and physical properties; ii) its dynamic capability to assemble into filaments that undergo constant disassembly into monomers generating a treadmilling process, controlled by several actin binding proteins (ABPs), that maintains filament length

while ensuring polarized growth of their fast growing ends for generation of protrusive forces.

5.3 Actin cytoskeleton architecture

The actin cytoskeleton plays a pivotal role in maintaining the cell shape and structure and in promoting cell migration. The capability to control such a diverse array of cellular functions derives from its ability to organize filaments into higher-order, crosslinked structures, which sustain these biological processes and often correlate with specialized cellular functions. These features include protrusions such as microvilli, filopodia and lamellipodia. Microvilli and microvilli-like structures are finger-like protrusions, most recognizable at the luminal side of intestinal and kidney epithelial cells, but that can be found in a variety of polarized cells, including hepatocytes and lymphocytes. Intestinal microvilli are 1-2 μM long and 100 nm wide, supported by a single axial bundle of actin filaments [5]. Within the bundle, filaments are densely packed and uniformly polarized, with their plus ends towards the plasma membrane at the tip of the protrusion (Figure 3). Microvilli are very stable in length and shape, even if it has been recently demonstrated that actin filaments turnover takes place in the actin bundles, with continuous actin incorporation at the plus ends.

Lamellipodia and filopodia are instead highly dynamic protrusive structures, present at the cellular leading edge and involved in cell migration.

The lamellipodium is a sheet-like structure. It starts at the leading edge of the cell and, depending on the cell type, can vary in breath from 1 to 5 μm. It is composed by a dense array of branched actin filaments and is a primary site of actin incorporation (Figure 3). The filaments are oriented with the plus ends toward the plasma membrane, thus polymerization at the plus end can lead to membrane pushing and deformation [6].

Filopodia are finger-like structures that frequently emerge from the lamellipodium at the cellular leading edge. They are formed by bundles of 10 to 30 actin filaments, all parallel

together with the plus ends oriented toward the plasma membrane (Figure 3). Somewhat similar to filopodia are microspikes, often considered precursors of filopodia extension, albeit this is still matter of debate, since they are generally present embedded within the lamellipodium, rather than extending beyond the leading edge [6] [7].

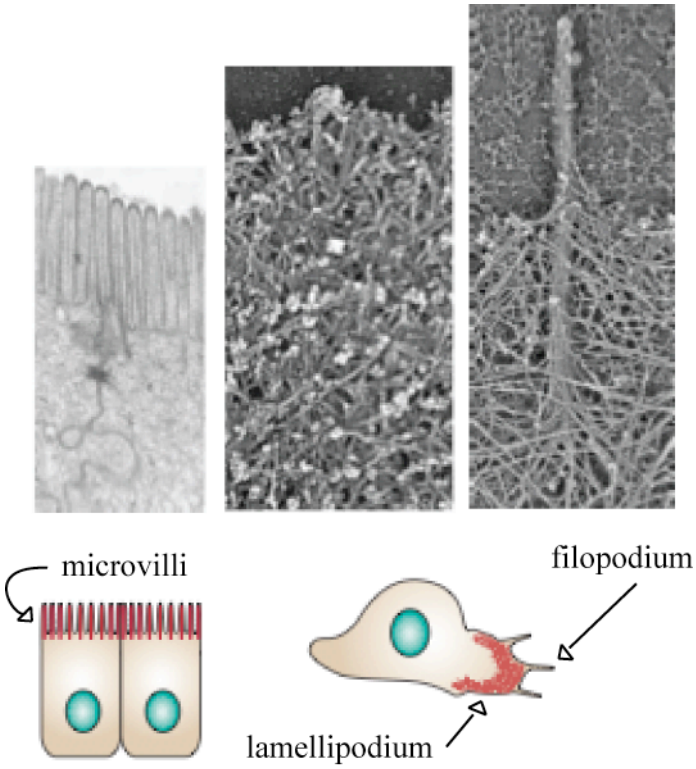

Figure 3: Actin based structures

Bundles of actin filaments sustain a variety of cellular structures.

Top part: EM images of intestinal microvilli on the apical surface of intestinal epithelial cells (right), a lamellipodium (centre) and a filopodium (left) at the cellular leading edge. Bottom part: cartoon representation of the three different structures. In the cartoon actin is represented in red. Modified from [5].

5.3.1 Crosslinking proteins

The formation and the maintenance of each type of these structures is precisely controlled and determinated by actin bundling or crosslinking proteins that mediate the interaction between the filaments and thus their organization into different cellular structures [5].

Several different classes of crosslinking proteins exist, each with slightly different biochemical properties. The heterogeneity of bundling proteins contribute to the plasticity of the actin cytoskeleton by finely tuning actin bundle stiffness and structural organization in order to adapt to the diverse mechanical requirement of the different cellular processes they form. Generally, actin crosslinking proteins bind F-actin through a bivalent interaction, needing to contact at least two filaments in order to crosslink them together. Often, however, crosslinking proteins have only one actin binding region, and is the dimerization of the molecule that leads to their activation as crosslinkers. This mechanism has been described for instance for Villin, a crosslinking protein mainly involved in microvilli organization [8]. Villin belongs to the gelsolin superfamily. It possesses six gelsolin like repeats, that form the core of the protein, and a carboxyl-terminal region called the headpiece domain. Two F-actin binding sites have been identified in the protein, one in the core and one in the headpiece domain. The F-actin interacting region in the core is solely responsible for a severing activity of the protein, while the headpiece domain is responsible for filament binding. This latter domain consists in a cluster of basic amino acids in which a KKEK motif is essential for the interaction with the actin filaments [9]. Activation of the crosslinking activity of the protein arises from its dimerization, with the headpiece domains of each monomer contacting a different filament.

The distance between the two domains involved as actin binding sites and their orientation is emerging as crucial in determining the ultrastructural properties of the actin filament network. Fascin, for example, is a small monomeric actin-bundling protein. It contains two actin binding sites, located in the N and in the C terminus of the protein. The two F-actin binding domains are thus very close together, correlating with Fascin capacity to organize actin in very tight and stiff bundles, as the ones present along filopodia [1] (Figure 4). Filamin, instead, forms parallel dimers, each subunit containing two actin binding motifs separated by a very long and flexible region. This structural organization

allows Filamin to crosslink widely disperse actin filaments, playing a key role in organizing the branched array in the lamellipodium [5] (Figure 4).

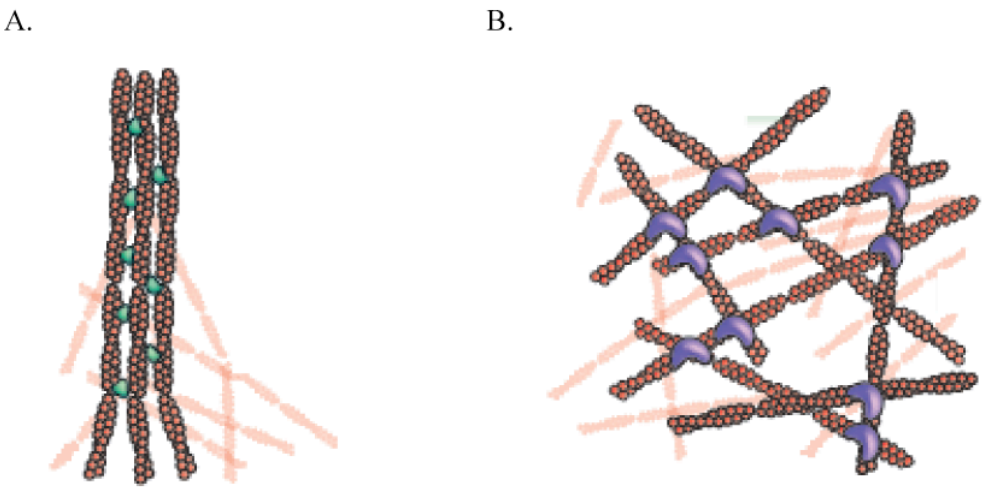

Figure 4: Crosslinkers affect the structural organization of the actin network

Actin filaments network stiffness correlates with the structural properties of the crosslinking proteins that mediate its organization.

A. Fascin is a monomeric crosslinking protein. It organizes actin in very tight and stiff bundles, as the ones present along filopodia.

B. Filamin mediated actin filaments crosslinking. Filamin crosslinks widely disperse actin filaments, playing a key role in organizing the branched array in the lamellipodium. Modified from [1].

5.4 Actin dynamics

Actin is among the most abundant and highly conserved protein in eukaryotes. In many cells, it accounts for more than the 10% of the total cellular protein content. Actin can polymerize into helical filaments changing from a monomeric or globular form (also called G-actin) to a filamentous one (also called F-actin). Upon polymerization, monomers undergo a change in their conformation that activates the ATPase activity of actin.

5.4.1 Actin monomer structure

Actin is a globular protein of 43kD. It stably binds an atom of Ca^{2+} or Mg^{2+} and a molecule of ATP or ADP. Actin consists of four subdomains, named from one to four. In the context of the filament, which is formed by two parallel protofilaments, the subdomains 1 and 2

are referred as the outer domains, while the 2 and 4 subdomains are reffered as the inner domains, because of their position with respect to the filament axis, where the inner domains are closer to the helix axis. Between the four subdomains there is the inner hydrophobic cleft in which the nucleotide and the metal ions are bound. The first high-resolution structure of monomeric actin was reported in 1990, in complex with Dnase I, a monomeric binding protein that prevents actin polymerization [10]. Since then, several other structures have been solved of actin bound to different actin binding proteins, including profilin [11], gelsolin [12], vitamin-D-binding protein [13], and an hybrid between Gelsolin domain 1 and Thymosin-β4 [14]. In these structures actin appeared bound either to ADP or ATP, but crystals were invariably grown in the ATP state, thus ADP actin was only obtained after hydrolysis of ATP within the crystal. Only in 2001, instead, the first structure of isolated ADP-bound actin was reported [15]. In this case crystals were obtained in the presence of ADP and a small macrolide molecule, the fluorescent probe tetramethyl-rhodamine-5-maleimide (TMR), was used to avoid actin polymerization. It must be noticed that all these structures are largely superimposible and can be classified into two major categories, referred to as “open”, as observed in the profilin:actin and in the TMR:actin structure, or “close” conformation [16], as is seen in all the other cases. The main differences between the close and the open conformation are in the three dimensional organization of a loop of subdomain 2 (called D-loop) and in the surfaces between the two halves of actin that cause an opening of the nucleotide binding cleft (Figure 5). Since the close conformation is the one resolved by the majority of the published structures it is likley to represent the physiological and most thermodynamically favored form of an actin monomer. However, most of the proteins used to stabilize actin in these structures inhibits also nucleotide exchange, causing a narrowing of the nucleotide binding cleft that result in a locked form of actin. Moreover in the profilin:actin complex structure, whose biologically occurrence and relevance is well established, G-actin adopts an open conformation. Thus, despite the wealth of structural information, whether the “real

structure" of an actin monomer is the close or the open conformation remains still a controversial issue. A possibility that may reconcile this controvery is that actin can adopt both conformations, and that the switch between the two forms is coupled to the ADP/ATP exchange. Once ADP-bound actin may adopt an open conformation that would be permissible for nucleotide exchange (that is indeed accelerated by Profilin), while when bound to ATP the nucleotide binding cleft closes allowing slow hydrolysis of the nucleotide.

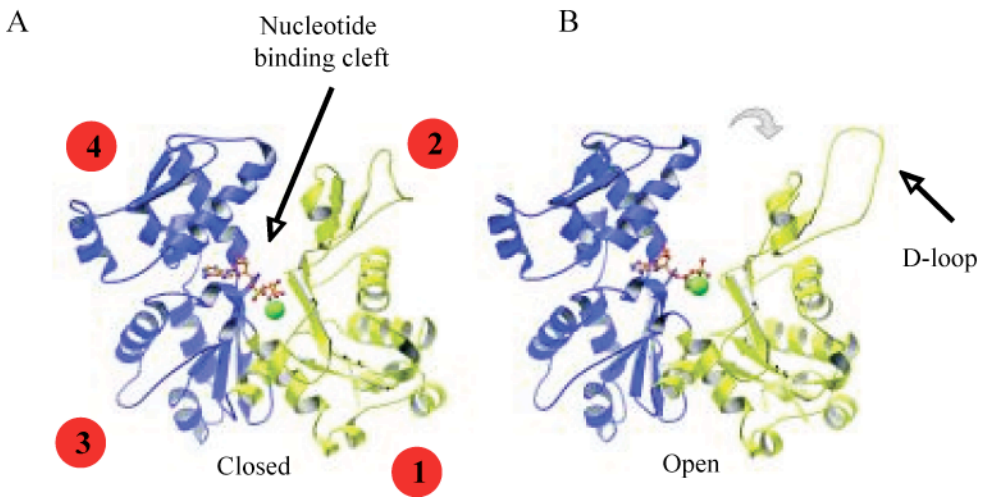

Figure 5: Monomeric actin structure

The structure of the actin monomer has been solved in a close and in an open conformation.

A. An example of the closed form of the actin monomer (PDB code 2BTF). The nucleotide (ATP) is shown as a ball-and stick representation and the metal ion as a green sphere. The four subdomains are indicated in red circles and the hydrophobic cleft in which the nucleotide and the metal ion can bind is also indicated.

B. The open conformation of the actin monomer (PDB code 1HLU). In the open conformation the two major structural differences are a change in the conformation of the D-loop in subdomain 2 and a slight rotation of the two halves of the monomer with an opening of the actin inner cleft. Modified from [16].

5.4.2 Actin filament structure

Actin monomers polymerize leading to the formation of a helical structure. The F-actin helix is usually referred to as a right-handed long-pitch helix, formed by two parallel protofilaments, with 13 monomers per turn. Along the helix monomers rotate by 167° and

have an axial translation of 27.5 Å. Monomers arrange head to tail all having the same orientation within the filament that thus results structurally polarized. Subdomains 1 and 3 are exposed at the plus or barbed end, while subdomains 2 and 4 are exposed at the minus or pointed end (Figure 6). Although the first atomic structure of G-actin appeared in 1990 [17], structural details of the F-actin monomers remained elusive since 2009 when a high-resolution structure of F-actin from analysis of X-ray fibre diffraction patterns was published [18].

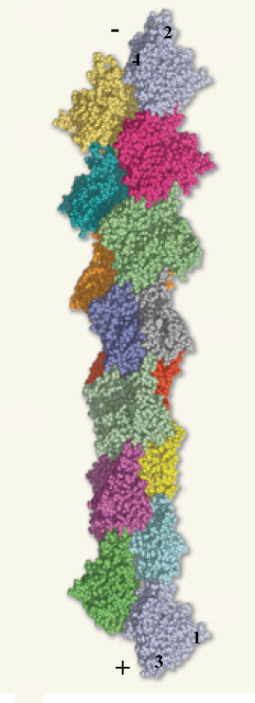

Figure 6: F-actin structure

Atomic model of the F-actin helix.

Actin filaments are formed by monomers that arrange head to tail. The resulting filaments are structurally polarized, with different monomer subdomains exposed at the two ends.

Each monomer of the helix is shown in a different colour. The exposed subdomains at the two extremities of the filament are indicated with numbers. Modified from [19].

This finding was a great breakthrough accounting for two major open questions in the field: the mechanism of activation of the ATPase activity of actin that occurs at the G- to F-actin transition; and the higher affinity of myosin for F-actin with respect to G-actin.

In the proposed model there is one essential difference between globular and filamentous actin. This change is a relative rotation of the two major domains of the actin monomer, the inner and the outer domain, by about 20° that flattens the molecule. This rotation brings an evolutionary conserved glutamine residue at position 137, which is implicated in the ATP hydrolysis mechanism, closer to the β and the γ-phosphate groups of the ATP

molecule. So it has been proposed that the rotation can be the switch for turning on the ATP-hydrolysis of actin. The rotation alters also the F-actin binding site of myosin, thus explaining the different affinity of myosin for F actin with respect to globular actin.

5.4.3 Actin filament assembly

Polymerization of actin filaments proceeds in three sequential steps. In a first phase the formation of a first oligomer of 3 or 4 actin monomers that assemble together occurs. This is the nucleation step, which represents a lag phase being kinetically unvafoured. After this first nucleation step the oligomers can act as seeds, which start to elongate in a filament with a rapid assemble of monomers into the filament. Both ATP and ADP bound monomers can associate and dissociate from either the plus or the minus end of the filament. Very different kinetic parameters, however, govern these reactions favouring the association of ATP bound actin at the plus end. The plus end, thus, represents the fast growing end of the filament during the elongation phase. As the filament grows the concentration of the free actin monomers that can assemble in the filament decreases until reaching an equilibrium, or steady state. At this stage, the polymerization at the plus end is counterbalanced by the depolymerization at the minus end, without change in the net length of the filament. The steady state is reached when the concentration of actin monomers is equal to the actin critical concentration (C_C), which is the minimal G-actin concentration required for assembly of filaments ends, resulting from the ratio of the rate constants of dissociation and association of monomers with actin filament ends [4] (Figure 7). Under typical *in vitro* conditions this value is equal to 0.1μM. The critical concentration is different between the two filament ends. At the plus end the C_C (C_C^+) is equal to 0.1μM, while at the barbed end the C_C (C_C^-) is equal to 0.8μM. At steady state this difference determines the net monomer association at the plus end and the net depolymerization at the minus end.

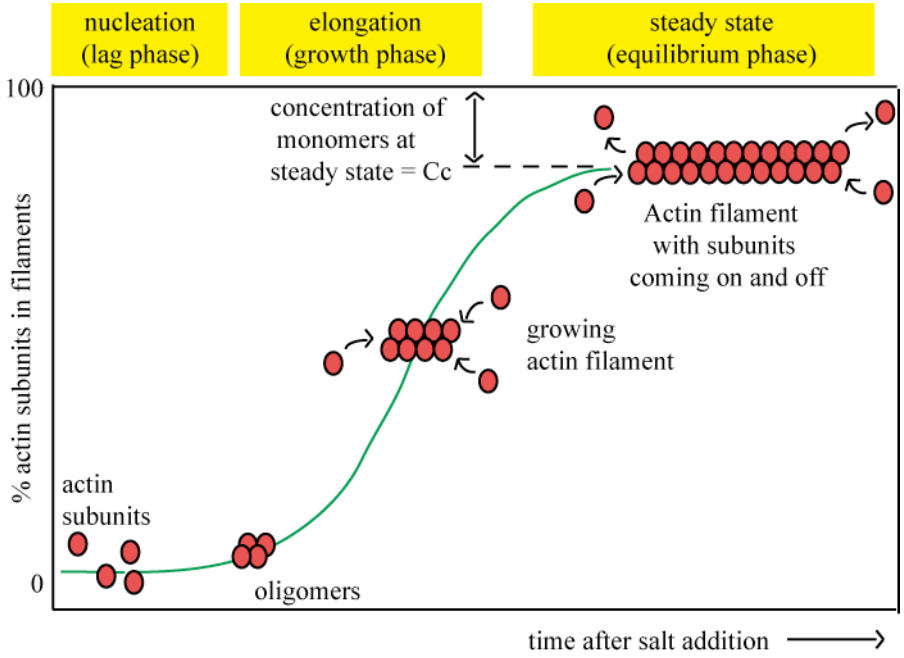

Figure 7: The three phases of actin polymerization

Actin filament assembly proceeds in three sequential phases.

During the first step (nucleation or lag phase) the actin monomers slowly assemble forming oligomers of 2 or 3 actin subunits. These oligomers then act as seeds and the filament rapidly elongates during the elongation or growth phase. At the end of this step a steady state is reached with no more net growth of the filaments. Here an equilibrium between F-actin and free G-actin is reached. This equilibrium depends on the actin critical concentration, equal to 0.1μM. Modified from (Molecular biology of the cell, Alberts, 2001).

5.5 Actin treadmilling

The two ends of actin filaments have different kinetic constants of association and dissociation of the actin monomers. The barbed end has higher association and dissociation rates for actin subunits than does the pointed end and thus dominates the dynamics of filament assembly [20]. In addition to this, there is an irreversible ATP hydrolysis that is associated with the incorporation of monomers at the plus end of filaments. These two events generate a difference in the critical concentration between the barbed and the pointed end [4], and create a flux of monomers along the filament with ATP bound actin monomers that associate at the plus end and ADP actin monomers that dissociate form the minus end. This process can be described as a cycle with ATP bound actin monomers that assemble at the plus end of actin filaments; as filament grows ATP is hydrolyzed and ADP

actin monomers dissociate from the minus end of the filaments. Once ADP actin monomers are free in the cytoplasm the ADP\ATP exchange occurs and new ATP actin monomers are formed that can be reassembled in the filaments (Figure 8).

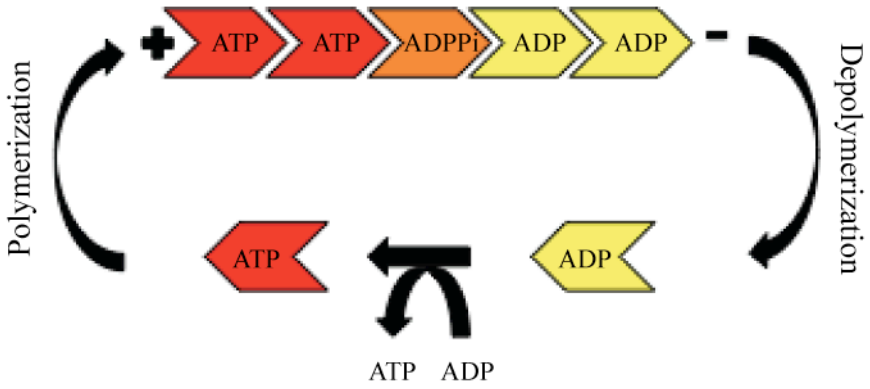

Figure 8: Treadmilling of the actin filaments

The treadmilling process describes the continuous assembly and disassembly of actin filaments.
ATP bound actin monomers associate at the plus end. As filaments polymerize ATP hydrolysis occurs and ADP bound actin monomers are formed that detach from the minus end of the filament. Once in the cytoplasm the ADP to ATP exchange occurs and new ATP actin monomers are formed that can associate with the plus end again.

The continuous process of assembly and disassembly of actin filaments, coupled with ATP hydrolysis, that maintains the constant length of the actin filaments at steady state, is called actin treadmilling [21]. Actin tredmilling is crucial for cell migration; indeed is the rapid filaments turnover that generates force propelling movement.

At the leading edge filaments are oriented with the plus ends towards the plasma membrane, and is a rapid assembly of these filaments that generates the protrusive force able to deform the membrane and enables the generation of filopodia and lamellipodia. While net polymerization occurs at the front, net depolymerization occurs at the rear of the lamella and moreover the total overall F-actin content of the cell remains constant [21]. Notably also pathogens such as *Listeria monocytogenes* or *Shigella flexineri* are able to mimic the dynamic behaviour of the filaments at the leading edge inducing a rapid actin

polymerization on their surfaces and thus exploiting actin based motility to move inside the cell. This dynamic behaviour is achieved thanks to actin binding proteins that are able to accelerate and regulate the actin treadmilling. *In vivo* actin treadmilling is 100 time faster with respect to pure actin *in vitro* with typically 3μm long filaments turning over in 1 minute [22]. The minimal set of proteins sufficient to sustain and accelerate actin treadmilling and actin based motility has been identified thanks to a series of *in vitro* biomimetic experiments in which actin-based motility of either bacteria or functionalized beads was reconstituted using purified proteins [23] [24, 25]. The identified proteins are able to promote actin nucleation, to influence actin depolymerization, and to block polymerization at the plus end. The first proteins that had been used in this assay were the nucleator complex Arp2/3 and its activators, ADF\Cofilin as depolymerizing factor and Gelsolin as a capping protein. Since then this assay has been widely used to identify proteins carrying one of these functions, by rescue experiments in which one of the established essential components of the system is substituted by the protein of interest [22].

5.5.1 Nucleating factors

The initial step of actin filaments assembly is kinetically unfavourable and thus inefficient. Nucleating factors directly nucleate actin thus overcoming this kinetic problem. For many years only the Arp2/3 complex, together with its activators, and Formins, had been known as actin nucleators. However more recently several new factors have been described as novel actin nucleators.

5.5.1.1 The Arp 2/3 complex

The first nucleating factor to be identified was the Arp2/3 complex. It is a 220kD complex, composed by seven stably associated proteins. These polypeptides include ARP2 and ARP3 and five additional subunits, named from ARPC1 to ARPC5 [26]. This complex localizes both at the cellular leading edge and on actin comet tails of rocketing vesicles or pathogens moving inside the cell [27]. The Arp2/3 complex is both able to nucleate and to

branch actin filaments. The complex binds to the side of a pre-existing actin filament and initiates the nucleation of a 70° angled, branched filament. EM analysis showed that the complex remains localized at the points of branching of actin filaments (Figure 9). Because of this property the Arp2/3 complex is thought to play a key role in the formation of the branched array of the lamellipodium. The isolated Arp2/3 complex is an inefficient nucleator. Its activity is increased by filament binding and by phosphorilation on Tyr residues in ARP2. To be fully active, however, the Arp2/3 complex requires the action of activators called nucleation-promoting factors (NPFs) [26].

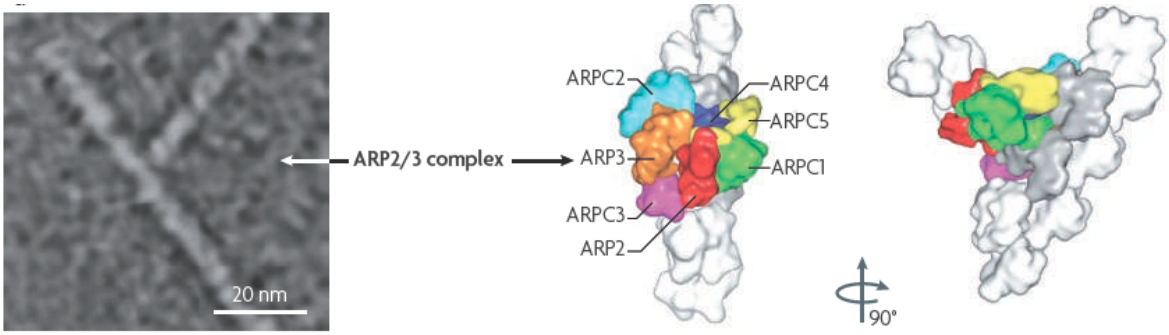

Figure 9: The Arp2/3 complex structure at branches

Structure of the Arp2/3 complex on actin filaments.

The morphology of the Arp2/3 complex and of the branched actin filaments is shown in an electron micrograph (left) and in a structural model based on electron tomography (right). The complex is formed by seven subunits and remains attached at the site of nucleation and branching of the new filament. Modified from [26].

The majority of Arp2/3 activators (called of CLASS I) interact with Arp2/3 through a WCA domain. This domain is composed by one or more WASP homology 2 (WH2) domains that bind actin monomers, an amphiphatic connector region and an acidic polypeptide. Within this region, the connector and the acidic part contact different subunits of the Arp2/3 complex, causing a conformational change that activates Arp2/3 as nucleator. The WH2 domain, instead, is able to bind actin, thus delivering monomers to the growing filament end (Figure 10).

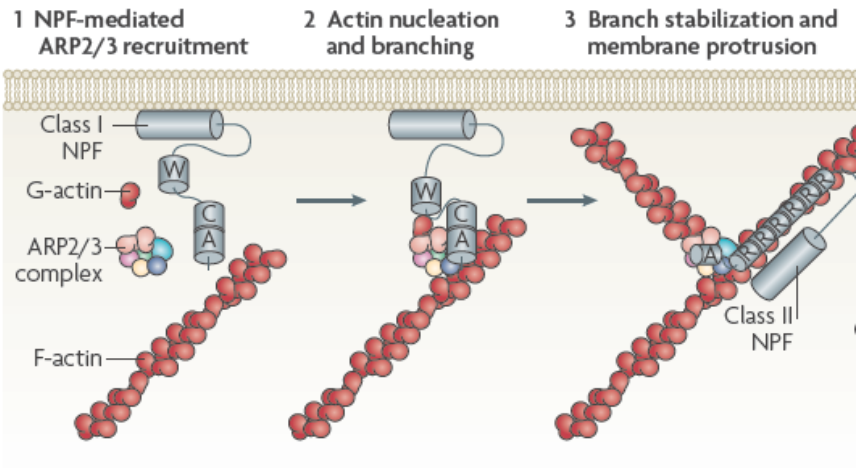

Figure 10: NPFs mediated Arp2/3 complex activation as an actin nucleator

The Arp2/3 complex is activated at the membrane by the action of class I and class II NPFs.

The Arp2/3 complex is recruited by the WCA domain of class I NPFs in proximity of the cell membrane (1). The complex is thus activated and the nucleation of a new branch filament occurs (2). The complex remains localized at the branch site, where it can be stabilized by Class II NPFs such as Cortactin (3).

The Class I NPFs comprises several subfamilies, distinct for their mechanism of action and their cellular localization. We can distinguish in particular five groups: WASP and N-WASP that were the first to be identified; three members of the WASP-family verprolin homologue (WAVE 1 to 3, also called SCAR); WASH (WASP and SCAR homologue) and WHAMM (WASP homologue associated with actin, membranes and microtubules); JMY (junction-mediating regulatory protein). WASP and WAVE subfamilies of NPF class I have a widespread tissues distribution, and play essential roles in a variety of general processes that relie on actin dynamics, ranging from vesicle and pathogens intracellular motility to cell migration [28]. The more recently identified NPFs display, however, more specialized functions: WASH for example mainly acts in endosomal and golgi traffic, whereas WHAMM is involved in golgi transport [26]. JMY instead has a double function acting both as an actin promoting factor and as a co-activator of p53. This double activity is reflected by its cellular localization. JMY is enriched in the nucleus upon DNA damage where it is though to mainly act in driving p53 response; in migrating cells JMY instead relocalizes to lamellipodia promoting cell migration. Intriguingly, JMY is also able to

promote actin polymerization possessing a nucleating activity and to influence cell adhesion controlling Cadherin levels. The precise mechanisms controlling JMY activities remain to be defined. This is reflected in the current open debate as to whether JMY acts as a convergent point connecting p53-dependent apoptotic and p53-independent migratory pathways, or whether JMY multiple activities betray moonlighting, unrelated functions [29] [30]. Mammalian cells posses also class II activators of Arp2/3, such as Cortactin family proteins. These factors do not posses canonical WH2 domains and are weaker activators of the Arp2/3 complex [26].

5.5.1.2 Formins

Formins are nucleating factors that, unlike Arp2/3, produce linear filaments. They are present in all eukaryotes. In mammals at least 15 Formins have been identified. The common feature of all the different Formins is the presence of two conserved Formin homology (FH) domains, named FH1 and FH2. The FH1 domain consists of a Proline rich region able to interact with SH3 and WW domains containing proteins. This region can also recruit Profilin-actin complexes, thus delivering the monomers at the plus end of filaments. The FH2 domain is sufficient *in vitro* to trigger actin nucleation [31].

Most notably, Formins act as processive nucleators, remaining attached to the plus end of the filaments while elongating. To perform this task, the FH2 domain is proposed to form a flexible homodimer that wraps around filament ends. One FH2 domain of the dimer, at time, detaches transiently from and moves toward the filament end, thus allowing the protein to remain attached while monomers become incorporated into the filament during elongation. As a result Formins act as ‘’leaky cappers” directly competing with and protecting the plus ends from binding to capping proteins (Figure 11). While the biochemical mode of action of Formins has by and large been identified, their functional role remains to be fully investigated. Their peculiar ability to promote linear filament

elongation has suggested their requirement in structures that need the presence of long, linear filaments, such as stress fibers and filopodia.

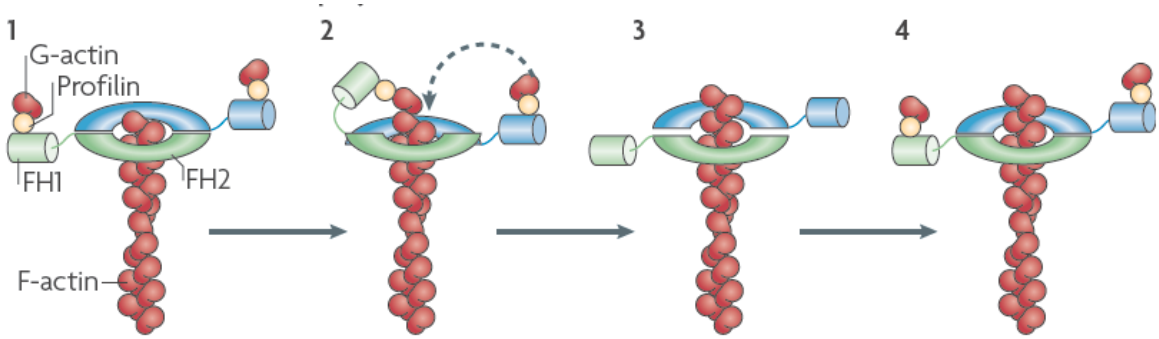

Figure 11: Elongation model of Formins

A model of actin mediated polymerization by Formins.

The FH1-FH2 domain localizes at the plus end of a growing filament. The FH2 domain adopts a dimeric conformation and wraps around the filament. The FH1 domain binds Profilin:actin and delivers the monomers to the growing end. The elongation proceeds in a stepwise manner with Formins remaining attached to the filament end. Modified from [26].

5.5.1.3 WH2 domain containing nucleators

More recently a new class of actin nucleators emerged whose common feature is the presence of a tandem cluster of G-actin binding motifs, including WH2 domains. The WH2 (WASP homology domain) is a 20-30 residues binding module that is found in many different regulators of the actin cytoskeleton. It forms a short (usually three turn) amphiphatic α-helix that usually contacts the hydrophobic pocket present between the subdomain 1 and 3 of the actin monomer [32] (Figure 12).

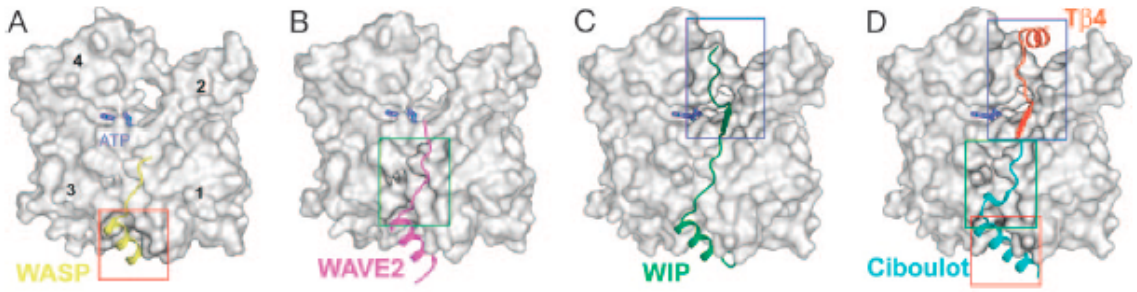

Figure 12: WH2 domain–actin structures

The WH2 domain is a common motif for actin monomer interaction.

A-C. Structures of the WH2 domains of WASP (A), WAVE 2 (B), WIP (C) in complex with actin. D. Superimposition of Ciboulot and Thymosin β-4 WH2 domains in complex with actin. Modified from [32].

This NPF class includes Spire, Cordonbleu (COBL) and Leiomodin families. Their WH2 domains are proposed to promote nucleation by tethering more actin monomers together thus favouring the first kinetic unfavourable monomer association.

Spire has been also described as a Formin interactor and a cooperation between the two proteins has been proposed to be important for enhancing Formin mediated actin nucleation and processive elongation [33] [34].

5.5.2 Depolymerizing factor

Actin depolymerizing factor (ADF, also called Cofilin) is an essential protein in controlling and accelerating the actin treadmilling. *In vitro* it is able to accelerate the turnover rate of actin filaments by more than one order of magnitude, and to accelerate actin based motility of pathogens such as *L.monocytogenes* [35]. ADF binds both G and F-actin, with a high preference for the ADP bound state. It binds actin filaments at the pointed ends (where ADP-bound actin monomers are present) and accelerates the depolymerization from these ends. The increased pointed end off rate is counterbalanced by an increase in the rate of assembly at the barbed end, elicited by an increase in the Critical Concentration and in the treadmilling rate [35]. ADF\Cofilin has also a severing activity, meaning that it is able to cut actin filaments. This activity is mainly due to a

conformational change of the filament induced by ADF binding, that destabilizes F-actin leading to severing.

5.5.3 Monomeric actin binding proteins

The rapid turnover and polymerization at the cellular leading edge depends on the monomeric G-actin concentration within the cell. G-actin concentration in the cytoplasm is much higher than the critical concentration required for filament elongation. This means that in the cells mechanisms are present that allow the maintenance of a steady state actin monomer concentration higher than the critical concentration at the plus end, without polymerization of the filaments. This is achieved though the presence of proteins that bind monomeric actin and that are able to control its availability for polymerization, its nucleotide binding and its localization.

5.5.3.1 Profilin

Profilins are among the most highly expressed proteins in the cytoplasm and are key regulators of the actin treadmilling. They are small (12-19 kD) monomeric actin binding proteins, with a higher affinity for ATP-bound than for ADP-bound actin (Kd = 0.1μM and 0.5μM respectively). Profilin acts by catalyzing the exchange of ADP for ATP. It achieves this function contacting the monomer between subdomain 1 and 3, and thus modulating the opening of the monomer cleft where the nucleotide binds. Moreover, Profilin inhibits ATP hydrolysis thus maintaining the actin monomers in an ATP-bound state. Thus the pool of ADP-G-actin monomers depolymerizing from the pointed end is converted into an ATP-bound Profilin actin complex that selectively associates at the plus end thus accelerating the treadmilling (Figure 13). This acceleration is particularly effective in the presence of ADF\Cofilin that acts on the other end of the filament. The synergistic effect of the two proteins can accelerate the treadmilling rate up to 125 fold [36].

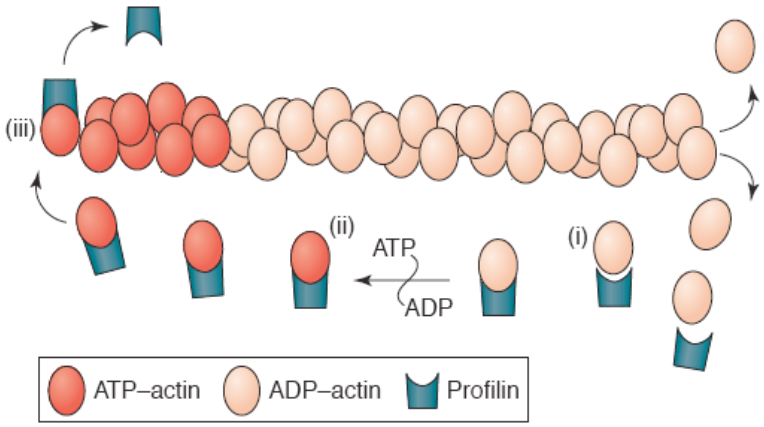

Figure 13: Role of Profilin in accelerating the actin treadmilling

Profilin binds ADP-actin monomers and accelerates the ADP/ATP exchange.

Profilin binds the ADP-actin monomers that detach from the minus end of the filament (i); Profilin then promotes the ADP/ATP exchange and ATP-bound Profilin actin complexes are formed (ii). These bound monomers can selectively associate only with the filament plus end thus leading to polymerization (iii). Modified from [37].

It is of note that profilin in addition to bind to monomeric actin can also associate with a variety of different proteins. Profilin possesses a poly-proline rich region through which it is able to interact with a plethora of ligands that are involved in different cellular processes. Most of these interactors are proteins that control cytoskeleton dynamics. For example, profilin binds WASP family proteins. This interaction acts in synergy with the binding of Cdc42 to promote WASP activation and thus Arp2/3-dependent actin polymerization [38]. Similarly, the binding of the prolifin:actin complex to the FH1 domain of Formins is crucial for the delivery of actin monomers to the active FH1-FH2 domain [31]. Notably, profilin has been also found to bind, through a mass spectrometry approach, proteins involved in membrane trafficking, such as clathrin or dynamin 1, suggesting a role of profilin in linking the actin cytoskeleton and the endocytic membrane machinery [39]. Finally profilin also binds nuclear-export receptors such as Exportin 6. In this latter case, Exportin 6 is thought to recognize specifically the profilin:actin complex and to ensure that this complex is transported into the cytoplasm and excluded from the

nucleus [37]. Profilin is, thus, emerging not only as a key regulator of different aspects of the actin cytoskeleton dynamics, but also as a central factor in the regulation of a complex network of molecular interactions.

5.5.3.2 β-thymosins

β-thymosins are a family of highly conserved actin binding proteins of about 5 kD present in vertebrates. Several family members exist with thymosin β-4 being the better characterized as an actin binding protein [40]. Thymosin β-4 interacts specifically with ATP-bound actin monomers through a WH2 domain. Upon binding it sequesters the monomers so that they cannot be incorporated in the filaments any more. NMR studies have shown that thymosin β-4 undergoes a dramatic conformational change upon binding to monomeric actin. In the cytoplasm the protein is mainly unstructured, while upon binding it adopts an L-shape conformation with a very extended central part and two external small α-helices at the N and C terminal that correspond to the actin binding surfaces. The key residues for the interaction with the actin monomer are found in the N-terminal helix, that binds the monomer between subdomains 1 and 3. The C-terminal helix contributes to the binding interacting with the actin subdomain 2 [41].

5.5.4 Capping proteins

Capping proteins bind the plus ends of actin filaments and block actin polymerization from these ends. They are essential for actin-based motility [23] and to accelerate the actin treadmilling. How Capping proteins may increase actin filaments turnover was firstly explained in 1997 by Carlier at al. [21] that proposed the so called “funnelling hypothesis”. According to this hypothesis capping of the fast-growing barbed ends of most of the actin filaments in the cell leads to an increase of the ATP-actin monomers concentration available for the polymerization of the few barbed ends that remained free. This would, ultimately, cause an increase in the steady-state concentration of monomeric actin and to a faster growth of the few free barbed ends (Figure 14).

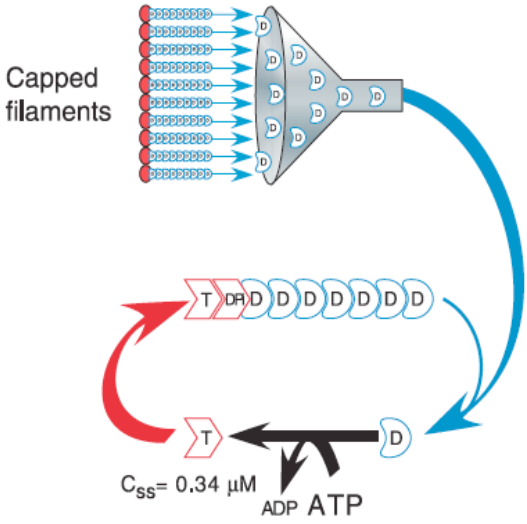

Figure 14: Regulation of the actin treadmilling by capping proteins: the funnelling hypothesis
According to the funnelling hypothesis capping proteins accelerate the treadmilling rate increasing the Cc of monomeric actin. Blocking the vast majority of filaments barbed ends would in fact lead to an increase monomeric actin concentration for the few barbed ends that remain free. Non-capped barbed ends therefore would growth faster. Modified from [22].

Recently, however, this model has been challenged by a series of experiments that revealed that a number of testable predictions (e.g. in the presence of cappers the amount of free monomeric actin should increase, the number of free barbed ends should decrease and there should be an increment in the rate of filament elongation) implicit in the funnelling model could not be experimentally verified [42]. It was, thus, proposed that capping proteins instead of generating a restriction, cooperate with actin nucleators (in particularly the Arp2/3 complex was used in the experimental setting) to increase filament nucleation, acting as "monomer gating". More precisely, cappers by blocking filament ends close to the surface where WCA-containing NPFs reach the maximal concentration, would compete with WH2 domain (part of the WCA) preventing its unproductive binding to filament ends, and favouring, instead, its association to actin monomers, which is required to prime Arp2/3 complex activation and filament nucleation. The role of capping proteins in actin-based motility would thus be not accounted by an increase in the treadmilling rate but by an increase in nucleation events.

Several families of capping proteins have been identified in mammals so far and considerable effort has been devoted to explore their structural mechanism of action.

Capping proteins display, indeed, a variable and not conserved domain organization, suggesting different modes through which they cap filament ends.

5.5.4.1 Capping Protein

CP (Capping Protein), known also as β-actinin or CapZ in skeletal muscle, is an αβ heterodimeric protein. It is very conserved in eukaryotes, but show no similarity with any other capping protein family [20].

CP α and β subunits adopt a very similar conformation, despite lacking any amino acidic sequence conservation. The overall three dimensional structure of CP displays a mushroom like shape. The N-terminal regions of the two subunits create a six-helix bundle structure (3 helices coming from each subunit) that forms the stalk of the mushroom. The remaining parts of the subunits form a very intertwined β sheet that creates the cap of the mushroom. Each subunit ends at the C-terminus with an α helix that extends perpendicularly on the top of the mushroom (Figure 15A). These two helices have been proposed to act as two tentacles for binding to the end terminal region of the filaments (Figure 15B) [20].

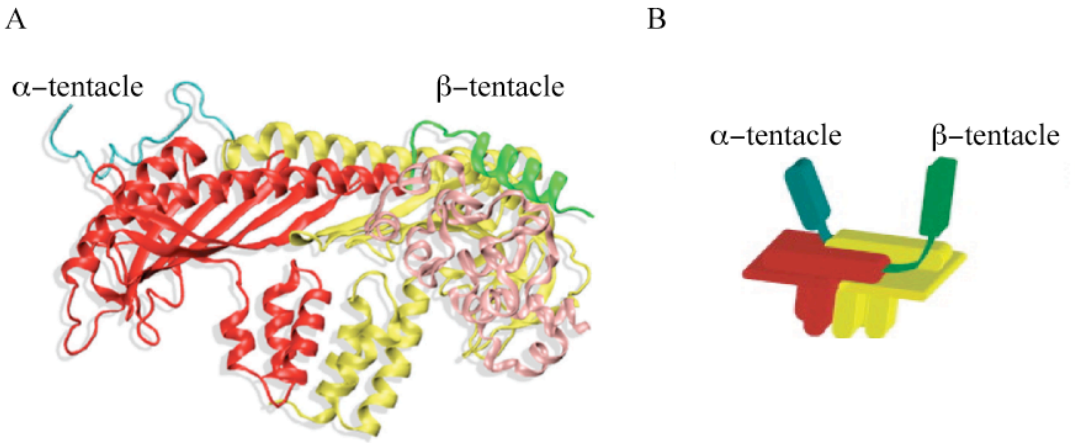

Figure 15: Three-dimensional structure of CP

CP forms a heterodimer that adopts a mushroom like shape with two α helices that act as tentacles for actin binding.

A. Ribbon representation of the 3D structure of the CP αβ heterodimer. The α subunit is depicted in yellow and the β subunit in red. The C-terminal α helices of the α and β subunits are represented in green and blue respectively.

B. Cartoon representation of the CP structure. The C-terminal α helices of the α and β subunits are flexible and can act as tentacles to bind the actin monomers at the filament end. Modified from [20].

This model has been more recently confirmed and refined by Narita and colleagues that analyzed by EM CP bound on the barbed ends of actin filaments [43]. They could unambiguously identify the α and β subunits and their position with respect to the actin monomers. According to these results, they proposed a two steps binding model for CP interaction with the plus end. The first event is the binding of basic residues of the C-terminal α subunit (first tentacle) with the acidic amino acids of the barbed end of a filament. Next, the amphipatic C-terminal β subunit (second tentacle) would dock into the hydrophobic pocket of the actin protomer, stabilizing the interaction with the filament end (Figure 16).

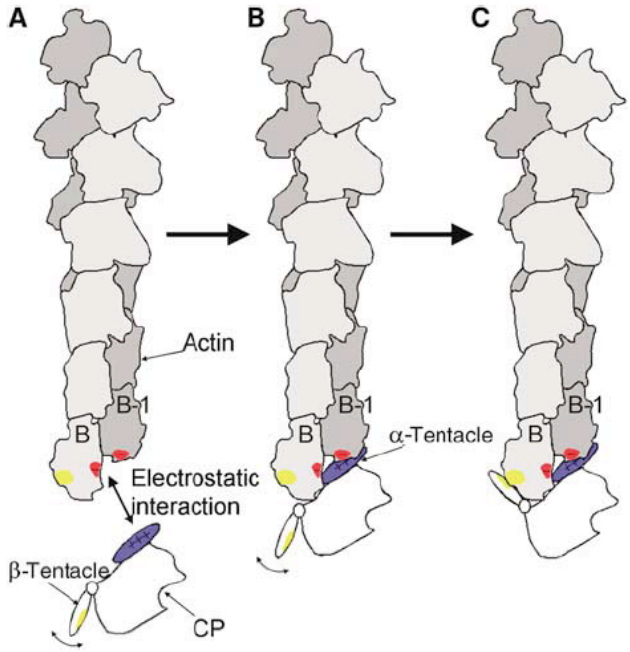

Figure 16: Two steps binding model for CP interaction with the plus end
According to the model proposed by Narita and colleagues the first interaction between CP and actin would be between the basic residues on the α tentacle and the acidic residues on the barbed end of the filament (depicted in red) (A). After this first interaction the β tentacle would bind contacting the hydrophobic cleft on the terminal protomer (depicted in yellow) (B and C). Modified from [43].

5.5.4.2 Gelsolin

Gelsolin is a member of a large family of actin binding proteins, including Villin and CapG.

It was discovered in 1979 and was named according to its ability to mediate the gel-sol transition of the cytoplasm, in a Calcium-dependent manner [44]. Indeed, Gelsolin binding to filament ends occurs only in the presence of micromolar concentrations of intracellular Calcium [44].

Gelsolin family is characterized by the presence of a variable number of homologous and repeated Gelsolin domains of about 100-125 amino acids [45].

Gelsolin itself contains six repeats (named from G1 to G6), distributed into two homologous parts of the protein. G1 to G3 are in the C-terminal, while G4 to G6 are in the N-terminal half of the protein, connected by a linker of 53 amino acids (Figure 17A). Within these repeats G1, G2 and G4 are able to interact with actin. At resting intracellular levels of Calcium, the protein assumes a very compact conformation and the actin interaction surfaces are hidden within the structure. Elevation of Ca^{2+} concentrations, releases latches within the constrained structure and produces large shifts in the relative positioning of the domains. This conformational change permits Gelsolin to bind to the actin filament. Firstly, an intramolecular contact between G6 and G2 is released revealing the G2 actin binding site. Secondly, in each half of the protein the third domain releases the first domain, thus exposing the actin binding sites in G1 and G4 [46].

Biochemical and structural studies of the two first Gelsolin domains, G1 and G2, indicated that these two modules are sufficient to mediate Gelsolin capping activity. The G1 domain binds and blocks barbed ends, while the G2 domain contacts the side of the filament and stabilizes the binding (Figure 17B).

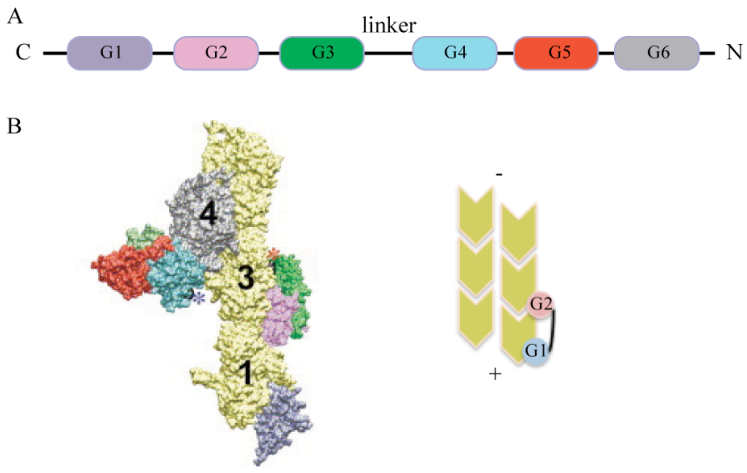

Figure 17: Gelsolin domains organization and actin binding

Gelsolin is composed by 6 repeats with the first two domains being required for plus end binding and capping.

A. Scheme of the domains organization of Gelsolin. Gelsolin contains 6 repeats (G1 to G6). The protein is organized in two symmetrical halves, with 3 repeats each, divided from a flexible linker. B. Binding of Gelsolin at filament ends. Left: binding of Gelsolin at the end of the filament. The G1 domain (depicted in blue-violet) binds the last monomer of the filament, while the rest of the protein contact the filament side. Right: cartoon representation of the G1-G2 domains binding at filament ends. These domains are sufficient to mediate the capping activity of Gelsolin. Modified from [45].

Gelsolin is also able to sever actin filaments upon binding. As for capping, also severing requires the activation of the protein upon calcium binding, which induces a complete opening of its conformation. Once activated the F-actin binding domain G2 is exposed and binds to the filament side. Next, the G1-G2 linker, the G3-G4 linker and G6 wrap themselves around the filament, positioning G1 and G4 onto their binding sites. Finally a coordinated pincher movement of G1 and G4 causes disruption of intermolecular interactions between actin monomers within the filament leading to severing [47] [45]. These two distinct protein functions render Gelsolin a key member in regulating actin dynamics.

5.5.4.3 Twinfilin

Twinfilin is a conserved protein that, as Gelsolin, possesses distinct and diverse biochemical functions, being able both to cap actin filaments and to sequester monomeric actin. Twinfilin has a modular structure, with two ADF homology domains separated by a 30 residue linker and followed by a C-terminal tail region of approximatively the same length [48] (Figure 18A). Twinfilin ADF domains have no sequence similarity but are structurally homologous to the Gelsolin domains (Figure 18B). Both ADF domains are able to bind monomeric actin and are required for the protein capping activity, with the ADF–C (for C-terminal) playing a critical role. The proposed mechanism for Twinfilin filament end capping is comparable to the one proposed for Gelsolin. Like Gelsolin G1 domain, the ADF-N domain is proposed to bind the end of the filament, while the ADF-C domain would stabilize the binding by contacting the side of the filament, in fashion similar to the Gelsolin G2 motif (Figure 18C).

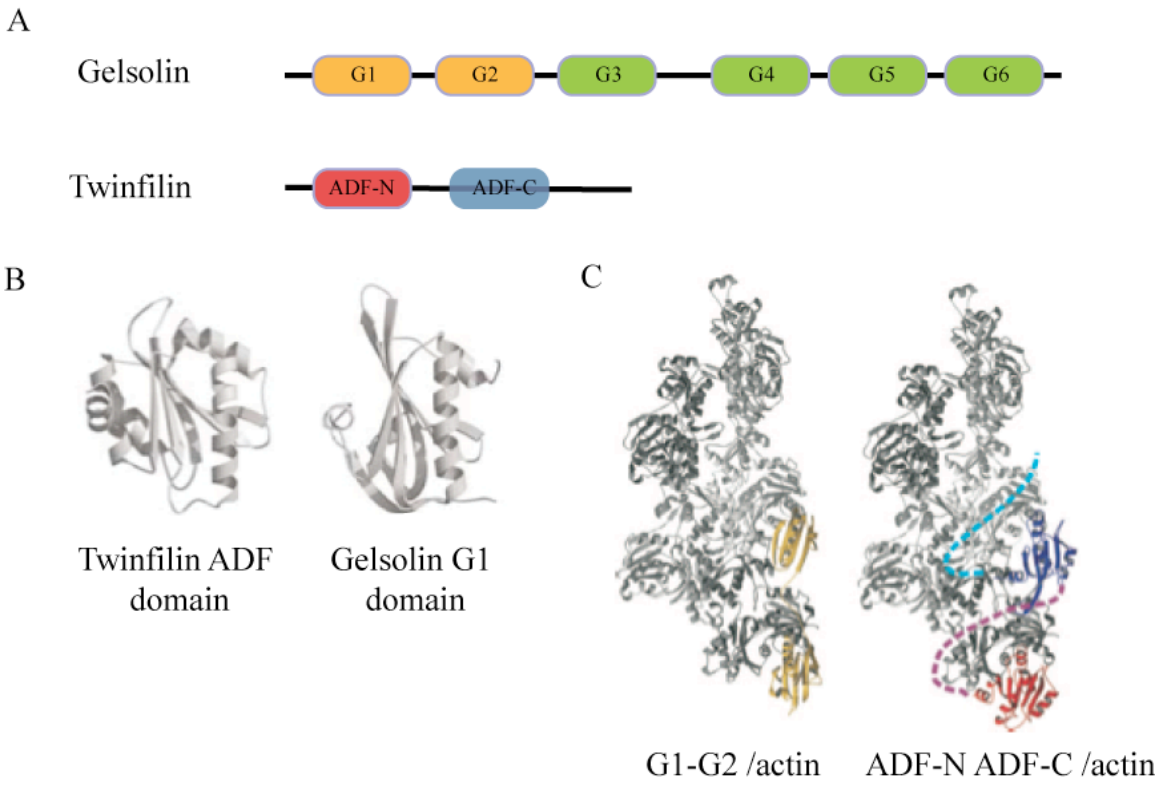

Figure 18: Comparison between Gelsolin and Twinfilin organization

Gelsolin and Twinfilin are two capping proteins that show similarities in their structural organization and mechanism of action.

A. Domain organization of Gelsolin and Twinfilin. Gelsolin is composed by six homologous domains, while Twinfilin is composed of two (N terminal and C terminal) ADF homology domains.

B. Comparison of the ribbon structure of the Gelsolin G1 domain and the Twinfilin ADF-H N terminal domain showing their structure similarity.

C. Comparison of Twinfilin and Gelsolin way of binding to filament ends. Model of Gelsolin G1-G2 and Twinfilin ADF-N and C domains bound to F actin (depicted in grey). Modified from [49].

5.5.4.4 Eps8 family

Eps8 (EGF receptor pathway substrate #8) family has been more recently described as a novel class of capping proteins [50] [51]. In mammalian three Eps8 homologous exist, named Eps8-L1, L2 and L3. Eps8 homologues are present also in *Drosophila melanogaster* and in *C.elegans,* indicating an important and conserved role of the protein throughout evolution [52]. Eps8 family members show a modular structure, with a N-terminal PTB domain, a central SH3 domain, and a C-terminal region, which retains the actin binding capability of the protein (Figure 19).

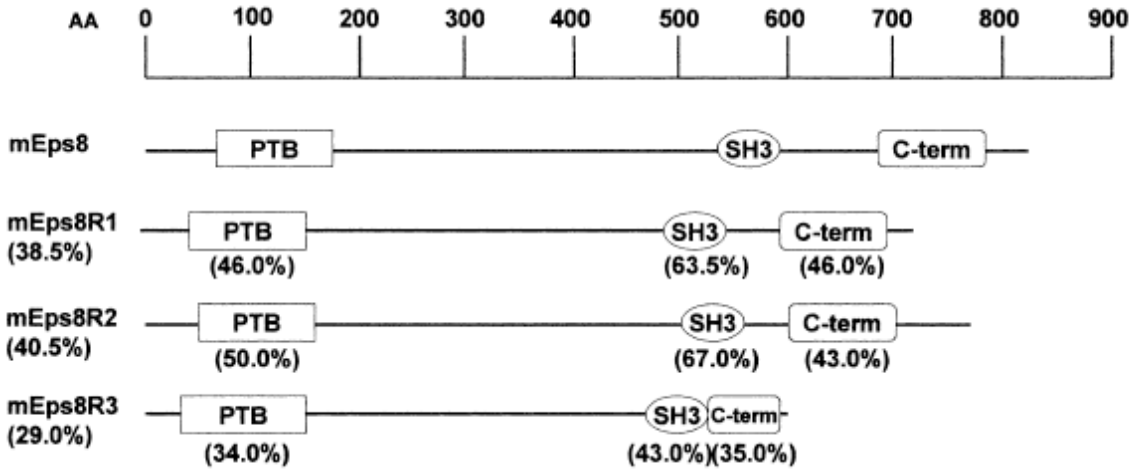

Figure 19: Schematic representation of the domain organization of the mammalian Eps8 family genes
The principal Eps8 domains are boxed. In parenthesis the percentage of amino acidic identity between Eps8 and each related protein is indicated, with respect both to the single domains and to the entire protein sequence. Modified from [52].

Eps8 and Eps8L2 have an ubiquitary pattern of expression, while Eps8L3 is selectively expressed in the colon and Eps8L1 in the prostate and in the colon. Functional redundancy between Eps8 and Eps8L2 is probably the cause of a lack of overt phenotypic alterations of EPS8-knock out mice. This latter notion is supported by the observation that in *C.elegans*, where only one *eps-8* gene is expressed, genetic interference with *ce-eps-8* causes early embryonic lethality, thus demonstrating an essential function of the protein in development [51]. The *ce-eps-8* gene can give rise to two alternative splice variants, one retaining the C-terminal region, including the conserved actin binding domain (named *eps-8a*), and a shorter that retains the PTB and SH3 domains only (named *eps-8b*). Remarkably, genetic disruption of the long isoform (*eps-8a* mutant) leads to strains that are able to overcome early embryonic lethality, suggesting that functions encoded by the N-terminal portion of *eps-8* are essential for early development. *eps-8a* mutant strains, however, display specific arrest at later larval stages (stage 4), with a defective intestinal morphogenesis and altered ultrastructural organization of intestinal microvilli, revealing a specific developmental function of the actin binding region of EPS-8 [51].

The mammalian Eps8 protein organization and its biochemical functions will be discussed in more details in the following session.

5.6 Eps8

Eps8 (EGFR pathway substrate #8) is a 97kD protein identified through an expression cloning approach for substrates of receptor tyrosine kinase (RTK) [53]. It has a modular structure typical of a signalling molecule, and possesses different biochemical functions that render the protein a key regulator of the actin cytoskeleton remodelling.

5.6.1 Eps8 structural organization

Eps8 displays a domain organization that includes an N-terminal Phospho-tyrosine Binding domain (PTB), a central Src homology-3 domain (SH3), two Proline rich regions and a C-terminal "effector region" [54] (Figure 20).

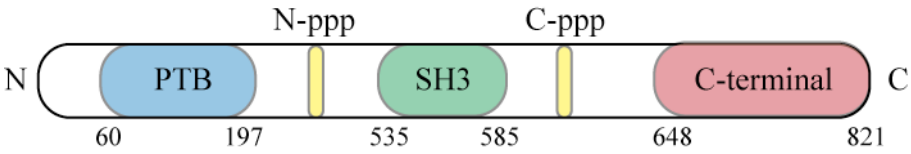

Figure 20: Eps8 structure

Eps8 has a modular structure typical of a signalling protein.

Eps8 domain organization is shown. Eps8 protein contains a PTB (Phospho-Tyrosine Binding domain), a central SH3 domain and a C-terminal effector region that mediates the interaction with actin. Two Proline rich regions are also present, flanking the SH3 domain.

The PTB domain is a protein-protein interaction module, binding to a variety of Tyrosine containing motifs [54]. No physiological interactors for the PTB domain of Eps8 have been identified so far and its cellular function remains to be elucidated. However, an *in vitro* interaction between this domain and specific integrins β tails has been shown [55]. The binding has been so far demonstrated only by pull down assays but it is consistent with recent works suggesting the involvement of Eps8 in the transduction of integrin-

induced signals. Eps8 has in fact been recently shown to control integrin mediated Rac1 activation and cell migration in Oral Squamous Cell Carcinoma (OSCC) [56] and to increase the expression and the activity of focal adhesion kinase (FAK) in Colon Cancer cells [57].

SH3 domains mediate protein:protein interactions with Prolin-rich motifs. The canonical SH3 domain structure is formed by two small β sheets, packed against each other approximately at right angles [58]. Eps8 SH3 domain is somehow unconventional. First, two crystallographic structures exist, one indicating a monomeric structure of the domain, and one indicating that the SH3 domain can form an intertwined, domain-swapped dimer [59]. Secondly, Eps8 SH3 domain binds preferentially peptides containing a PXXDY consensus sequence, instead of the classical PXXP motif [54]. Two known interactors of the SH3 domain of Eps8 are Abi1 and 2 and RN-tre, indicating a role of Eps8 both in the Rho GTPase signalling cascade and in endocytosis. Together with Abi1 and Sos1, in fact, Eps8 takes part of a trimeric complex that displays a specific Rac GEF activity *in vitro* and *in vivo* [60] [61]; RN-tre, instead, is a GAP for Rab5, Rab33 and Rab41 [62]. More specifically, RN-tre activity on Rab5, a protein essential for endosome biogenesis and maturation, revealed a role of Eps8 in RTKs internalization and recycling [54].

5.6.2 Eps8 functions

Eps8 has emerged as a key regulator in controlling actin cytoskeleton remodelling. It acts both by participating in signalling cascades downstream RTKs receptors, through its interaction with Abi1, Sos-1 and RN-tre, and by directly controlling the actin cytoskeleton dynamics and structural organization through its capping and bundling activity. All these functions are mediated by Eps8 C-terminal domain (aa 648-821), in which both the Sos-1 and the actin binding surfaces are located.

5.6.2.1 Eps8 in the Rho GTPase signalling cascade

Eps8 as a molecular adaptor participates to RTKs signalling cascade leading to Rac - dependent actin cytoskeleton remodelling [3]. At the molecular level, Eps8 was shown to enter into a multimolecular complex, together with Abi1, the non catalytic subunit of PI3K, p85, and the dual GEF for Ras and Rac, Sos-1. Within this complex, Abi1 acts as a scaffold facilitating the interaction between Eps8, p85, and Sos1 [63]. The assembly of this signalling unit enables through mechanisms that remain to be fully elucidated to unmask the otherwise silent Rac-specific GEF activity of Sos-1, mediating actin cytoskeleton remodelling in response to growth factors stimulation [60]. Notably, the C-terminal region of Eps8 mediates *in vitro* a direct low affinity interaction with Sos-1, sufficient, however, to activate the Rac-specific GEF of the latter protein in cells, suggesting that this region acts as a bona fide effector region within Eps8, mediating all the functions so far ascribed to the protein both as signal adaptor as well as actin regulatory binding interactor.

5.6.2.2 Eps8 and endocytosis

Eps8 involvement in endocytic processes derives from its ability to bind yet another SH3 interactor, RN-tre. RN-tre is a GAP specific for Rab family proteins, including Rab5 and Rab41 [64], indicating its involvement in trafficking processes. Most notably, RN-tre was originally demonstrated to function both *in vitro* and *in vivo* on Rab5, which is in turn essential for regulating multiple steps of internalization of various membrane receptors, including early endocytic events and early endosomal formation, maturation and trafficking [62].

In particular, Rab5 is essential for EGF receptor endocytosis upon ligand binding. Interaction between Eps8 and RN-tre has been shown to be required for the activation of the Rab5-GAP specific activity of the latter protein. This leads to the inhibition of the small GTPase accompanied by increased EGFR at the cell surface due to impaired receptor internalization and increased signalling [65]. RN-tre has also been demonstrated to be a

direct effector of Rab5 in RTK-induced pathways leading to actin cytoskeleton remodelling and in particular to circular dorsal ruffle (CDR) formation [66]. CDRs are transient actin based structures which form on the dorsal, apical cell plasma membrane implicated in macropinocytosis and three dimensional cell migration [67] [68]. Within this signalling cascade, RN-tre has been proposed to mediate a three-pronged interaction between Rab5, which localizes on CDRs, actin and the actin crosslinker actinin4 (the latter two proteins bind RN-tre C-terminal region) thus restricting the localization of these proteins on PM sites where remodelling of the actin network through crosslinking results in CDRs formation.

A recent work revealed an unexpected connection between Rab5-induced endocytosis and Rac activation. A Rab5 endocytic circuit was shown to be required for spatial restriction of Rac signalling at the plasma membrane leading to the generation of CDRs and impacting on the mode of tumour cell motility [69]. By activating endocytosis, Rab5 causes internalization of Rac, its activation in recycling endosomes and its subsequent redelivery through Arf6-dependent routes to specific regions of the plasma membrane [69]; there, polarized Rac dependent functions take place, leading to the formation of classical peripheral lamellipodia (PL), the first obligatory step in two-dimensional cell motility, and atypical, apically-restricted circular dorsal ruffles, a surrogate marker of macropinocytosis and 3D mesenchymal motility [70].

Thus, Eps8 may regulate Rac activity either directly through assembly of a PM-localized signalling complex that promotes optimal transmission of motogenic RTK signalling, and indirectly through endocytsosis that confers a spatial dimension to signalling that is ultimately required for regulation of polarized functions, first and foremost actin-dynamics based directional migration.

5.6.2.3 Eps8 and actin dynamics

Eps8 is also able to control directly the actin cytoskeleton remodelling through its capping and bundling activity. As a capping protein, Eps8 can accelerate actin treadmilling, blocking polymerization at filament ends. As a bundler, instead, Eps8 can regulate the architectural organization of the actin cytoskeleton. These biochemical properties make Eps8 a key regulator both of actin based motility and of the formation of specific structures such as protrusions at the cellular leading edge. Eps8 functions are both mediated and retained by the protein C-terminal region, in which the F-actin binding surface is located. The full-length protein is instead regulated by protein-protein interactions.

5.6.2.3.1 Eps8 capping activity

A more recent work revealed that Eps8 acts not only as a signalling molecule, but is also the prototype of a new family of capping proteins thus controlling directly actin dynamics [50]. Eps8 capping activity resides in its conserved carboxyl-terminal region (aa 648-821), which, in substoichiometric amounts with respect to actin, is able to inhibit barbed end growth up to 90% in *in vitro* polymerization assays using spectrin actin seeds [50]. Consistently with its capping activity Eps8 enables propulsion of N-WASP coated beads in *in vitro* actin based motility assays in the absence of Gelsolin or other cappers, and it localizes in cellular regions where there is high actin turnover. Consistently, the protein is found at lamellipodia tip, on filopodia and microspikes, and is enriched in peripheral and dorsal ruffles. Eps8 also localizes in rocketing tails propelling phosphatidylinositol-4,5-phosphate-(PI45P) enriched vesicles or intracellular pathogens such as *Listeria monocytogenes* or *Shighella flexneri* [50]. In keeping with this latter specific localization, eps8 -\- derived fibroblasts displayed a decrease in the number of PI5K-induced phosphatidylinositol-4,5-phosphate enriched vesicles and in the propulsion rate of intracellular pathogens [50]. While the isolated C-terminal region is fully active as a capper, the full-length protein is regulated by protein:protein interaction. Full-length Eps8

capping activity can only be induced upon binding to Abi1 [50]. While the mechanism of this regulation remains obscure, it is possible that the binding to Abi1 induces a conformational change that exposes the C-terminal region, which would otherwise be hidden in the context of full-length protein.

Notably, a triple complex formed by Eps8 and Abi1, together with Sos1, was already been shown to be involved in Rac activation leading to actin remodelling [60]. Moreover Abi1 has been shown to be involved in WAVE2 activation and to interact with N-WASP [71] [72]. Thus, collectively these observations support the possibility that Eps8 and Abi1 participate in actin cytoskeleton regulation by entering into different complexes, each possessing distinct regulatory activities. How the formation of these different protein complexes is regulated in space and time and the impact of these interactions on actin dynamics warrant further investigation.

Eps8 capping activity is conserved throughout evolution. Like in mammalian cells, also in *C.elegans*, EPS-8A, the longer EPS8 isoform retaining the effector region, has been demonstrated to efficiently cap actin filaments through its C-terminal domain [51]. This isoform was also shown to be specifically required for proper intestinal microvilli morphogenesis and this phenotype was correlated with the capping activity of the protein [51]. The more recent discovery of the bundling properties of Eps8 raised the question whether the bundling, rather than the capping activity, could be linked to this specific gut phenotype. This issue will be specifically experimentally addressed in this work.

5.6.2.3.2 Eps8 bundling activity

Eps8 has been described to influence the architecture of the cytoskeleton by promoting bundle formation in at least two ways [73]. Firstly, it has been shown to possess a weak bundling activity *in vitro*, encoded by its C-terminal effector region. Remarkably, this domain is not only able to bind filament ends blocking their further growth and thus acting as capping device, but it also interacts with the side of filaments to mediate the

crosslinking into bundles. The bundling activity of the isolated C-terminal region of Eps8, however, can only occur when the c-terminal region is fused to GST. Since GST drives the formation of dimers, it is possible that the bundling activity of Eps8 is specifically, but somewhat artefactually, observed only under these peculiar *in vitro* conditions that may or may not reflect a physiological situation. This issue will be specifically addressed in the thesis results session and ensuing discussion.

Secondly Eps8 has been found to form a constitutive, relatively stable and abundant molecular complex together with the protein IRSp53 (Insulin Receptor Tyrosine Kineses Substrate of 53kD, also known as BIAP2 for binding partner of the Brain Specific Angiogenesis Inhibitor 1). This interaction is functional to the activation of the bundling activity of the complex. IRSp53 is, indeed, able to bind actin filaments through its N terminal IMD domain, which consistently possesses a weak bundling activity that is, however, autoinhibited in the context of the full length protein. The formation of an Eps8:IRSp53 complex is thought to release this inhibition, although an alternative possibility is that the dimeric nature of IRSp53 enhances the crosslinking activity of Eps8. Whatever the case, the enhanced bundling property of the Eps8:IRSp53 complex likely accounts, *in vivo*, for the increased filopodia protrusive activity that can be observed when the two proteins are concomitantly expressed in cells. IRSp53 has long been known to induce the formation of filopodia-like protrusions in a variety of cellular systems, mainly through its IMD domain [74], while Eps8 expression alone has no effect on filopodia formation. The concomitant expression of the two proteins, however, leads to a dramatic increase in filopodia number, length and arborisation.

Several evidences suggest that this complex acts downstream of Cdc42: i) Cdc42 mediated filopodia formation requires both Eps8 and IRSp53; ii) IRSp53 binds active Cdc42 and mediates the formation of a triple complex Eps8-IRSp53-Cdc42. Notably, however, Cdc42 has no effects on the *in vitro* biochemical bundling properties of either Eps8 or IRSp53, while it induces *in vivo* a redistribution of Eps8 and IRSp53 into

membrane-rich cellular fractions. Based on this evidence, Cdc42 has been proposed to act by promoting the recruitment of the IRSp53:Eps8 complex at plasma membrane clusters, where the combined membrane deforming property of IRSp53 and increased bundling activity of the complex may initiate the formation of filopodia.

6. RATIONAL

The dynamic assembly of actin filaments and their architectural organization into higher ordered arrays is essential for a variety of cellular processes and is at the basis of cell motility. A large number of actin binding proteins (ABP_S) regulates the turnover and the spatial organisation of actin filaments [75]. Among these are in particular capping and cross-linking proteins. Capping proteins cap the fast growing ends of filaments (barbed or plus end), and allow the actin treadmilling to take place playing an essential role in cell migration [25]. Several classes of capping proteins have been identified in mammalian cells and considerable effort has been devoted to explore their structural mechanism of action. Capping Proteins display a variable, not conserved domain organization, suggesting that they adopt different modes to cap actin filaments, and possibly exert different and specialized roles in controlling actin cytoskeleton dynamics.

Cross-linking proteins, instead, organize actin into highly dynamic and architecturally diverse subcellular scaffolds. This is achieved by linking through a bivalent interaction adjacent actin filaments to form networks that support cellular structures such as lamellipodia, filopodia, stress fibers, focal adhesions or microvilli [76].

Eps8 defines a new family of capping proteins, $Eps8L_S$ (Eps8-like), which displays no homology with other known cappers, suggesting that it uses novel mechanisms to exert its biochemical function [50]. Eps8 and its family members are also capable of side-binding and bundling actin filaments, thus playing an essential role in controlling not only the dynamics, but also the architecture of the actin cytoskeleton. The isolated C-terminal domain (residues 648-821) is sufficient to mediate both the capping and the bundling activity of the protein. This region however displays no similarity with any other capping or crosslinking proteins, suggesting that Eps8 exerts its biochemical activity through molecularly and structurally peculiar mechanisms that have remained by and large elusive.

The aim of my project was thus to unveil the structural and molecular mechanisms underlining the different activities of Eps8, with the objective of defining features enabling this protein and in particular its C-terminal domain to exert the various and different functions associated to the protein.

To this end, we utilized a multidisciplinary approach that combined biochemical and molecular biology with genetic approaches and structural analysis by Electron Microscopy (EM).

First, we biochemically characterized the C-terminal region of the protein in order to identify the actin binding surfaces. We used several independent approaches such as biochemical assays of actin polymerization, mass spectrometry analysis and *in vitro* binding experiments to fluorescently labelled actin. We combined this approach with a structural analysis by EM to reconstruct tridimensionally the mode through which Eps8 interacts with actin filaments. These biochemical and structural information were validated by point mutagenesis, which allowed us to dissect the minimal surfaces of Eps8 responsible for its capping and bundling activity *in vitro* as well as in mammalian cell and in the nematode *C.elegans* as an *in vivo* model system.

7. MATERIALS AND METHODS

7.1 Common laboratory Solutions

7.1.1 Phosphate-buffered saline (PBS)

137 mM NaCl

2.7 mM KCl

10 mM Na_2HPO_4

2 mM KH_2PO_4

The solution is prepared by dissolving 8 g of NaCl, 0.2 g of KCl, 1.44 g of Na_2HPO_4, and 0.24 g of KH_2PO_4 in 800 ml of distilled water. The pH is adjusted to 7.4 with HCl and distilled H_2O is added to 1 litre.

7.1.2 Tris HCl (1M)

The solution is prepared by dissolving 121.1 g of Tris base in 800 ml distilled H_2O. The pH is adjusted with HCl, and distilled H_2O is added to 1 litre.

7.1.3 10X Tris EDTA (pH 7.4-8.0)

100 mM Tris HCl (pH 7.4-8.0)

10 mM EDTA (pH 8.0)

7.1.4 50x TAE (Tris-Acetate-EDTA)

242 g/l Tris

57.1 ml/l Acetic acid

20 ml/l 0.5 M EDTA pH 8

The pH is adjusted to 8.5 with HCl and distilled H_2O is added to 1 litre.

7.1.5 Tris-buffered saline (TBS)

137mM NaCl

2.7mM KCl

25mM Tris

The solution is prepared by dissolving 8 g of NaCl, 0.2 g of KCl, and 3 g of Tris base in 800 ml of distilled H_2O. The pH is adjusted to 7.4 with HCl and distilled H_2O is added to 1 litre final volume.

7.1.6 1.4x JS lysis buffer

50 mM HEPES PH 7.5

50 mM NaCl

1% glycerol

1% Triton X-100

1.5 mM $MgCl_2$

5 mM EGTA

To this solution phosphatases and proteases inhibitors are freshly added:

Protease inhibitor cocktail (Roche, Basel, Switzerland)

1 mM DTT

20 mM Na pyrophosphate pH 7.5

50 mM NaF

0.5 M Na-vanadate in HEPES pH 7.5

7.1.7 5x (2x) SDS-PAGE Sample Buffer

10% (4%) SDS

500 mM (200mM) Tris pH 6.8

30% (12%) glycerol

0.03% (0.0012%) saturated bromophenol blue

15% (6%) (v/v) β-mercaptoethanol (14M)

Stored at 4°C, protected from light by foil.

7.1.8 10x SDS-PAGE Running Buffer

144 g/l Glycine

30 g/l Tris base

1% SDS

7.1.9 10x Western Transfer Buffer

144 g/l Glycine

30 g/l Tris base

Diluted at 1x concentration in 20% EtOH.

7.1.10 Ponceau S

0.1% (w/v) Ponceau ($C_{22}H_{12}N_4Na_4O_{13}S_4$) (Sigma)

5% Acetic acid

7.2 Reagents and antibodies

The following antibodies were used: anti-actin (sigma aldrich), anti-GST (produced by the IFOM-IEO Campus Antibody facility). TRITC phalloidin was from Molecular Probes (Eugene, OR). The proteins Thymosin β4, Ciboulot, Gelsolin, ADF\Cofilin, Profilin and spectrin actin seeds were a kind gift from Dr Marie-France Carlier (LEBS-CNRS-Gif sur Yvette, France). Lifeact-cherry was a kind gift from Roland Wedlich-Soldner.

7.3 Cloning techniques

7.3.1 Agarose gel electrophoresis

DNA samples were loaded on 0.8% - 2% agarose gels along with DNA markers. Gels were made in TAE buffer containing 0.3μg/ml ethidium bromide or GelRedTM Nucleic Acid 1:10000 (Biotium, Italy) and run at 90V until desired separation was achieved. DNA bands were visualized under a UV lamp.

7.3.2 Minipreps

E.coli Top10 Cells (Invitrogen) picked from individual transformed colonies were used to inoculate 3 ml LB (containing the appropriate antibiotic) and grown overnight at 37°C in 15ml Falcon tubes. Cells were pelleted for 15 minutes at 2500 rpm. Minipreps were performed according to the manual instructions (Promega, Wizard Plus SV Minipreps). The final elution was made in 80μl of milli-Q water. DNA was checked performing an agarose gel electrophoresis using 5μl of the elution.

7.3.3 DNA digestion

Between 0.5 and 2 μg DNA was digested for 2 hours at 37°C with 10 units of restriction enzyme (New England Biolabs). For digestion, the volume was readjusted to 10 μl with the appropriate buffer and ddH_2O (20μl in case of double digestions).

7.3.4 Large Scale Plasmid Preparation

E.coli Top10 Cells (Invitrogen) containing the desired DNA vector were expanded into 500 ml cultures overnight with the appropriate antibiotics. Plasmid DNA was isolated from

these cells using the Qiagen Maxi-prep kit (Qiagen,Valencia, CA) according to the manufacturer's instructions.

7.3.5 Transformation of competent cells

E.coli Top10 cells (Invitrogen) were used for cloning and large scale DNA preparation, while *E.coli* BL21 cells (Promega) were used for protein production. The transformation protocol used was the same for both strains.

50 μl of fresh competent cells were thawed on ice for approximately 10 minutes prior to the addition of plasmid DNA. Cells were incubated with DNA on ice for 20 minutes and then subjected to a heat shock for 45 seconds at 42°C. Cells were then returned to ice for 2 minutes. Then, 0.4 ml of LB were added and the cells were left at 37°C for 60 minutes (with 200 rpm shaking) before plating them onto plates with the appropriate antibiotic.

200 μl of the transformed bacterial were usually plated. Plates were incubated overnight at 37°C.

7.3.6 DNA elution from agarose gel

Dna elution from agarose gel was performed using the QIAquick Gel Extraction kit (Quiagen, Valencia, CA), following manufacturer's instructions.

7.3.7 PCR (Polymerase Chain Reaction)

Sense and antisense oligos, of 20-30 nucleotides each, were generated, one annealing in 5' (forward) and the other in 3' (reverse) to the target sequence. The primers were designed of similar length and annealing temperature. Melting temperature of the primers was calculated according to the formula: Tm = 81.5+0.41(%GC) - 675\N - % mismatch. These

primers were used in a PCR reaction together with the DNA template and the high fidelity Pfu polymerase (Promega).

Reaction mixture	
reaction buffer 10x (Promega)	5 μl
DNA template	100-300 ng
primer forward	0.2 μM
primer reverse	0.2 μM
dNTPs mix	0.2 mM
Pfu (Promega)	5 U
ddH_2O	to a final volume of 50 μl

There are three major steps in a PCR (denaturation, annealing and extension), which were repeated for 18 cycles. This was done on an automated cycler (GeneAmp PCR system 9700, Applied Biosystems), which can heat and cool the tubes with the reaction mixture in a very short time.

Cycling parameters:

Step	**Temperature**	**Time**	**N° of cycles**
A)	denaturation at 95°C	30 seconds	1
B)	denaturation at 95°C	1 minute	18
	annealing at X°C	30 seconds	
	extension at 72°C	(2 minutes/each kb of target length)	
C)	extension at 72°C	7 minutes	1

7.3.8 Site directed mutagenesis

Site directed mutagenesis was performed using the Quick Change mutagenesis kit (Stratagene), following manufacturer's instructions. Briefly, a sense and an antisense oligo of about 30-45 nucleotides each, carrying the desired mutation in the middle of the

sequence, were generated and used in a PCR reaction using the wild type construct (100-300 ng) as template. PCR was performed using the Pfu TURBO polymerase for 18 cycles.
For the amplification step, 18 PCR cycles were performed with a denaturation step of 30 seconds at 95ºC followed by an annealing step of 1 minute at 55ºC and an extension step at 68ºC of 2 minutes/each kb of plasmid length.
After amplification, 1 µl of DpnI restriction enzyme, which selectively cuts methylated DNA at the GATC sequence, was added to digest the wild-type parental DNA. After one-hour incubation at 37˚C, the PCR product was used to transform competent *E. coli* Top10 cells (Invitrogen) and single colonies were sequenced for the presence of the desired mutation and the absence of other, unwanted, base changes. The presence of the desired DNA amplification was also checked by DNA electrophoresis of 10µl of the product in a 1-2 % agarose gel.

7.3.9 Generation of EPS8 constructs

Eps8 constructs containing different fragments of the C-terminal region of the protein (aa 648-821) were obtained through PCR, using as template the pGEX6P1 vector (Pharmacia Biotech) containing the cDNA sequence of murine Eps8 C-terminal region (aa 648-821) cloned into BamH1-EcoR1 restriction sites.

To clone the different constructs specific primers were designed flanked by BamH1 and EcoR1 sites.
The DNA fragments were first cloned in a TOPO pCR 2.1 vector (Invitrogen) using the TOPO TA Cloning kit (Invitrogen) according to manufacturer's instructions.
DNA fragments were then subcloned in an empty pGEX6P1 vector after BamH1-EcoR1 double digestion and subsequent ligation.

USED PRIMERS:

constructs	Primers	
H1 (aa 674-703)	Fwd:	5’ ggatcctacaaacaactcccagtgg 3’ (Tm=59.1°C)
	Rew:	5’ gaattcagcactgcgccc 3’ (Tm=56.2°C)
H5 (aa 765-788)	Fwd:	5’ ggatccgtctgcccggaaggtg 3’ (Tm=63.6°C)
	Rew:	5’ gaattcattactgtcctccaaagcagc 3’ (Tm=62.5°C)
H1-2 (aa 674-737)	Fwd:	5’ ggatcctacaaacaactcccagtgg 3’ (Tm=59.1°C)
	Rew:	5’ gaattctccctttgactgcagccaagtc 3’ (Tm=69.5°C)
L-H2-H5 (aa 701-821)	Fwd:	5’ ggatcccagcctggtctgcctggg 3’ (Tm=59.1°C)
	Rew:	5’ gaattcattactgtcctccaaagcagc 3’ (Tm=62.5°C)
H2-5 (aa 717-788)	Fwd:	5’ ggatccgtgatcaatatcacttatgactcc 3’ (Tm=58.5°C)
	Rew:	5’ gaattcattactgtcctccaaagcagc 3’ (Tm=62.5°C)

7.3.10 Generation of EPS8 point mutants

The different EPS8 mutants were generated performing site directed mutagenesis using the Quick Change mutagenesis kit (Stratagene), following manufacturer’s instructions (see also section 7.3.8). Specific primers were designed:

constructs	Primers
Δbundling (Villin) mut L757A K759A	5’ ggagcacaactcttttct**gc**caac**gc**agacgaactgagg 3’
Δcapping (H1) mut V689D L693D	5’ cccagatggaagagg**a**tcaggatgag**ga**cttccagaggc 3’
Δbundling (Villin) mut *C.e.* L849A K851A	5’ gccaatctattctcc**gc**gtca**gc**attgcatctgcaacaagc 3’
Δcapping (H1) mut *C.e.* L784E V788E	5’ gaatcctcaagaga**tt**caagaag**a**gactgaaactgtggg 3’
Linker mutant R706A F708A	5’ gcgcagtgctgcgcag**gc**gaag**gc**ccacgtgccacggc 3’

7.4 Cell culture

7.4.1 Cells culture

MEF (mouse embryonic fibroblasts) and Phoenix cells were grown in Dulbecco's modified Eagle's medium (DMEM, Life Technologies, Inc.) supplemented with 10% foetal bovine calf serum (FCS), 100 µg/ml streptomycin, 100 µg/ml penicillin and 2 mM glutamine. Cells were grown at 37°C in 10% CO_2.

7.4.2 Transfection

Transfections were performed using either the calcium phosphate method or electroporation.

Phoenix cells were transfected using the calcium phosphate procedure. In this case DNA (10 µg for a 10 cm plate) was diluted in 439 µl of ddH_2O and 61 µl of 2M $CaCl_2$ were added. This solution was added, drop-wise, to 500 µl of HBS 2x. After 15 minutes incubation, the precipitate was added to the cells (plated on 10 cm dishes) and removed after 12-16 hours.

Electroporation was used to transfect MEF cells for the live imaging experiments, using the MicroPorator system (Digital Bio Technology) according to manufacturer's instructions. Cells were microporated with one pulse of 30 ms at 1350 V, with a cell density of $5*10^6$ cells\ml.

2x HBS pH 7.5

50 mM Hepes pH 7.5

10 mM KCl

12 mM dextrose

280 mM NaCl

1.5 mM Na_2HPO_4

7.4.3 Retroviral infection

Stable MEF Eps8 -/- cells re-expressing wt GFP-Eps8 FL or expressing GFP Eps8 FL carrying the different mutations (Δcap, Δbundle, and ΔcapΔbundle mutants) were generated by retroviral infection using a pBABE-GFP vector (Cellbiolabs) in which the different constructs had been cloned. Retroviruses were produced by transfecting Phoenix cells using the calcium phosphate procedure (2 plates of 10bcm diameter for each construct). 48 and 72 hours after transfection, supernatants were collected and passed through a 0.45 μm filter. 8 μg/ml Polybrene (Sigma-Aldrich) was added to the viral supernatant. Viral supernatant was added to cultured MEF Eps8 -/- cells in a 6 well plate. Two cycles of infection were performed, of 4h each. Infected cells were selected with Puromycin for 2 weeks. Expression of the different constructs was controlled by GFP expression and by Western Blot analysis.

7.4.4 Cell lysis

After washing with PBS 1x, cells were lysed in JS buffer directly on the plates using a cell-scraper. About 200 μl of JS buffer/10 cm plates were used. Lysates were incubated on ice for 10 minutes and spun at 12000 rpm for 10 min at 4ºC. The supernatant was transferred into a new eppendorf and protein concentration was measured by the Bradford assay (Biorad), following manufactur's instructions.

7.5 Imaging techniques

7.5.1 Immunofluorescence

To perform immunofluorescence, cells were fixed in 4% paraformaldehyde (in PBS) for 10 minutes, washed with PBS and permeabilised in PBS 0,1% Triton X-100 for 10 minutes at

room temperature. To prevent non-specific binding of the antibodies, cells were then incubated with PBS in the presence of 0.2 % BSA for 20 minutes.

The coverslips were then gently deposited, face down, on 30 µl Alexa 594-conjugated phalloidin (Molecular Probes) at a concentration of 6.7 U/ml.

After three washes in PBS, coverslips were mounted in mowiol (20% Mowiol (Sigma), 5% Glycerol, 2.5% DABCO (Molecular Probes), 0.02% NaN3 in PBS) and examined by fluorescent optical microscopy.

7.5.2 Cell Spreading

The spreading experiment was performed using MEF cells stabling expressing GFP Eps8 (WT or mutated) produced with Retroviral infection (see section 7.4.3).

Coverslips were coated with Fibronectin (5-7 µg\ml in PBS) o\n at 4°C.

Cells were trypsinized and incubated with warm complete medium for 30 minutes under the hood. Cells were then plated on fibronectin coated coverslips. Attaching of the cells to the coverslips was monitored using a microscope with a 10X objective. After 30 minutes cells were fixed in 4% Paraformaldeyde and immunofluorecence was performed as described in section 7.5.1.

7.5.3 Live cells imaging

MEF -\- cells were co-microinjected with Myc-phosphaditylinositol 4,5 kinase (PI(4,5)K), lifeact-cherry and the different Eps8 constructs fused to GFP.

100.000 cells for each condition were plated on 35mm dishes (Ibidi) with glass bottom.

Cells were imaged using a spinning disk confocal microscope (Olympus) with a 60X oil objective. Cells were checked for GFP expression and then five minutes movies were taken, following only the cherry-lifeact signal.

The velocity of rocketing endomembranes was determined by manually tracking individual vesicles in at least 5-10 different cells using the ImageJ software. Statistical significance was evaluated with the Turkey-Kramer HSD test.

7.5.4 FRAP experiments

FRAP experiments were performed by Dr. Klemens Rottner.

The experiments were performed on Mouse melanoma cells (B16-F1), from American Type Culture Collection (ATCC CRL-6323). Cells were maintained in DMEM (Invitrogen, Germany) with 10% FCS (PAA Laboratories, Austria) at 37°C in the presence of 5% CO_2.

Cells were observed in an open, heated chamber (Warner Instruments, Reading, UK) at 37°C on inverted microscopes. FRAP experiments were performed using a double-scan-headed confocal microscope (Fluoview1000, Olympus), allowing simultaneous imaging of EGFP- and/or RFP-tagged probes (with 30 mW 488 nm multilane argon and/or 20 mW 561 nm solid-state lasers, respectively) and photobleaching/activation using a 20 mW 405 nm diode laser.

7.6 Biochemical procedures

7.6.1 SDS polyacrylamide gel electrophoresis (SDS PAGE)

Gels for resolution of proteins were made from a 30%, 37.5:1 mix of acrylamide:bisacrylamide (Sigma). As polymerisation catalysts, 10% ammonium persulphate (APS) and TEMED (Fluka) were used.

7.6.2 Western blot

Desired amounts of proteins were loaded onto 0.75-1.5 mm thick polyacrylamide gels for electrophoresis (Biorad). Proteins were transferred in Western transfer tanks (Biorad) to nitrocellulose (Schleicher and Schuell) in Western Transfer buffer 1x (diluted in 20% ethanol) at constant Voltage (100V for 1 hour, 80V for 2 hours, or 30V overnight). PonceauS colouring was used to reveal roughly the amount of proteins transferred on the filters. Filters were blocked 1 hour (or overnight) in 5% milk or 5% BSA in TBS 0.1% Tween (TBS-T).

After blocking, filters were incubated with the primary antibody, diluted in TBS-T 5% milk, for one hour at room temperature, or overnight at 4˚C, followed by three washes of five minutes each in TBS-T and then incubated with the appropriate peroxidase-conjugated secondary antibody diluted in TBS-T for 1 hour. After the incubation with the secondary antibody, the filter was washed three times in TBS-T and the bound secondary antibody was revealed using the ECL (Enhanced Chemiluminescence) method (Amersham).

7.6.3 GST-fusion proteins production

All the GST fusion proteins used were product in bacteria using *E. coli* BL21 cells transformed with the pGEX6P1 vector in which the desired construct had been cloned.

7.6.3.1 Bacterial culture

E. coli BL21 cells picked from individual colonies, transformed with the indicated GST-fusion constructs, were used to inoculate 50 ml of LB medium (containing ampicillin at 25 μg/ml) and were grown overnight at 37°C. 5 ml of the overnight culture was diluted in 0.5 litre of LB and was grown at 37°C (240 rpm shaking) till it reached approximately OD=0.6.

Then IPTG was used to induce the protein production using different conditions depending on the protein:

Construct	IPTG concentration	time	temperature
Eps8 648-821 wt \ carrying all the different mutations	1mM	2h30	37°C
Eps8 H1 (aa 674-703)	0.5mM	o/n	16°C
Eps8 H1-H2 (aa717-788)	0.5mM	o/n	16°C
Eps8 H5 (aa 765-788)	0.5mM	o/n	16°C
Eps8 L-H2-H5 (aa 701-821)	0.5mM	o/n	16°C
GST	1mM	2h	37°C

After the induction cells were pelleted down at 4000 rpm for 15 minutes at 4°C and pellets were used immediately or conserved at -80°C after washing in PBS 1X.

7.6.3.2 Protein production

Pellets were suspended in GST-lysis buffer (20ml for 1l culture). Samples were sonicated 3 times for 30 seconds/each on ice and were pelleted down at 40000 rpm for 45 minutes at 4°C using a 55.2 Ti Beckman rotor. 1 ml of glutathione-sepharose beads (Amersham), previously washed 3 times with GST-lysis buffer, was added to the supernatants and samples were incubated 1 hour at 4°C while rocking. Beads were then washed 3 times (with 10 minutes of incubation at 4°C each) in the GST-lysis solution. Proteins were then eluted from the beads as GST fusion proteins or cleaved using prescission protease.

GST-lysis solution

50mM Tris pH 7.5

500mM NaCl

1mM $MgCl_2$

0.1% triton X100

protease inhibitor cocktail (Roche, Basel, Switzerland) (freshly added)

1 mM DTT (freshly added)

7.6.3.3 GST-fusion protein elution and PreScission protease cleavage

Beads were washed once in the washing solution and than subjected to four cycles of elution (15 min each at RT) in the elution buffer. Eluted proteins were finally purified through gel filtration using a Superdex 200 10\30 column (GE Healthcare Life Science) on an AKTA purifier system (Amersham Bioscience) in the final storage buffer. Proteins were flesh frozen using liquid Nitrogen and stored at –80˚C.

Washing buffer

10 mM Tris-HCl pH 8.5

75 mM NaCl

Elution buffer

20 mM Tris-HCl pH 8.0

500 mM NaCl

20 mM glutathione (Amersham)

Storage buffer

50 mM Tris-HCl pH 7.5

50 mM NaCl

1 mM DTT

5% glycerol

Proteins were cleaved from the GST using the PreScission protease (Amersham Pharmacia Biotech) according to the manufacturer's instructions. Cleaved protein was then further purified and stored as described above.

7.6.4 PPDM cross-linking of Eps8 (648-821) and actin

G-actin and Eps8 (648-821) were solubilized in a buffer containing 5 mM Hepes pH 7.8, 0.2 mM $CaCl_2$ and 0.2 mM ATP by using a D-Salt Extracellulose Desalting column (PIERCE). G-actin and Eps8 (648-821) were mixed and incubated for 5 and 10 minutes with 16 μM of PPDM (N,N'-(1,4-Phenylene)dimaleimide) (Fluka) at room temperature. Following addition of 10 mM DTT, samples were resolved by SDS-PAGE.

7.6.5 Gel filtration analysis

Size exclusion chromatography was performed on a Superdex 200 10\30 column (GE Healthcare Life Science) on an AKTA purifier system (Amersham Bioscience). Proteins were centrifuged for at least 10 minutes at 13.000 rpm before loading.

Proteins were loaded in 500 μl volume using a Hamilton syringe. Typical flow rate was 0.5 ml\min.

To study the EPS8-actin complex proteins were run in G buffer: 2 mM TRIS pH 7.8, 0.2 mM ATP, 1 mM DTT and 0.1 mM $CaCl_2$.

To perform the hydrodynamic analysis and to evaluate the proteins stability elutions were performed in buffer A or in buffer F:

Buffer A: 50 mM TRIS pH 8, 1 mM DTT, 1 mM EDTA, 50 mM NaCl, 10% glycerol

Buffer F: 2 mM TRIS pH 7.8, 0.2 mM ATP, 1 mM DTT, 0.1 mM $CaCl_2$, 1 mM $MgCl_2$ 0.2 mM EGTA, 0.1 M KCl.

7.6.6 Hydrodynamic analysis

Hydrodynamic analysis was performed coupling size exclusion chromatography and glycerol density gradient.

7.6.6.1 Size exclusion chromatography

Size exclusion chromatography was performed on a Superdex 200 10\30 column as described above (see section 7.6.5) in buffer A. Markers of known Stoke radius were run in the same buffer. Elution volumes of the markers (bovine thyroglobulin, rabbit aldolase, hen egg albumin, and ribonuclease A) were plotted against their known Stokes radii to generate a calibration curve (R^2 = 0.9775) from which the Stokes radius of GST-Eps8 (648-821) was determined.

7.6.6.2 Glycerol density gradient

The glycerol density gradient was performed in a final volume of 5 ml.

3 ml of a 10% glycerol buffer (100 mM TRIS pH 8, 1 mM DTT, 1 mM EDTA, 500 mM NaCl, 10% v\v glycerol) were put in a 5 ml tube. Putting a syringe on the bottom, the tube was filled with a 40% glycerol buffer (100mM TRIS pH 8, 1mM DTT, 1mM EDTA, 500mM NaCl, 40% v\v glycerol). The gradient was then created using a Gradient Master machine (Biocomp). 75 μl of the different proteins were placed directly on the top of the gradient. Centrifugation was protracted for 13h at 55.000 rpm on a Beckman SW41Ti swinging bucket rotor at 4°C, with low acceleration and no brake deceleration velocities. The gradient was fractionated in 250 μl volume fractions that were analysed by SDS-page.

Sedimentation volume of the markers (Bovine Pancreas Chymotrypsinogen, albumine, aldolase and catalase) were plotted against their known Svedberg coefficient (2,58S, 4,22S, 7,4S and 11,4S respectively) to generate a calibration curve from which the Svedberg coefficient (**s**) of GST-Eps8 (648-821) was determined.

The molecular weight was calculated from the Stokes radius (**a**) in Ångstroms and from the sedimentation volume (**s**) according to the Monty-Siegel equation:

MW = **α a *s**

where $\alpha = (6\pi\eta_0 N)/(1 - \nu\rho)$, N is Avogadro's number (6.02×10^{23}), η_0 is the viscosity of medium (g/(cm·s)), ρ is the density of the medium (g/ml), and ν is the partial specific volume of the analyzed particle (ml/g). In our experimental setting we calculated $\alpha = 0.41$.

7.7 Mass Spectrometry analysis

The Mass Spectrometry analysis was performed in collaboration with the Mass Spectrometry facility of the IFOM-IEO Campus.

7.7.1 Crosslinking reaction

The complex between murine Eps8 (648-821) and actin was purified by gel filtration and crosslinked using 1:1 mixture of the bis [sulfosuccinimidyl]glutarate (BS^2G-d0) and its deuterated version (BS^2G-d4) (Pierce). The reaction was carried out at room temperature using 100-fold molar excess of the crosslinker reagent with respect to the protein complex in a final volume of 200 µl of 50 mM Hepes pH 7.5 and 150 mM NaCl. BS^2G contains a spacer of 7.7 Å length and crosslinks Lysines with side chains that can extend up to 6.0 Å. The reaction was stopped after 20 min with 5 µl of 1 M ammonium bicarbonate (Sigma).

7.7.2 Protein digestion and chemical crosslinked peptide purification

The protein sample was resolved by SDS-PAGE. Two bands with higher molecular weights, as compared to the control in absence of crosslinkers, were excised from the gel and Trypsin-digested. The enzymatic reaction was stopped by adding trifluoracetic acid (TFA) to a final concentration of 1%. The acidified peptide mixture was desalted and concentrated before injecting, via an Agilent 1100 Nano HPLC, into a C18 column (Reprosil-Pur C18-AQ 3 µm; Dr. Maisch GmbH) packed into a spray emitter (100 µm internal diameter, 8 µm opening, 70 mm length; New Objectives). The peptides were eluted in a gradient from buffer A (5% acetonitrile and 0.5% acetic acid) to buffer B

(acetonitrile and 0.5% acetic acid) going from 0% to 20% in 10 min at 300 nl/min-1. Spectra were recorded on a LTQ-FT mass spectrometer (Thermoelectron).

7.8 Biochemical actin-based assays

The following assays and the set of required purified proteins were generated following specific protocols derived from Marie-France Carlier Lab (CNRS, Gif-sur-Yvette, France).

7.8.1 Common buffers

Same buffers are commonly used in actin-based assay.

G buffer is used to keep actin in the monomeric state (G = globular)

Buffer G

5 mM Tris-HCl pH 7.8

0.2 mM ATP pH 7.0

1 mM DTT

0.1 mM $CaCl_2$

F buffer is used to keep actin in the polymerized state (F = filamentous)

Buffer F

5 mM Tris-HCl pH 7.8

0.2 mM ATP pH 7.0

1 mM DTT

0.1 mM $CaCl_2$

1 mM $MgCl_2$

0.2 mM EGTA

0.1 M KCl

7.8.2 Actin purification

Actin was purified starting from Rabbit muscle acetone powder (Pel-Frezez Biologicals, Rogrs, Arkansas) according to the following protocol.

Nine gr of acetone powder were extracted with 270 ml cold buffer X on ice in a 500 ml beaker. Buffer was slowly added with gentle stirring with a glass rod to thoroughly wet powder. The resuspension was set on ice for 30 min and stirred gently once every 10 min. The preparation was then centrifuged at 25000 xg at 4˚C for 45 min. Supernatant was filtered using a cotton lint into a graduated cylinder and transferred into a beaker. Solid KCl was added to a final concentration of 3.3 M while stirring (at RT until temperature reaches 15˚C) and moved back on ice without stirring until temperature returned to 5˚C. The sample was centrifuged at 25000xg, for 30 min at 4˚C. Tight white pellets, if any, is actinin. Supernatant was dialyzed vs 32 volumes of buffer D overnight. Final KCl concentration was 0.1 M.

After overnight dialysis 4M KCl was added to give a final concentration of 0.8 M and the prep was stirred for 1.5 hours at 4˚C in order to solubilize tropomyosin. The prep was then centrifuged at 100000xg for 3.5 hours at 4˚C. Supernatant was discarded. Pellets were homogenized with a potter in 25 ml buffer X. Once added 0.075 ml $MgCl_2$ 1 M and 0.375 ml KCl 4 M, the volume was adjusted to 38.6 ml with buffer X and the prep was left at 4˚C overnight without stirring.

The day after 9 ml KCl 4 M and 2.37 ml of buffer X were added and the prep was stirred for 1.5 hours at 4˚C and then centrifuged at 100000 xg for 3.5 hours at 4˚C. Pellet was homogenized in buffer X (20-30 ml) and the resuspension was dialyzed vs 1l G buffer.

The day after the prep was briefly sonicated in the dialysis bag, 1 x 10 seconds. Dialysis buffer was changed.

After 2 days of dialysis in G buffer (with daily change of the buffer) actin was clarified at 230000 xg for 2 hours at 4˚C. The prep was loaded onto a Superdex 200 26/60 column

(GE Healthcare) and run using an Amersham Biosciences AKTA Purifier. Fractions of 5 ml were collected. The protein concentration was measured using UV absorbance (290nm instead of 280 nm because ATP interferes at 280 nm wavelength). Actin concentration was calculated using the following formula:

[μM] = (OD 290nm\0.617) * (1\42)

where 0.617 is the OD of actin at 290nm when concentrated 1mg\ml, and 42 is the actin molecular weight (kD).

Buffer X

2 mM Tris-HCl pH 7.8

0.5 mM ATP pH 7.0

0.1 mM $CaCl_2$

1 mM DTT

Buffer D

2 mM Tris-HCl pH 7.8

1 mM $MgCl_2$

1 mM DTT

7.8.3 Pyrenyl-actin labelling

Actin was purified as described above and the labelling protocol was started at the end of the third day. Actin is labelled on cysteine 374.

After centrifugation the pellet was resuspended in buffer A to a final concentration of 2 mg/ml. 1:100 volume of N-(1-pyrenyl)iodoacetamide (Molecular Probes, Invitrogen) at 14 mg/ml in DMF was added and the sample was gently mixed until it became white. Actin was then incubated overnight at 4°C rocking. From this moment actin has to be kept always in the dark.

After overnight incubation DTT was added to 1 mM final concentration and the sample was centrifuged at 4000xg for 15 min. Supernatant was then centrifuged again at 100000 xg for 3.5 hours at 4˚C. Pellet was homogenized in 5 ml of buffer G and dialyzed vs 1 l of buffer G overnight at 4˚C.

The day after the prep was briefly sonicated in dialysis bag, 1 x 10 seconds and the dialysis buffer was changed.

After 2 days of dialysis in G buffer (with daily change of the buffer) actin was clarified at 230000xg for 2 hours at 4˚C. The prep was loaded onto a Superdex 200 26/60 column (GE Healthcare) and run using an Amersham Biosciences AKTA Purifier. Fractions of 5 ml were collected. The protein concentration was measured using UV absorbance (290 instead of 280 nm because ATP interferes at 280 nm wavelength). Actin concentration was calculated using the following formula:

[μM] = (OD 290nm\0.617) * (1\42)

where 0.617 is the OD of actin at 290nm when concentrated 1mg\ml, and 42 is the actin molecular weight (kD).

To evaluate the actin labelling OD was measured at 343 nm, that is the wavelength of maximum absorbance for Pyrene (N-(1-pyrenyl)iodoacetamide).

The following formula was used to calculate the concentration of the labelled actin:

[μM] labelled actin = OD 343 nm\54000

where 54000 (M^{-1} cm^{-1}) is the Pyrene ξ value at 343 nm.

To evaluate the percentage of actin labelling the ratio between labelled and total actin concentration was then calculated.

Buffer A

5 mM Tris-HCl pH 7.8

0.5 mM ATP pH 7.0

1 mM DTT

0.1 mM $CaCl_2$

2 mM $MgCl_2$

0.1 M KCl

7.8.4 NBD-actin labelling

Actin was purified as described above and the labelling protocol was started at the end of the third day. Actin is labelled on lysine 373.

After centrifugation the pellet was resuspended in buffer A without DTT to a final concentration of 2 mg/ml.

NEM (N-ethylmaleimide) (Molecular Probes, Invitrogen) was added to a final concentration of 2.5 mM, starting from a solution of 100 mM NEM in water. The solution was incubated first 15 min at RT, then 15 min at 15°C and finally 3 hours at 4°C. After the incubations 5 mM DTT was added in order to stop the reaction and the sample was centrifuged for 2h at 200000xg at 4°C. The surnatant was then taken and diluted two times in buffer G with DTT. The solution was dialyzed overnight in G-buffer (without DTT) at 4°C. Dialysis was continued for 2 days in G buffer changing the buffer daily. Actin was then centrifuged 2 hours at 200000xg and the pellet was resuspended in F buffer (without DTT). Actin was let polymerize overnight in the dark at 4°C.

The day after NBD (7-cloro-4-nitrobenzene-2-oxa-1,3 dyzole) was added to a final concentration of 0.4 mM and the sample was incubated 5 hours at 15°C.

Actin was then centrifuged 2 hours at 200000xg and the pellet was resuspended in buffer G (with DTT). Actin was dialyzed overnight towards G buffer (with DTT).

Actin was then clarified at 200000xg for 2 hours at 4˚C. The prep was loaded onto a Superdex 200 26/60 column (GE Healthcare) and run using an Amersham Biosciences AKTA Purifier. Fractions of 5 ml were collected. The protein concentration was measured using UV absorbance (290 instead of 280 nm because ATP interferes at 280 nm wavelength). Actin concentration was calculated using the following formula:

[μM] = (OD 290 nm\0.617) * (1\42)

where 0.617 is the actin OD at 290nm when concentrated 1mg\ml, and 42 is the actin molecular weight (kD).

To evaluate the actin labelling OD was measured at 590 nm, that is the wavelength of maximum absorbance for NBD.

The following formula was used to calculate the concentration of the labelled actin:

[μM] labelled actin = OD 590 nm\13500

where 13500 (M^{-1} cm^{-1}) is the NBD ξ value at 590nm.

To evaluate the percentage of actin labelling the ratio between labelled and total actin concentration was then calculated.

Buffer A

5 mM Tris-HCl pH 7.8

0.5 mM ATP pH 7.0

0.1 mM $CaCl_2$

2 mM $MgCl_2$

0.1 M KCl

7.8.5 Actin polymerization assays

Initial rate of filament growth from the barbed and the pointed ends was monitored by the increase in fluorescence of 10% pyrenyl-labeled actin using a Perkin Elmer (LS55) fluorescence spectrophotometer. Pyrenyl fluorescence increases of about 25 times from G- to F-actin. Filaments growth can thus be followed looking to the increase of fluorescence.

The used wavelengths are 366 nm for the absorption, 407 nm for the emission.

Actin polymerization is induced starting from seeds, preformed nuclei of 2 or 3 actin subunits from which the polymerization can start avoiding the first lag phase. Either spectrin actin seeds or gelsolin actin seeds can be used, where spectrin and gelsolin are

proteins that bind specifically the plus and the minus end respectively. Spectrin actin seeds have thus only free barbed ends allowing actin polymerization only from the plus ends. Gelsolin actin seeds, at the contrary, can polymerize only from their minus ends.

Seeded polymerization was induced by addition of 0.1 M KCl, 1 mM $MgCl_2$ and 0.2 mM EGTA to a solution of Ca-ATP–G-actin (2.5 μM) in G-buffer containing spectrin–actin seeds (0.25 nM) or gelsolin actin seeds and the desired amount of purified protein in a final volume of 100 μl.

Gelsolin-actin seeds were prepared by adding gelsolin and 2.5 molar equivalent Ca ATP-G-actin in G-buffer. Spectrin actin seeds were a kind gift of Marie-France Carlier laboratory.

The affinity for barbed ends was derived as follows: the initial rate of polymerization was taken as a measure of the free barbed ends at t_0 (C_0, equal to the concentration of actin seeds at t_0). The following equation was used to fit the data, in which [C_0] and [B_0] are the total concentration of barbed ends and of the Eps8 fragments, respectively, and Kcap represents the equilibrium dissociation constant of the complex of Eps8 with barbed or pointed ends [*BC*]. The fraction *R* of Eps8-bound barbed ends is:

$$R = [BC]/[B_0] = (V_0 - V_C)/(V_0 - V_{min})$$

$$= ([C_0] + [B_0] + K \pm (([B_0] + [C_0] + Kcap)^2 + 4[B_0].[C_0])1/2)/2[B_0]$$

in which V_0 is the initial rate of polymerization in the absence of capping proteins, V_C is the initial rate of polymerization in the presence of capping proteins at total concentration [C_0], and V_{min} is the initial rate of polymerization in conditions of maximum inhibition (determined experimentally).

7.8.6 *In vitro* actin-based motility assays

This protocol describes the execution of an assay that reconstitutes the propulsion of N-WASP-functionalized microspheres in a minimum motility medium containing Arp2/3

complex, ADF, gelsolin (or other capping proteins), profilin, and actin [23].

7.8.6.1 Beads coating

Polystyrene carboxylated microspheres of diameters from 0.2 to 3 μm were incubated in N-WASP buffer A containing 400 nM N-WASP (added from a 4 μM stock) for 1 hour on ice. The quantity of microspheres in a 50 μl suspension was adjusted so that the total surface of solid per unit volume of solution was 7.5 x 10^9 μm^2/ml, independent of the diameter of the microspheres. 5μl of 10 mg\ml BSA were added to block free adsorption sites and incubated 15 minutes on ice. The microspheres were then centrifuged 5 minutes at 1000xg at 4°C and then washed twice, each time by adding 250 μl N-WASP buffer A and centrifuging 5 minutes at 1000xg at 4°C. Final pellet was resuspended in 50 μl of N-WASP buffer C containing 1 mg\ml BSA. Functionalized microspheres were stored on ice and used for up to 1 week without any change in their motile properties.

7.8.6.2 motility assay

Polystyrene carboxylated beads coated with N-WASP were placed in a reconstituted motility medium that consisted of 7 μM F-actin, 3.5 μM ADF, 2.4 μM profilin, 100 nM Arp2/3 complex, 50 nM capping protein (gelsolin or GST–Eps8-648–821), 4 μl ADP/DABCO/DTT mix in assay buffer 1% BSA (final volume 24 μl). An aliquot of 2.5 μl of the mix was placed between a slide (Superfrost plus, Menzel-Gläser, GmbH) and a coverslip, sealed with Valap (vaselin:lanolin:paraffin 1:1:1), and observed in phase contrast or in fluorescence using a CCD camera (Hamamatsu ORCA II ER) on an Olympus AX70 microscope equipped with a motorized stage (Märzhäuser). MetaMorph 4,6 software for microscope control and image acquisition was used to calculate the speed of the beads in time-lapse experiments.

Assay buffer:

10 mM HEPES pH 7.5, 0.1 M KCl, 1 mM $MgCl_2$, 0.1 mM$CaCl_2$, 1mM ATP, 1 % BSA)

ATP/DABCO/DTT mix:

15 µl of 0.2 M ATP, pH 7.0, and 6µl of 1M $MgCl_2$ were added to 79 µl of distilled water to obtain a 30 mM ATP\60mM $MgCl_2$ stock solution. The ATP\DABCO\DTT mix was prepared by mixing 40µl of the 30mM ATP\60mM $MgCl_2$ stock solution with 20 µl of 2.2mM 1,4-diazabicyclo[2.2.2]octane (DABCO; Molecular Probes) and 10 µl 0.2M DTT. The mix was stored in ice and used within 3 days.

Methylcellulose,1%:

1% (w/v) methylcellulose was prepared in distilled water, heated to 60°C, and stirred until the solution cleared.

Mg-F-actin

100 µl of Mg-F-actin were obtained by adding 5 µl of KME (2M KCl, 20 mM $MgCl_2$, 4 mM EGTA) to 95 µl Ca-G-actin in G-buffer.

N-WASP buffer A:

20 mM sodium phosphate buffer pH 7.8**,** 5% (v/v) glycerol**,** 0.3 M NaCl **,** 0.1% (v/v) Tween 20**.** Just before used, 1mM PMSF, 5 µg/ml leupeptin, 5 µg/ml chemostatin, 5 µg/ml pepstatin, 10 µg/ml benzamidine were added.

N-WASP buffer C: 20mM sodium phosphate buffer, ph 7.5, 5% (v\v) glycerol, 0.3 M NaCl, 10mM imidazole , 1mM DTT.

7.8.7 Actin low speed co-sedimentation assays

This assay is used to evaluate the capacity of a protein of interest to bundle actin filaments. After a low speed centrifugation, actin filaments remain in the surnatant, and only actin bundles, if present, go to the pellet. The bundling activity of a protein can be thus evaluated looking at the presence of actin in the pellet fraction. Bundling proteins would go into the pellet together with actin.

Monomeric rabbit G-actin was induced to polymerize at RT in F-actin buffer (polymerization buffer). Recombinant proteins or control buffer were subsequently incubated with F-actin for 60 min at room temperature and centrifuged for 30 min at

10000xg in a Eppendorf 5415D table-top centrifuge. Equal amounts of starting materials, supernatants and pellets, were solubilized in SDS-PAGE sample buffer, boiled and resolved on an SDS-PAGE gel. Actin and Eps8 proteins were revealed by Western Blot analysis using specific antibodies.

7.8.8 Fluorescence microscopy of actin bundling

Monomeric rabbit G-actin was induced to polymerize at RT in F-actin buffer (polymerization buffer) and was then diluted in F-buffer to a final concentration of 2 μM.

A mix was then prepared, putting 5 μl of 2 μM actin, the protein of interest at the desired concentration, and bringing to a final volume of 10 μl with F-buffer.

The reaction mix was incubated at room temperature for 30 min.

9 μl of the reaction mix were then transferred into a new tube and mixed with 1 μl TRITC Phalloidin (very slowly, using cut tips). The reaction was incubated 10 minutes at room temperature in the dark. The reaction was then added to 2.5 μl of a 1:1 mixture of 0.1% DABCO and 0.1% Methyl Cellulose with careful mixing.

The samples were finally mounted between a slide and coverslip coated with poly-Lysine and imaged by fluorescence microscopy with a 100x objective.

7.8.9 NBD-actin and AEDANS -actin binding assays

The change in fluorescence of NBD- or AEDANS-labelled actin was used as a probe for the formation of complexes of G-actin with Eps8 (648-821), H1-H2 or H5. Static fluorescence measurements were carried out on a LS55 fluorescence spectrometer from Perkin Elmer. Excitation and emission wavelengths were 475 nm and 530 nm for NBD-actin and 340, 460 nm for AEDANS actin, respectively. The amount of complex was determined by setting at 100 % the change of fluorescence measured in the presence of saturating amounts of Eps8 (648-821), H1-H2, or H5. The equilibrium dissociation

constant (Kd) for the complex was derived from the curve obtained determining the different concentrations of the complex with respect to the total concentration of Eps8 (648-821), H1-H2, or H5 using the following equations:

$[A] + [CA] = [A_0]$

$[C] + [CA] = [C_0]$

$[CA] = (1/2)\{[A_0] + [C_0] + Kc + (([A_0] + [C_0] + Kd)^2 - 4[A_0].[C_0])^{1/2}$

where $[A]$, $[A_0]$, $[C]$, $[C_0]$ are the free and the total concentrations of G-actin and of the binding proteins (either Eps8 (648-821), H1-H2, or H5); [CA] is the concentration of the complex.

7.8.10 Nucleotide Exchange on G-actin

Kinetics of nucleotide exchange on monomeric actin were monitored using the change of fluorescence of εATP upon binding to G-actin.

ATP-G-actin 1:1 complex was obtained by Dowex-1 treatment. Free nucleotide was removed just before starting the experiment by treatment with 20% v\v of a 50% suspension of Dowex 1-X2 ion exchange resin (sigma aldrich) for 4 minutes at 4°C. The Dowex resin was removed by filtration through a Millipore filter of 0.45 μm pore size.

Actin was then diluted to 1 μM in the reaction buffer (5 mM Tris HCl, 0.1 mM $CaCl_2$, 1 mM DTT) in the presence of Eps8 (648-821). The increase in fluorescence (λ_{exc} = 350nm, λ_{em}= 410nm) upon addition of 5 μM εATP was monitored using a Safas flx spectrofluorometer.

The observed first order rate constant displayed hyperbolic saturation behaviour with the concentration of Eps8 (648-821). The equilibrium dissociation constant for the Eps8 (648-821)-actin complex was derived from the dependence of the apparent exchange rate constant on the concentration of Eps8 (648-821) as follows:

$[A] + [CA] = [A_0]$

$[C] + [CA] = [C_0]$

$k_{obs} = (k_1[A] + k_2[CA])/[A_0] = ([A]/[A_0])\{k_1 + k_2([C_0]-[A_0] + [A])/k_c\}$

with

$[A] = (1/2)\ \{[A_0] - [C_0] - K_c \pm (([A_0] - [C_0] - K_c)^2 + 4K_c[A_0])^{1/2}\}$

$[CA] = (1/2)\ \{[A_0] + [C_0] + K_c \pm (([A_0] + [C_0] + K_c)^2 - 4\ [A_0] * [C_0])^{1/2}\}$

where $[A]$, $[A_0]$, $[C]$, $[C_0]$ are the free and total concentrations of G-actin and Eps8 (648-821) and $[CA]$ is the concentration of the complex; k_1 and k_2 are the rate constants for nucleotide dissociation from G-actin and from the CA complex, respectively; K_C is the equilibrium dissociation constant of the CA complex. The values of k_1 and k_2 were determined experimentally in the absence and in the presence of saturating amounts of Eps8 (648-821). The value of K_C was derived from the adjustment of the calculated curves k_{obs} ($[C_0]$) to the data.

7.9 Electron microscopy

Electron microscopy was performed in collaboration with Doris Hanein laboratory in La Jolla, California.

7.9.1 grids preparation

Rabbit skeletal muscle actin was prepared and stored as described in section 7.8.2. Filamentous actin (F-actin) was used within two to three weeks of preparation. F-actin samples were diluted to 0.03-0.07 mg/ml in buffer A just before the application to glow-discharged 400-mesh copper grids coated with lacy carbon film. All protein samples (excluding F-actin) were spun at 4º C for 10 min at 15,000 rpm prior to dilution (Buffer A). Following 30-60 seconds of incubation in a humidity chamber, the sample was blotted and stained with 2% aqueous uranyl acetate. Images were recorded at a dose of ~50 $e^-/Å^2$ with a Tecnai G2 T12 electron microscope (FEI Company, Hillsboro, OR) at 120 keV with a nominal magnification of 52,000 and 1.5 μm defocus. Images were digitized using a

SCAI scanner (Integraph Coorporation, Huntsville, AL) with pixel size of 0.4 nm on the sample.

Buffer A:

5 mM NaPi pH 7.0

20 mM NaCl

1 mM $MgCl_2$

0.1 mM EGTA

2 mM NaN_3

7.9.2 Image Processing

To reconstruct Eps8 C-terminal domain (residues 535-821) bound to F-actin a modified version [77] of the iterative helical real space refinement method [78] was applied in order to select filaments that clearly showed decoration by visual inspection. The first step of the procedure is the selection of overlapping boxes containing short helical segments. A box size of 80x80 pixels with a 0.54 nm pixel size was used. This corresponds to about 15 asymmetric units of the helix, a little over one actin crossover. An overlap of 60 pixels was chosen, allowing every asymmetric unit to contribute to four different views of the helix. A total of 36550 units contributed to the average. The twist of the reconstruction refines to 2.14 subunits per turn, which corresponds to a rotation of -168º between symmetry neighbours along the short-pitch helix. Control reconstructions of F-actin alone were also calculated resulting in a twist of 2.16 subunits per turn, a rotation of -166.66º. After compensating for the difference in twist, the EPS8-decorated and undecorated F-actin reconstructions were optimal aligned using the density-fitting module of CoAn [79] and difference maps were calculated.

7.9.3 Docking and modelling of EPS8 C-terminal domain bound to F-actin

The difference density resulting from subtracting the control F-actin reconstruction from the Eps8 bound reconstruction was used to dock the atomic model of helices H2-H5 using the statistics-based density docking method implemented in CoAn [79, 80]. The statistical analysis indicated a rotational degeneracy along its long axis. The H1 model and its interactions with actin were taken straight from the Ciboulot crystal structure (1sqk) [81]. H1 could bind in two ways between subdomains 1 and 3, either with the N-terminal at the front or at the back of the actin subunit. Both modes of binding have been observed for different actin binding proteins [82]. The modelled configuration (N-terminus at the back) is more consistent with the crosslinking studies presented here. The linker was modelled directly into the density using PyMOL [83]. Stereo chemistry constraints to avoid clashes and ensure connectivity were imposed using REFMAC [84]. Molecular representations were generated with Chimera [85]

7.10 *C. elegans* techniques

7.10.1 *C. elegans* strains and mantainment

Worms were growth at 20°C on NGM agar plates seeded with the *Escherichia coli* strain OP50, a genetic modified bacteria not to overgrowth, under standard laboratory conditions. Cleaning worms protocols before performing IF experiments and freezing conditions of worm strains were performed following standard protocols listed below.

The wild-type *C. elegans* was variety Bristol, strain N2.

The *eps-8(by160)* strain was previously isolated and characterized in our laboratory [50, 51]. The DLG-*1::RFP* strain was kindly provided by Martha Soto (Rutgers University).

eps-8(by 160) strains carrying different arrays in DLG-1 ::RFP trensgene-expressing strain were obtained by crossing.

NGM agar plates for growing cultures

3 gr NaCl, 2.5 gr Bacto-peptone and 17 gr Bacto-agar were dissolved in 800ml dH_20. The solution was adjusted to a 1L volume and sterilized by autoclaving. After sterilization 1 ml of cholesterol (5mg\ml in EtOH), 1 ml $CaCl_2$, 1 ml 1M $MgSO_4$ and 25 ml 1M KH_2PO_4 pH6 were added. Each plate was seeded with an overnight colture of *E.coli* OP50. The plates were put at 37°C overnight and then stored at 4°C.

7.10.2 Cleaning worm cultures

Two alternative procedures were followed.

Bleaching protocol:

Plates with many gravid adults and eggs were usually selected for this procedure. Plates were washed with dH_2O and the worm suspension was transferred to a 15 ml falcon tube. Worms were centrifuged at 1500 rpm for 1 min at room temperature. The worm pellet was then resuspended into 2.5 ml of dH_2O. An equal volume of 2X bleaching solution was added and the worm suspension was shacked for 5 min (or until no more worms were visible).

The volume was brought to 15 ml with dH_2O and the mixture was centrifuged at 1500 rpm for 1 min at room temperature. The worm pellet was washed twice with dH_2O.

Finally the supernatant was discarded and the pellet was resuspended in 50-100 μl of dH_2O. The egg suspension was plated onto NGM plates seeded with OP50.

If the bleaching procedure was done in order to obtain a synchronous worm population, the egg suspension was left overnight at room temperature to allow hatching. The L1 perfectly synchronized were then plated onto NGM plates seeded with OP50.

2X Bleaching solution

250 ml dH_2O

1 ml of Alkaline Hypochlorite

1.25 ml 2 N NaOH

Sucrose protocol:

Worms were washed off from plates with dH_2O and placed in a 50 ml falcon tube. The worm suspension was putted on ice for 10 min and then centrifuged at 1700 rpm for 2 min at 4°C. The cold worm pellet was moved to 15 ml of cold 70% sucrose and a cold 35% sucrose was added very carefully in order to let it stratify onto the 70% phase.

The mixture was then centrifuged for 2 min at 1700 rpm at 4°C. After centrifugation, bacteria, debris and dead worms were recovered on the bottom, while cleaned worms formed a ring between the 35% and the 70% sucrose solutions. Cleaned worms were taken from the ring and washed extensively with dH_2O in order to eliminate the residual sucrose.

7.10.3 Freezing worms

It is important to enrich the worm population in L1 and L2 larvae, which better survive to the freezing procedure. Worms were washed off from 1 large plate or 3 medium plates with dH_2O and then centrifuged for 1 min at 1500 rpm at room temperature. The worm pellet was resuspended in 2 ml of dH_2O. An equal volume of 2X freezing solution was added and the suspension was mixed up well. One ml of the worm mixture was distributed in each cryogenic vial (from Nalgene). The freezing vials were moved to styrofoam boxes at –80°C, in order to cool worms very slowly. After one week one vial was thawed (just by warming the vial between hands) and the surviving rate was verified. If successful, the remaining three vials were moved to liquid nitrogen.

2X Freezing solution:

100 mM NaCl

50 mM KH_2PO_4

30 % glycerol

The solution was prepared in a final volume of 2 L in dH_2O and sterilized by autoclaving. 300μM $MgSO_4$ was then freshly added.

7.10.4 Crossing

Crosses were carried out by placing few young adult virgin hermaphrodites together with an excess of young adult males (3:7 ratio). Small NGM agar plates were used in these experiments. Hermaphrodites and males were moved to a new fresh plate every 12 hours, at least three times. In the case of successful mating, males will represent half of the progeny on the small plate.

Source of males for crossings. Males are rarely found in a population of self-fertilizing hermaphrodites, thus it is necessary to have a source of males when crossing are planned. Method 1: crossings between hermaphrodites and the rare males found in the plates were performed. The worm population with a high number of males was kept in culture by picking few hermaphrodites and a large number of males. Method 2: the spontaneous male frequency was increased by heat shock treatment. From 10 to 20 hermaphrodites at mid L4 stage were incubated for 6 hours at 30°C, then animals were kept at the usual temperature of growth. In the progeny of the heat shocked hermaphrodites the percentage of males should be between 2% and 5%.

7.10.5 *C. elegans* injection

cDNAs of the wild-type (WT) EPS-8A or mutants were cloned under the intestinal *opt-2* promoter into the pPD95.75 vector that provides a C-terminal GFP tag (kindly provided by A. Fire, Stanford University, USA) and sequence verified.

Mutants were EPS-8A Δcap = L784E, V788E; EPS-8A Δbund = L849A, K851A; EPS-8A ΔcapΔbund = L784E, V788E, L849A, K851A.

EPS-8 constructs were injected into *eps-8(by160)* heterozygous animals at a concentration of 5-20 ng ml^{-1}.

In details, DNA, coming from a maxi preparation, was centrifuged for 30 min at 4°C to pellet down debris and small particles that could clog the needle.

DNA was injected into the cytoplasm of the syncytial mitotically active gonads, together with the *ttx-3p::RFP* selection marker expressed in the AIY neuron, in order to facilitate the identification of the transformants in the progeny.

Injected animals were single out on different small plates and the F1 generation was analyzed for the presence of transformants. After two generations, the injected DNA is stably inherited to the progeny through the germline and maintained as an extrachromosomal array.

7.10.6 Rescue experiments and phenotypical analysis

Rescue of lethality was tested in two different transgenic lines for each construct. At least 100 GFP positive L1 larvae (F1), from heterozygous *eps-8* animals (F0), were individually plated and allowed to grow and self-fertilize. Rescued homozygous *eps-8* mutants were recognized by loss of the genetic balancing markers (*unc-26, dpy-4*) and positivity for GFP expression. Confirmation for homozygosity for the mutated *eps-8* allele was obtained by PCR. Alternatively, the entire progeny (ranging from 30 to 120 F1 animals) of at least three heterozygous adults was individually plated and allowed to grow and self-fertilize. Rescue of lethality analysis was performed as described above.

Homozygous *eps-8(by160)* mutant worms are characterized by intestinal alterations, namely paleness, gut constipation, presence of clumped and more refractile gut granules. Rescue of this phenotype was scored in live L1/L2 larvae (at least 100) under a Zeiss Axioplan 2 plus microscope with Nomarski optics and epifluorescence. For the analysis of the gut phenotype in *eps-8(by160)*;[opt-2:EPS-8AΔbund] and *eps-8(by160);*[opt-2:EPS-

8A-ΔbundΔcap], homozygous larvae were identified by growth retardation respective to siblings in a synchronous F1 progeny from heterozygous worms.

7.10.7 Single worm PCR

A single worm was transferred into 10 μl of lysis buffer, in a cap of a 0.2 ml tube. After spinning it down for few seconds at maximum speed, the animal was incubated at 65°C 1 hour, then at 95°C 5 min to inactivate the Proteinase K.

The reaction was cooled to 4°C. The DNA worm preparation was either immediately used for a PCR reaction or stored for one night at 4°C.

For the *eps-8(by160*) allele, primers used are:

Forward: 5'-CGCCACTGTCGCAAATTCAAATTAC-3'

Reverse: 5'-GGATTACATTGTGTTGGGAGC-3'

The wt band is 2229 bp, while the deleted one is 730 bp

Lysis buffer

50 mM KCl

10 mM TrisHCl pH 8.3

2.5 mM MgCl2

0.45% NP40

0.45% Tween 20

0.45% Gelatin

Before use, Proteinase K was added at a final concentration of 200 μg/ml

7.10.8 *C. elegans* imaging

Living animals, anesthetized into 2% of sodium azide, were transferred to a 2% agarose pad mounted on a slide, coverslip was then applied.

Nomarski and epifluorescence images were acquired on a Leica TCS SP2 AOBS confocal microscope. A 633/1.4 NA oil-immersion objective (HCX PL APO 63X Lbd Bl, Leica Microsystems) was employed for analysis. Image acquisition conditions were set to remove channel crosstalk, optimizing spectral detection bands and scanning modalities. Leica Confocal Software and ImageJ were used for data analysis.

8. RESULTS

8.1 Eps8 C-terminal region (aa 648-821) binds monomeric ATP and ADP actin

Eps8 is a modular protein with a C-terminal domain (aa 648-821) that mediates the interaction with actin filaments and that is responsible for its biochemical activities: capping and bundling [50, 73]. This region displays no similarity with other known capping proteins or actin binding motifs and its mode of interaction with actin remains thus elusive. We investigated whether this region is also able to bind monomeric actin, a property that is displayed by several other capping and bundling proteins, such as Gelsolin, Twinfilin, and CP [45, 49]. Studying this interaction may provide novel insights into the mode of Eps8 association with actin contributing to elucidate Eps8 functions. We tested the possibility of an Eps8:monomeric actin interaction by monitoring the ability of the Eps8 C-terminal region to bind to fluorescent labelled, monomeric NBD-(7-chloro-4-nitrobenzofurazan)-actin. In this fluorimetric *in vitro* assay the binding of a protein to the actin monomer can be monitored following the changes in the fluorescence intensity of the emission spectrum of the NBD fluorophore that is conjugated with actin. We, thus, measured the emission spectra of NBD-actin alone or in the presence of Eps8 (648-821). The addition of Eps8 C-terminal region significantly increased (by as much as 20%) the NBD-actin fluorescence, in low ionic strength condition (G-buffer), thus indicating its ability to bind monomeric actin (Figure 21A). Dose dependence analysis of the binding curves indicated a saturation binding mode, consistent with the formation of a 1:1 complex between monomeric actin and Eps8 C-terminal region and an equilibrium dissociation constant Kd of 50 nM in low ionic strength conditions (G-buffer) and 1.7 μM, when physiological salt conditions (F-buffer) were used (Figure 21B and C respectively).

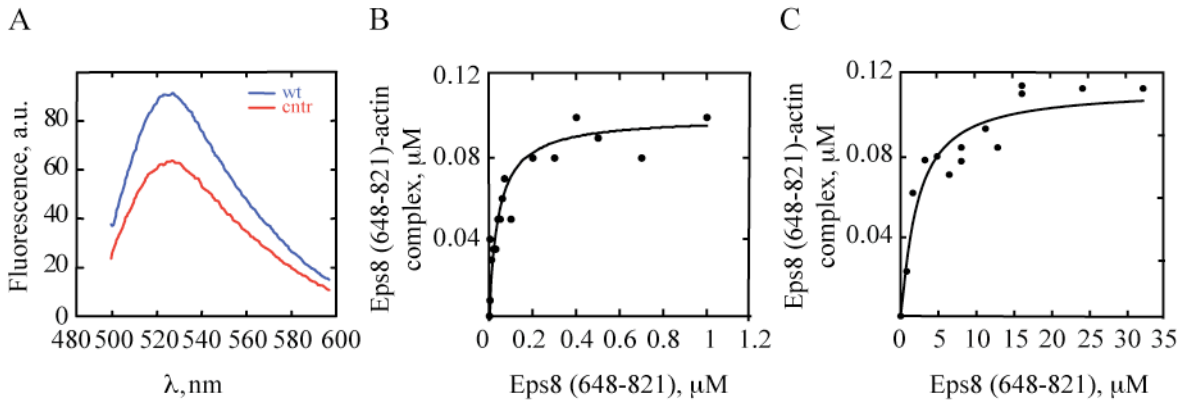

Figure 21: Eps8 C-terminal region (648-821) binds monomeric actin

A. Fluorescent spectra of NBD-actin in the presence or absence of Eps8 (648-821).

NBD-labelled actin (1.5μM) was incubated in the absence (red line) or in the presence (blue line) of 200nM Eps8 (648-821) for 60 minutes, before recording fluorescent spectra between 480nm and 600nm of wavelength.

B-C. Binding affinity of Eps8 (648-821) for monomeric actin.

(B) The change in fluorescence of 0.1μM NBD-Actin-actin was measured at different concentrations of Eps8 (648-821) in low salt (G-buffer).

(C) The change in fluorescence of 0.1μM NBD-Actin-actin was measured at different concentrations of Eps8 (648-821) in high salt (F buffer) containing 0.1 M KCl and 1 mM MgCl2.

Symbols indicate data; solid line indicates fitted binding curve for a complex with a 1:1 stoichiometry. The curve is calculated using the equation 1 in the "Experimental Procedure".

Monomeric actin can be present in the cell in an ATP or ADP bound state. Several monomeric actin binding proteins show a preferential interaction with either ATP or ADP actin, that often correlates with their cellular role [86]. We thus tested whether also the Eps8 C-terminal region could bind preferentially one of the two nucleotide bound forms of actin, monitoring the binding capacity of the C-terminal region of Eps8 to either ATP or ADP bound NBD-labelled actin. We score similar Kds values for both ADP and ATP actin (Kd = 120 nM and Kd = 75 nM respectively), indicating a similar affinity of Eps8 for both nucleotide-bound forms of actin (Figure 22A).

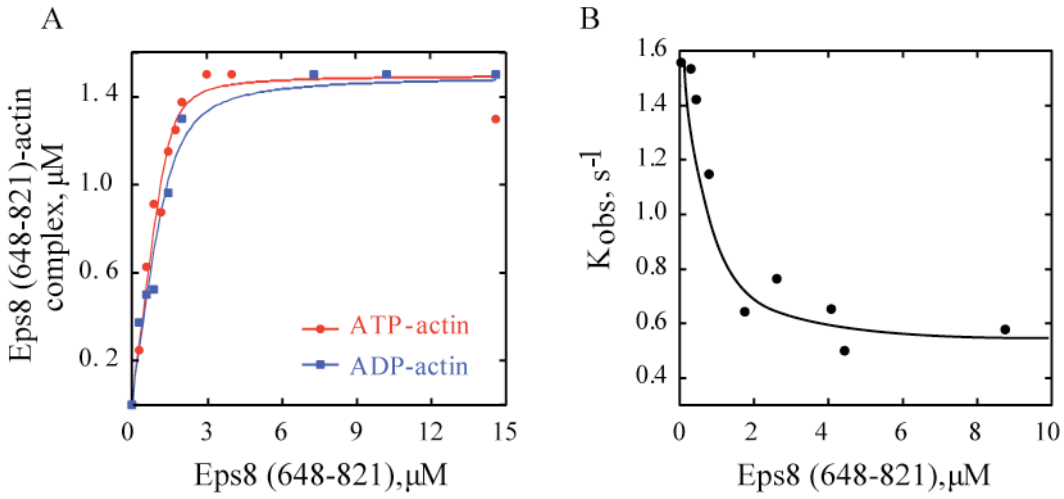

Figure 22: Eps8 (648-821) binding to ADP\ATP actin

A. Eps8 (648-821) binds ATP or ADP monomeric actin with the same affinity.

The change in fluorescence of 1.5 µM NBD-ADP-G-actin (blue line, closed squares) or NBD-ATP-G-actin (red line, closed circles) was measured at different concentrations of Eps8 (648-821), in G-buffer. ATP to ADP exchange was performed using Hexokinase in the presence of 10 mM $MgCl_2$ and 1 mM glucose. Symbols indicate data; solid lines indicate fitted binding curves for a complex with 1:1 stoichiometry. The affinity constants calculated from these plots using the equation described in "Experimental Procedures" were Kd(ATP-Ca-G-Actin) = 75 nM, Kd(ADP-Ca-G-Actin) = 120 nM.

B. Eps8 (648-821) inhibits the dissociation of ATP from ATP-G-Actin.

ATP-G-actin (2 µM, in G-buffer containing 20 µM of $CaCl_2$) was supplemented with the indicated concentrations of Eps8 (648-821). The dissociation of bound ATP was monitored by adding 5 µM of εATP at time 0 and recording the subsequent increase of fluorescence of εATP. The pseudo-first order exchange rate constant is plotted versus the total concentration of Eps8 (648-821).

Different G-actin binding domains are also able to modify the nucleotide dissociation rate from G-actin. WH2 or ADF homology domains, for instance, decrease the nucleotide dissociation rate from G-actin, while others, like profilin, enhance it. Among capping proteins, Twinfilin inhibits the nucleotide exchange from ADP-G-actin [87], whereas Gelsolin blocks nucleotide exchange from ATP-G-actin [88]. The presence of this effect on nucleotide dissociation rate upon binding could give thus also an indirect indication on the kind of structural interaction of a protein with the actin monomer. We tested the effect of Eps8 (648-821) on nucleotide exchange by monitoring the association of a fluorescent ξ-ATP analogue to ATP-G-actin. Eps8 (648-821) significantly diminished the nucleotide

exchange rate on G-actin by 5-fold (Figure 22B), similarly to what has been reported for the WH2 containing protein Ciboulot [89]. These results suggest that the Eps8 (648-821):G-actin complex shares biochemical and, likely, structural features with G-actin in complex with either WH2 domains, S1-gelsolin, or Twinfilin.

8.2 Eps8 C-terminal region (aa 648-821) and monomeric actin form a 1:1 complex

We decided to further investigate the stochiometry of the Eps8 (648-821)-actin complex in other to confirm the 1:1 ratio that the fluorimetric experiments indicated.

We used two independent techniques: a chemical cross-linking analysis and size-exclusion chromatography.

In the first approach, we crosslinked either Eps8 (648-821) or actin alone, or the two proteins together, for different time points. At the end of the reaction we could detect a single band, only when both proteins were incubated together. This single covalently cross-linked protein had a size of ~ 60 KD, equivalent to the sum of the molecular weights of Eps8 (648-821) and monomeric actin (Figure 23) and was thus a further indication of a 1:1 ratio of the complex.

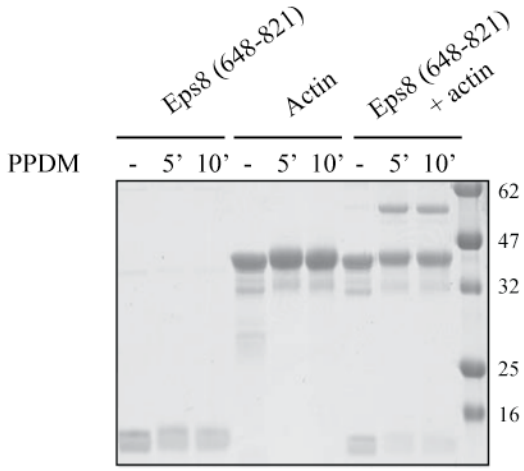

Figure 23: Eps8 (648-821) forms a 1:1 complex with monomeric actin

Chemical crosslinking between Eps8 (648-821) and monomeric actin.

10 μM Eps8 (648-821) and actin, either alone or in combination, were incubated for various lengths of time in the absence or in the presence of PPDM, separated by SDS-PAGE and detected by Comassie blue staining. Lines 1,2,3: 10μM of Eps8 (648-821) incubated in the absence (Lane 1) or in the presence of the crosslinker for 5 min (Lane 2) or 15 min (Lane 3); Lanes 4,5,6: 10μM of actin incubated in the absence (Lane 4) or in the presence of the crosslinker for 5 min (Lane 5) or 15 min (Lane 6); Lanes 7,8,9: 10μM of Eps8 (648-821) and actin incubated in the absence (Lane 7) or in the presence of the crosslinker for 5 min (Lane 8) or 15 min (Lane 9).

We then used a gel filtration analysis in order to investigate the elution profile of the two proteins, either alone or in combination. When we run Eps8 (648-821) or G-actin alone, the two proteins eluted in distinct fractions, according to their respective molecular weight. Conversely, when mixed in a 1:1 molar ratio, they co-fractionated, forming a stochiometric complex. Addition of two fold molar excess of Eps8 (648-821) saturated the amounts of G-actin and the excess of the former eluted with the expected retention volume (Figure 24). Collectively, all these experiments demonstrate the formation of a complex between actin and Eps8 C-terminal region with a 1:1 stochiometry.

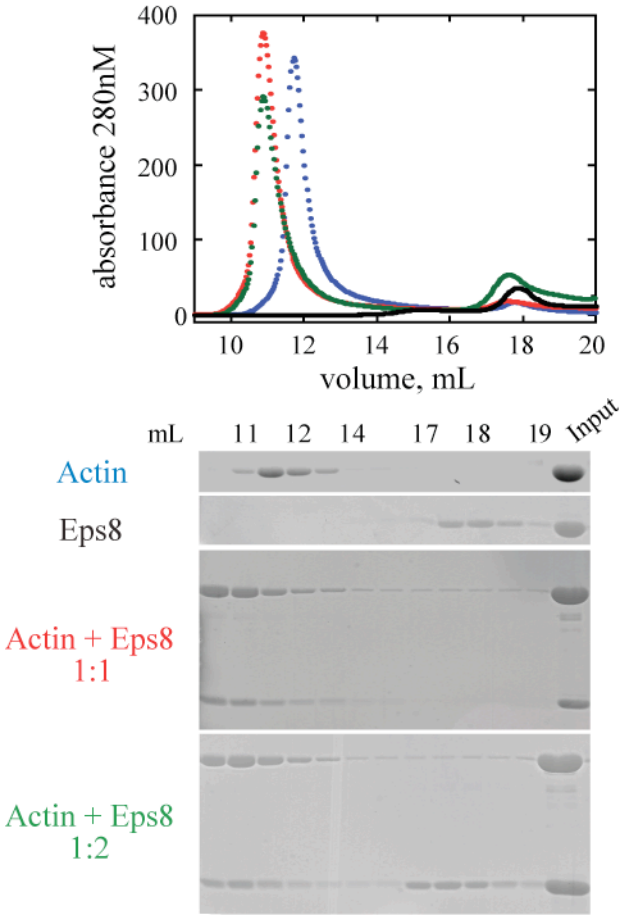

Figure 24: Eps8 (648-821) and actin form a 1:1 complex in gel filtration

Eps8 C-terminal domain and actin co-elute in gel filtration forming a 1:1 complex.

Size exclusion chromatography experiment on a Superdex 200 10/30 column in G buffer (2mM TRIS pH 7.8, 0.2mM ATP, 1mM DTT, 0.1mM $CaCl_2$). Purified Actin and Eps8 (648-821) were analyzed by gel filtration either alone (blue and black line, respectively) or after pre-incubation on ice for 1h in a 1:1 or 1:2 molar ratio (red and green line respectively). In each case, 30µL fractions were collected and analyzed by Comassie staining on 10% SDS-PAGE gel that is shown beneath the elution profile.

8.3 Eps8 C-terminal region sequesters monomeric actin

The formation of an Eps8 (648-821):G-actin complex prompted us to revisit the effect of Eps8 (648-821) on actin assembly. Actin filaments expose ATP-actin monomers at the plus end, while at the minus ends monomers are in an ADP bound state. Due to the capability of Eps8 to bind both ATP and ADP actin, Eps8 could in principle affect filaments assembly at both ends of the filament. We thus measured Eps8 (648-821) activity on both extremities. At the plus end Eps8 is known to act as a capping protein [50].

We used spectrin actin seeds, purified actin oligomers with blocked pointed, but free barbed ends, to follow its capping activity. As previously reported, Eps8 (648-821) capped the plus ends of actin filaments with nM affinity (Kcap = 15nM) (Figure 25).

To monitor Eps8 effect at the other side of the filament, we used instead gelsolin actin seeds, which have blocked barbed but free pointed ends. Eps8 (648-821) also inhibited, in a concentration-dependent fashion, actin polymerization from pointed ends. In this latter case, however, stoichiometric concentrations of Eps8 (648-821) with respect to G-actin were required, with an apparent K_i (Constant of inhibition) of Eps8 (648-821) for pointed end filament growth of around 2.5 μM (Figure 25). Under these conditions, an Eps8 (648-821):G-actin complex is formed that cannot be incorporated into a nascent filament; the complex, thus, fails to support pointed end growth, and this is reflected in the sequestration of monomeric actin.

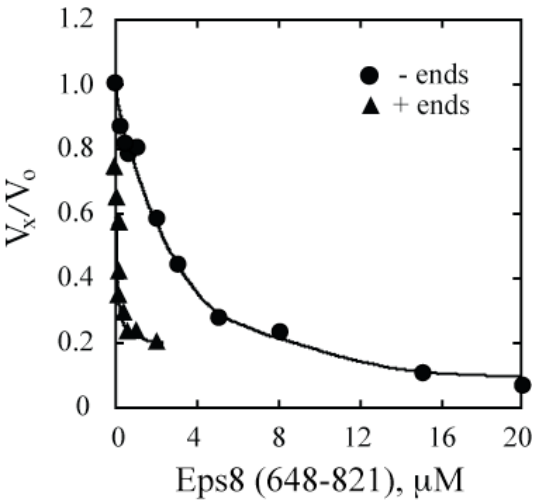

Figure 25: Eps8 (648-821) affects actin growth both at the plus and at the minus end

Barbed and pointed end elongation rate of actin in the presence of Eps8 (648-821).

The rate of elongation was measured from pointed ends (circles), using gelsolin-actin seeds (5nM) and 2 μM of G-actin (10% pyrenyl-labeled), or from barbed ends (triangles) using spectrin-actin seeds, in the presence of increasing concentrations of Eps8 (648-821), as indicated. Rates are normalized taking as 100 % the rate of elongation from either pointed or barbed ends measured in the absence of Eps8 (648-821).

We thus showed that the C-terminal region of Eps8 (648-821) is able to bind monomeric actin and shares some properties of the WH2 actin binding domains. The formation of an Eps8:G-actin complex leads to the sequestering of the actin monomer that can not be incorporated in the filament any more.

8.4 The minimal actin binding region of Eps8 C-terminal domain encompasses its amphiphatic H1 helix

The C-terminal region of Eps8, that has no homology with any other actin binding domain, is very conserved among Eps8 homologues and hortologues (Figure 26).

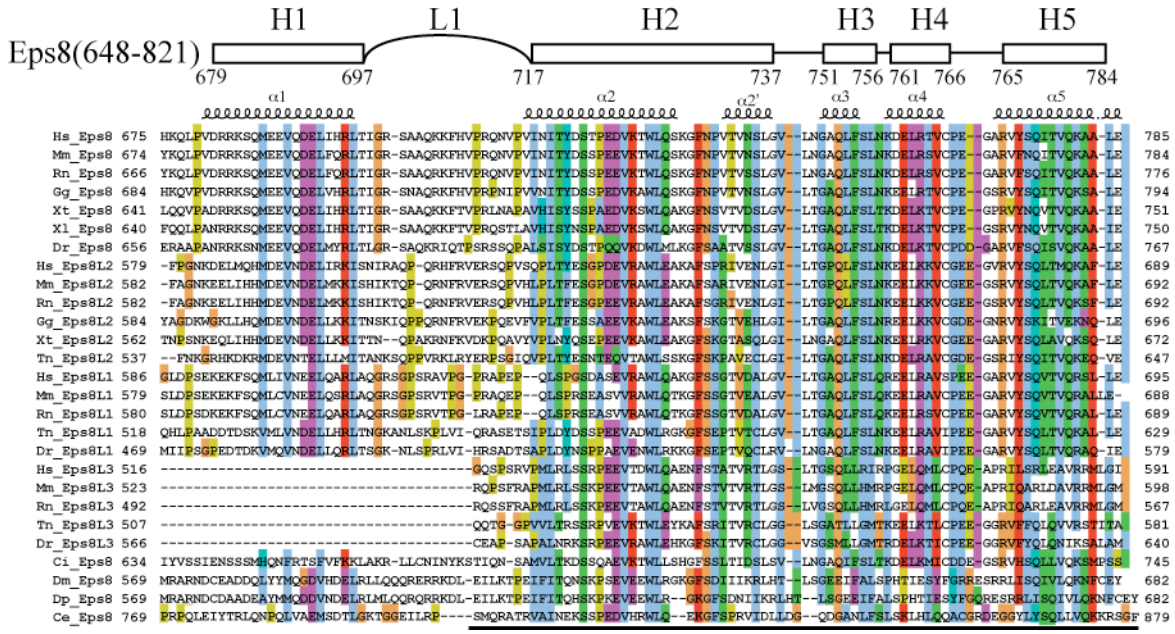

Figure 26: Eps8 C-terminal region (648-821) is highly conserved

Sequence comparison and secondary structure predicted organization of the Eps8 actin binding domain. Multiple sequence alignment of a collection of the C-terminal regions of Eps8 and its homologues. Protein sequences were aligned using the ClustalW program. Manual adjustments were introduced on the basis of secondary structure information, and the picture was produced using Jalview. Secondary structure prediction was made by using the prediction server SAM-T99. On top, a schematic organization into the predicted helices of the C-terminal actin binding domain of Eps8 is shown. Numbers indicate murine aa.

Due to this sequence similarity the secondary structure prediction is the same for the different Eps8 homologues. The domain is predicted to be organized in five α-helices, with a long linker connecting the first helix (H1) to the second one. An exception is represented by Eps8L3 proteins, which have a shorter domain lacking the first H1 helix and part of the linker region. Consistently, this member of the family is devoid of actin capping activity [50]. In order to investigate the minimal regions of the domain implicated in the binding to monomeric actin we created different fragments encompassing the different helices, alone or in combination, and we tested them for their ability to bind monomeric actin using NBD-labelled actin as a probe (Figure 27A). We discovered that the fragments encompassing the first two helices of the domain, H1-H2 (residues 674-737), and the last helix of the domain, H5 (residues 765-788), are the minimal fragments capable of increasing NBD-actin fluorescence by 17% and 12% respectively (Figure 27B). Next, we performed a dose response experiment using different concentrations of the two proteins in order to determine the affinity of these fragments for monomeric actin. The H1-H2 fragment displays a high affinity for monomeric actin (Kd = 50nM), similar to the affinity of the whole C-terminal region (Figure 27C). The H5 helix displayed instead a lower affinity (Kd =3μM) (Figure 27D). Due to the formation of a 1:1 complex between actin and Eps8 (648-821), and to the similar affinity of the H1-H2 fragment and the whole C-terminal domain for G-actin, we concluded that the H1-H2 region represents the major surface of interaction between Eps8 and the actin monomer, and that the interaction that we see with the H5 could probably be hidden in the context of the whole C-terminal domain.

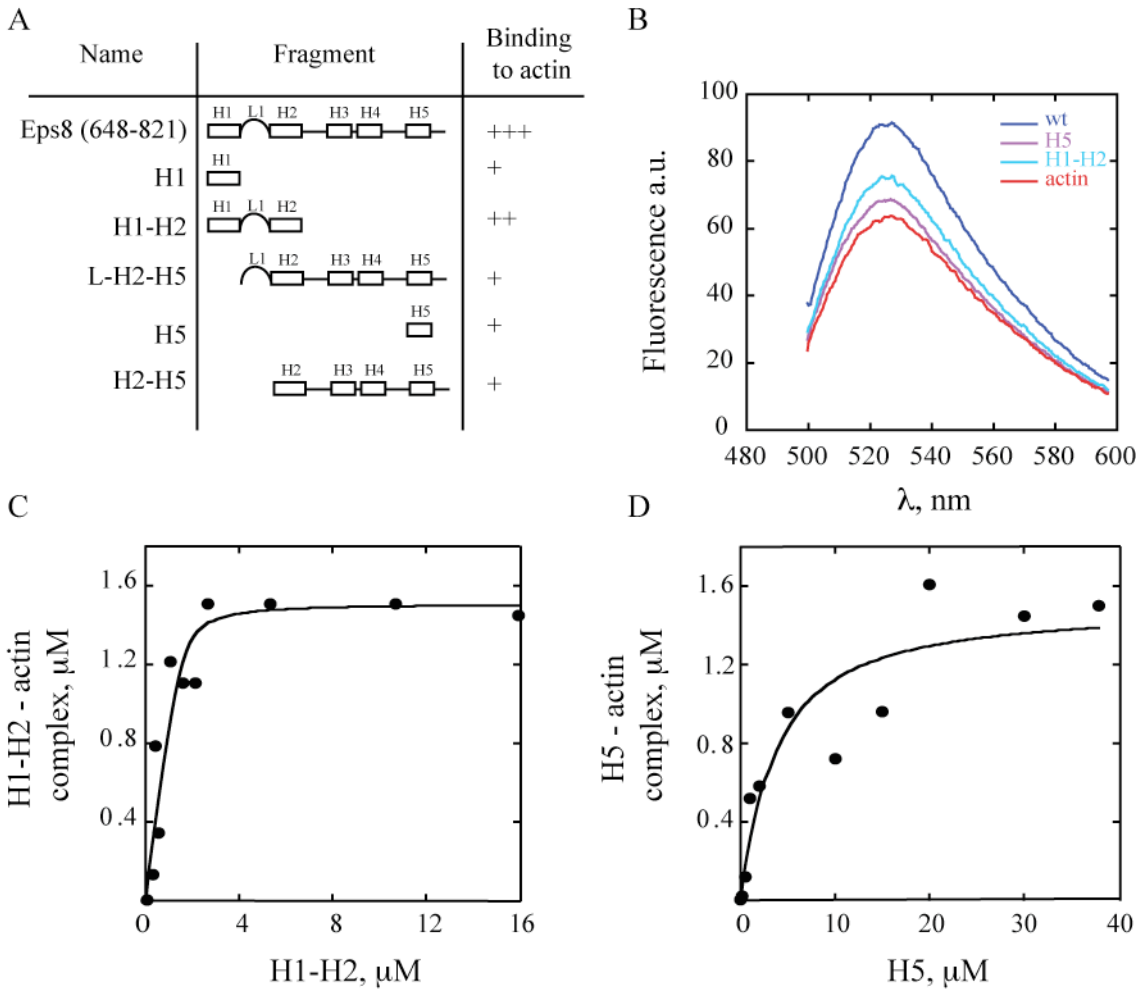

Figure 27: Eps8 (648-821) possess two monomeric actin binding surfaces: H1-H2 and H5

Summary of the binding ability of various helices of Eps8 (648-821) to G-Actin.

A. The change in fluorescence of 1.5 μM NBD-Actin-actin was measured in the presence of the indicated Eps8 fragments in G-buffer. A change in fluorescence caused by the formation of the complex between actin and Eps8 fragments of at least 10% with respect to actin alone was scored as positive (+).

B. Fluorescent spectra of NBD-actin in the presence or absence of either H1-H2, or H5 or Eps8 (648-821). Monomeric NBD-labelled actin was incubated in the absence (red line) or the presence of 20 μM of Eps8 (648-821) (blue line), or H1-H2 (light blue line) or H5 (violet line) for 60 min, before recording fluorescent spectra between the indicated wavelengths.

C, D. HI-H2 and H5 bind G-actin in a concentration-dependent manner.

The change in fluorescence of 1.5 μM NBD-Actin-actin was measured at different concentrations of either H1-H2 (C) or H5 (D), in low salt (G buffer). Symbols indicate data; solid lines indicate fitted binding curves for a complex with 1:1 stochiometry.

To further characterize both fragments we decided to investigate their biochemical activities towards the two ends of the actin filament.

The H1-H2 fragment was able to inhibit actin polymerization at both ends of the filament. At the plus end substochiometric amount of H1-H2 were able to completely block actin polymerization, with a calculated Kcap of 200nM (Figure 28A). This result indicates that H1-H2 is still able to cap in a significant way actin filaments, even if the lower activity with respect to the wt protein suggests that other structural determinants are likely involved in the capping of the filaments. Sequestration of ATP-G-actin by H1-H2, instead, completely accounted for the concentration dependent inhibition of pointed ends growth, in a stochiometric range of concentrations with respect to G-actin, with a Kseq of 2.5μM, identical to that calculated for the Eps8 (648-821) (Figure 28A).

H5 was also able to inhibit actin filaments growth at the 2 ends of the filament. In this case, however, the thermodynamic parameters of inhibition were in the micromolar range ($Kseq_{pointed}$ = 32μM; $Kcap_{barbed}$ = 40μM) indicating that supra-stochiometric amounts of H5 were required to block filament end growth, consistent with low sequestering activity (Figure 28B).

To provide additional evidence that low affinity binding to filaments did not accounted for the observed inhibition, we performed barbed end polymerization assays at two different actin concentrations. Higher concentrations of H5 were required to inhibit polymerization when the concentration of G-actin was increased from 2 to 4 μM, accounting for the shift toward the right of the curves (Figure 28C). This result demonstrated that the inhibition by H5 is solely dependent on its ability to sequester monomeric actin and is not due to low affinity binding to filament ends.

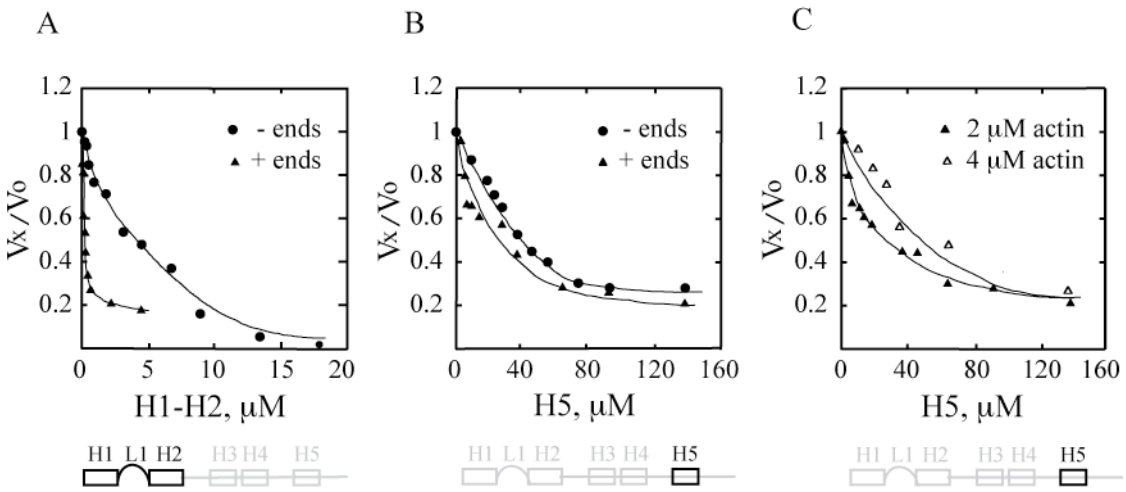

Figure 28: H1-H2 and H5 influence the actin filaments elongation rate with different thermodynamic constants

A, B. H1-H2 and H5 inhibit barbed and pointed end elongation rates with different thermodynamic constants. The rate of elongation was measured from pointed ends (circles), using gelsolin-actin seeds (5nM) and 2 μM of G-actin (10 % pyrenyl-labeled), or from barbed ends (triangles), using spectrin-actin seeds (2nM), in the presence of increasing concentrations of H1-H2 (A) or H5 (B), as indicated. Rates are normalized taking as 100 % the rate of elongation measured in the absence H1-H2 or H5. Kd_s are reported in the text.

C. H5 sequesters G-actin, but does not cap filaments ends.

The rate of elongation from barbed ends was measured using actin seeds and 2 μM (closed triangles) or 4 μM (opened triangles) of G-actin (10 % pyrenyl-labeled) in the presence of increasing concentrations of H5. A shift toward the left of the rate of elongation by H5 as the concentration of G-actin used increased indicates that stoichiometric concentrations of H5 with respect to actin are required for the inhibition.

Collectively, these data indicate that Eps8 C-terminal region binds monomeric actin mainly through a surface that encompasses the two first helices of the domain, H1-H2. This region retains also a significant capping activity and is thus probably binding actin monomers in a region that is exposed at the plus end thus blocking the further addition of actin subunits in the filament. The H5 shows instead a low binding to the actin monomer, is not able to cap actin filaments and retains only a low sequestering activity. This helix is thus likely to represent a secondary site of binding in the context of the full-length protein, contributing in Eps8 stabilization at the plus end of the filament.

8.5 The Amphiphatic H1 helix of Eps8 contacts the hydrophobic pocket between subdomain 1 and 3 of the actin monomer

Our results indicated that the main surface of interaction between Eps8 C-terminal region and the actin monomer is represented by the H1-H2 fragment. Remarkably, sequence analysis of the single helices encompassing this minimal active fragment of Eps8, revealed that H1 helix possess all the feature of a WH2-like domain. WH2 domains consist of an α-helix, with a few exposed hydrophobic side chains [82]. Similar features are shared by H1 helix, which forms a short amphiphatic helix thus representing a WH2-like motif (Figure 29).

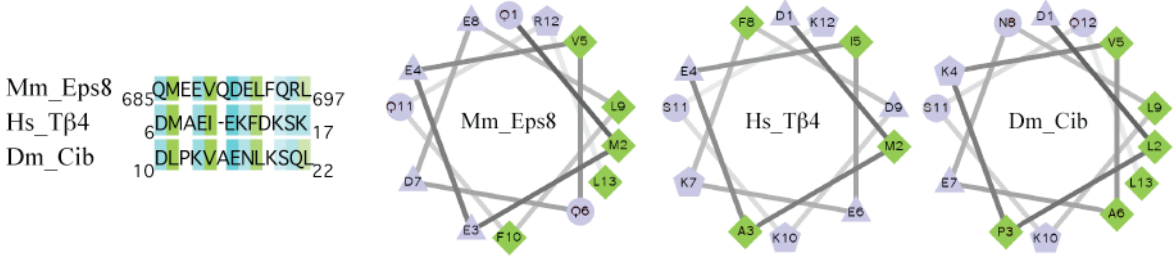

Figure 29: Helical wheel analysis of the predicted helix H1 of Eps8

Eps8 H1 helix is predicted to be amphipathic.

Left: alignment of mouse Eps8 H1 helix with the WH2 domains of either human Thymosin β-4 and Drosophila Ciboulot.

Right: helical wheel analysis of the amphipathic helices of mEps8, hThymosin β-4 and DCiboulot. The helix is projected along its axis going into the page. The hydrophilic residues are presented as circles, hydrophobic residues as diamonds, potentially negatively charged as triangles, and potentially positively charged as pentagons. Hydrophobicity is colour coded as well: hydrophobic residues are green, hydrophilic residues are coded blue with the potentially charged residues in light blue.

WH2 domains usually contact actin on a hydrophobic cleft present between subdomain 1 and 3 of the actin monomer. This cleft is exposed at the plus end of the filament being a key point of interaction between monomers within the filament.

The binding to this cleft can, thus, provide a way to cap filament ends preventing the addition of new actin monomers.

We thus investigated whether Eps8 binds to this cleft similarly to other WH2 domain containing proteins. To this end, we performed competition assays using NBD-labelled actin and saturating amounts of proteins that are known to bind the hydrophobic actin cleft, such as Ciboulot and Tymosin β–4 (which binds through a WH2 domain) or ADF/Cofilin [82, 90]. NBD-G-actin saturated with either Thymosin β-4 or Ciboulot displayed levels of fluorescence higher than NBD-G-actin in complex with Eps8 (648-821). The addition of increasing concentrations of Eps8 (648-821) to either Thymosin β-4:NBD-G-actin or Ciboulot:NBD-G-actin led to a decrease in fluorescence to levels consistent with the displacement of these proteins from actin and the concomitant formation of a Eps8(648-821):actin complex (Figure 30A,B). Similarly, Eps8 (648-821) competed with ADF/cofilin for binding to ADP-G-actin. Binding of ADF/cofilin did not significantly affect the fluorescence of NBD-ADP-actin, but caused a large increase in the apparent Kd for binding of Eps8 (648-821) (Kd Eps8 648-821 = 50nM and Kd = 5μM in the absence and in the presence of Cofilin respectively) (Figure 30C). Thus, Eps8 (648-821) competes with Thymosin β-4, Ciboulot and ADF/cofilin for binding to monomeric actin, suggesting that the three proteins share the same interaction surfaces. We performed similar assays utilizing Ciboulot and either the isolated H1-H2 or H5. Only H1-H2, but not H5, displaced Ciboulot from actin (Figure 30D,E).

These results suggest that the two Eps8 fragments, H1-H2 and H5, bind actin on two different surfaces, and that the H1-H2 region contacts the hydrophobic cleft on the actin monomer similarly to a WH2 domain. To further validate a bivalent mode of interaction of Eps8, we performed a competition experiment between the two isolated Eps8 fragments and actin. H1-H2 bound NBD-G-actin with identical affinity in the absence or presence of H5, at low ionic strength (Figure 30F) in keeping with the notion that the two regions bind to different actin surfaces. Notably, the increases in fluorescence of NBD-actin due to the

binding of H5 and of H1-H2 are additive, consistent with simultaneous binding of the two fragments.

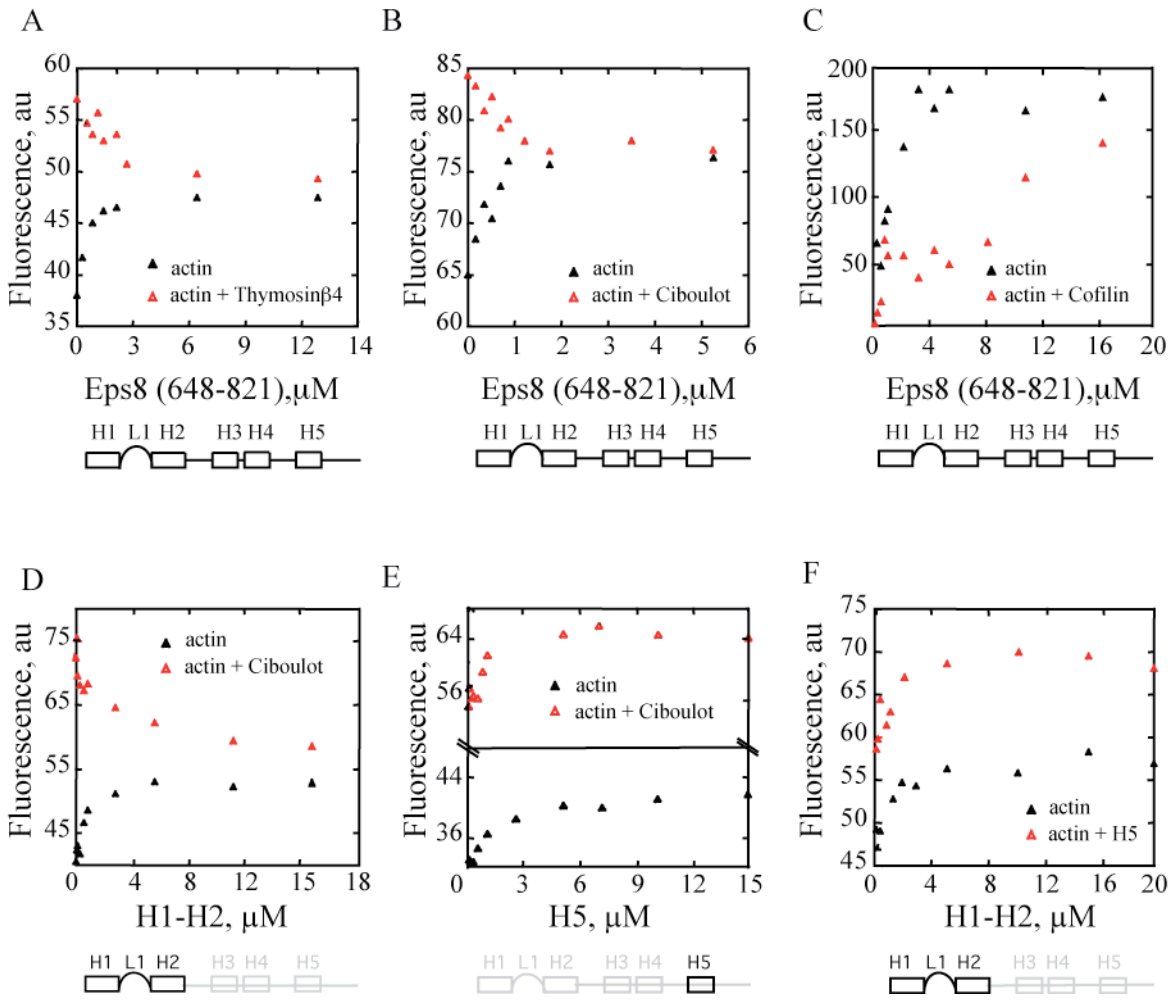

Figure 30: Eps8 (648-821), Thymosin β4, Ciboulot and ADF/Cofilin share common binding surfaces on actin

A-C. Eps8 (648-821) competes with Thymosin β-4, Ciboulot and ADF/Cofilin for binding to monomeric actin.

The change in fluorescence of 1.5 μM NBD-Actin-actin was measured in the presence of the indicated, increasing concentrations of Eps8 (648-821) and/or saturating amounts (25 μM) of either Thymosin β-4 (A), Ciboulot (B), or ADF/Cofilin (C) in low salt buffer (G-buffer). In the case of ADF/Cofilin (C), NBD-ADP-actin was used.

D, E. H1-H2, but not H5 competes with Ciboulot for actin binding.

The change in fluorescence of 1.5 μM NBD-Actin-actin was measured in the presence of the indicated, increasing concentrations of Eps8 H1-H2 (D) or H5 (E) helices alone or together with saturating amounts (25 μM) of Ciboulot, in low salt buffer (G-buffer).

F. H5 and H1-H2 do not compete for binding to monomeric actin.

Change in fluorescence of NBD-Actin-actin in the presence of increasing concentrations of Eps8 helices (H1-H2) alone or together with saturating amounts (25 μM) of Eps8 (H5) in low salt buffer (G-buffer).

We validated our findings by using also another type of labelled actin, 5-(2((acetyl)amino)ethyl)amino-naphthalene-1-sulfonate (AEDANS)-Actin-G-actin, in an high salt buffer, which reassemble the physiological situation. Under these conditions we could confirm the competition between Thymosin β-4 and either Eps8 (648-821) or H1-H2 (Figure 31A,B). In high salt however the interaction between actin and H5 was very weak and could not reliably be monitored. Thus, we were unable to perform competition assays using this Eps8 fragment.

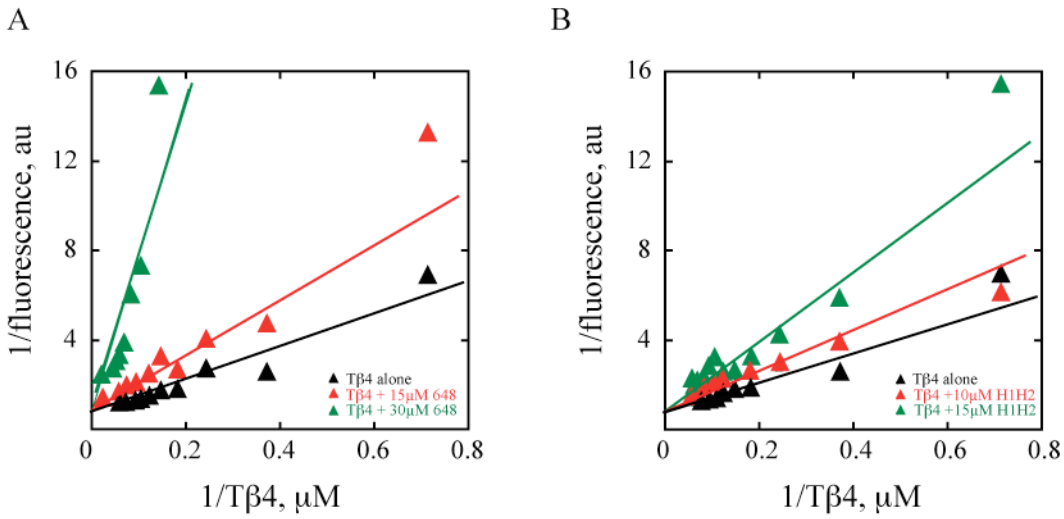

Figure 31: Competition experiments between Eps8 and Thymosin β4 for actin binding

A. Eps8 (648-821) competes with Thymosin β4 for AEDANS actin binding at high salt (F-buffer).

The change in fluorescence of 1.5 μM AEDANS-Actin-actin was measured in the presence of increasing concentrations of Thymosin β4 and 0, 15 μM or 30 μM of Eps8 (648-821) in 0.1M KCl and 1mM $MgCl_2$. Under these conditions, the Kd of Thymosin β4 is 3 μM, and the K_{app} (K apparent) are 9 μM and 14 μM in the presence of 15 μM and 30 μM of Eps8 (648-821), respectively.

B. The H1-H2 fragment is sufficient to compete with Thymosin β4 for binding to monomeric actin.

The change in fluorescence of 1.5 μM AEDANS-Actin-actin was measured at increasing concentrations of Thymosin β4 and 0, 10 μM or 15 μM of H1-H2 in presence of 0.1M KCl and 1mM $MgCl_2$. In these conditions, the Kd of Thymosin β4 is 3 μM, and the K_{app} (K apparent) are 6 μM and 11 μM in the presence of 10 μM and 15 μM of H1-H2, respectively.

To obtain direct validation of our findings with an independent approach, we performed mass spectrometry analysis after crosslinking of actin and Eps8 (648-821).

We generated isopeptide bonds between side chains of actin and Eps8 (648-821) by incubating these proteins alone, as a control, or in combination with a crosslinking agent (see Matherials and Methods). SDS-PAGE separation of the resulting reaction products, revealed two slower-migrating protein species, only when Eps8 (648-821) and actin were simultaneously present in the crosslinking mixture (Figure 32A). We isolated these products and subjected them to mass spectrometry analysis (Figure 32B). A number of Eps8-actin, crosslinked peptides could be identified (Figure 32C). All actin-derived peptides contained either K330, located in subdomain 3, or K375, located in subdomain 1, whereas, Eps8-derived fragments contained K675 and K683, which are located just before or in the predicted H1, respectively, or K707, located in the linker region connecting the predicted H1 and H2 (Figure 32D).

These results are in good agreement with our biochemical mapping, confirming the binding between the Eps8 region encompassing the H1-H2 helices and the subdomain 1 and 3 of actin. These findings corroborated the notion that H1 helix plugs into the hydrophobic cleft of the actin monomer, similarly to a WH2 domain.

Notably, we isolated also one crosslinked peptide that is the result of an intramolecular interaction within Eps8 (648-821), occurring between H1 and the linker region, thus suggesting the possibility that these regions of Eps8 may fold one over the other in a configuration that may be relevant for regulation of the protein activity.

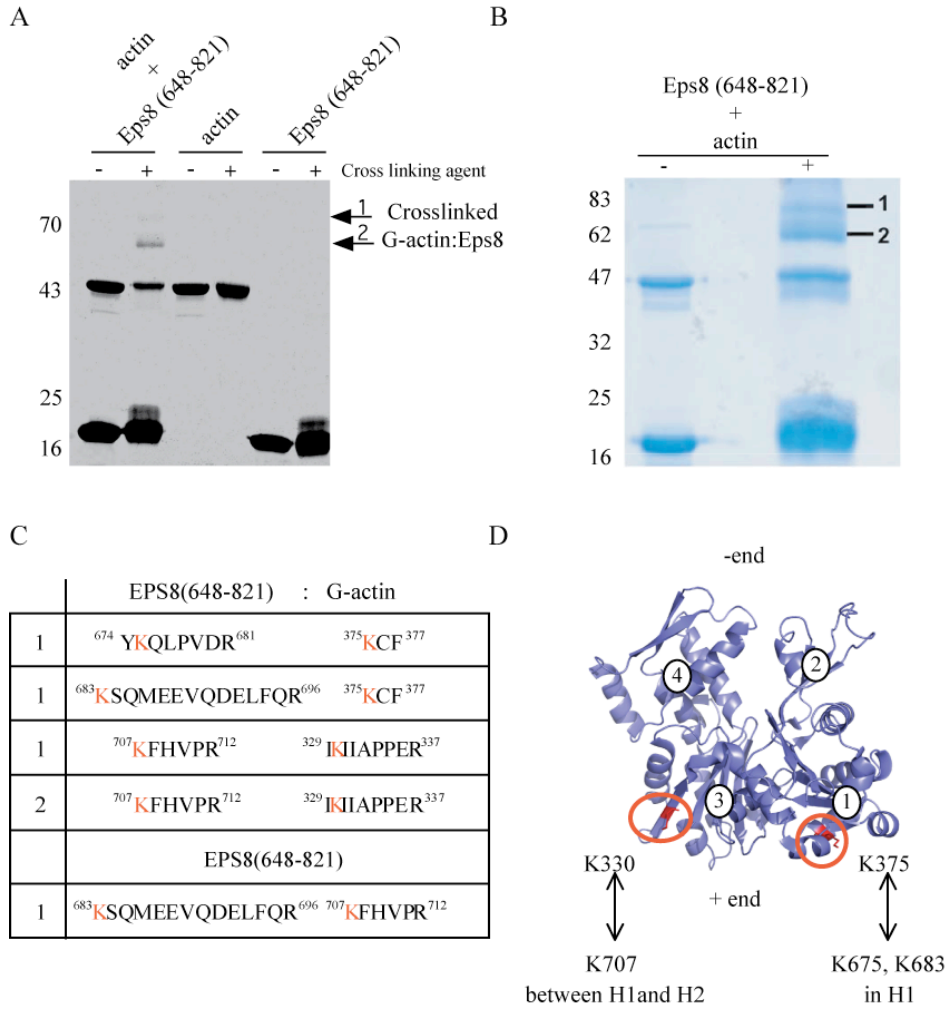

Figure 32: Mapping of the interaction surfaces between Eps8 (648-821) and G-actin by mass spectrometry

A. Crosslinking of Eps8 (648-821) and actin.

Eps8 (648-821) and actin, either alone or in combination, were incubated in the absence (-) or presence (+) of BS2-GD4 (Bis(sulfosuccinimidyl02,2,4,4-glutarate-d4), as a crosslinker, for 45 min. The reaction products were separated by SDS-PAGE and detected by Coomassie blue staining (shown in greyscale). Two cross-linked protein bands, indicated as 1 and 2, were specifically detected only when actin and Eps8 (648-821) were concomitantly incubated with the cross-linker.

B-D. Identification of Eps8 (648-821)-Actin chimaeric peptides by mass spectrometry.

B. Eps8 (648-821) and G-actin were incubated in the absence (-) or presence (+) of the crosslinking agent, as described above. The two indicated cross-linked species were subjected to mass spectrometry analysis.

C. Table summarizing the sequences of peptides derived from mass spectrometry analysis of gel band 1 and 2 of the Eps8 (648-821):G-actin complex or of Eps8(648-821), containing crosslinked lysines (K). Numbers on the left indicate the number of times the peptide was found in a typical mass spectrometry analysis.

D. The positions of BS2G-d0-cross-linked Lysine residues of the peptides identified by mass spectrometry on actin are indicated in red and circled. The corresponding crosslinked Lysines of H1 and H2 helices of Eps8 (648-821) are indicated at the bottom. Actin subdomains (1-4) are also indicated.

8.6 H1 is connected to the H2-H5 globular core via a cleavable linker

In order to better understand the way of binding of Eps8 on the actin filaments we set out to obtain structural information on the three dimensional organization of murine Eps8 C-terminal region.

To this end, we took advantage of a recently solved NMR structure of the C-terminal region of human Eps8L2 (residues 612-697, 1WWU), a member of the Eps8L family protein [91] and of human Eps8 (residues 699-784, 2E8M) (Figure 33), deposited in the PDB database (Structural genomic program- RIKEN Genomic Sciences Center, Yokohama 230-0045, Japan).

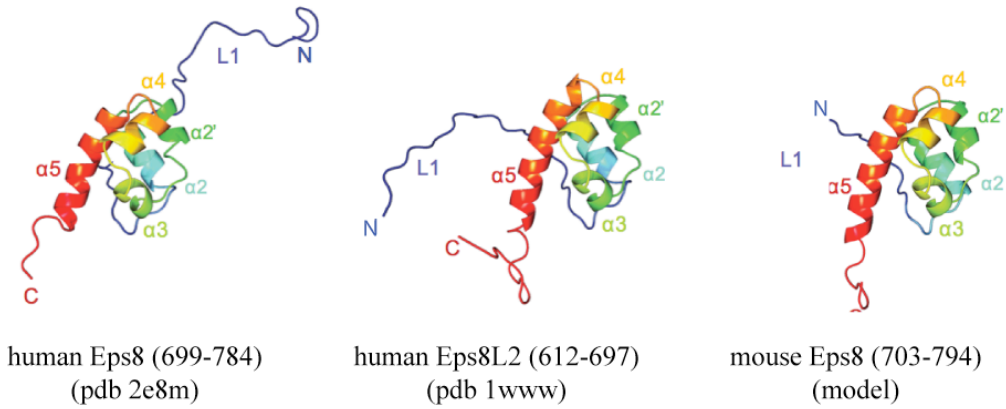

Figure 33: Modelling Eps8 tertiary structure

Ribbon diagrams of the resolved, NMR, tertiary structures of the C-terminal region of human Eps8 (aa 699-784) (PDB ID: 2E8M), human Eps8L2 (aa 612-697) (PDB ID: 1WWU) and of the predicted tertiary structure of the C-terminal region of murine Eps8 (703-794) obtained by Phyre software. Please note that in the NMR structures of human Eps8 (PDB ID: 2E8M) and Eps8L2 (PDB ID 1WWU) the linker, L1, appears in a disorder state suggesting that is not part of the compact globular core (not shown).

These fragments, which include the most C-terminal four helices, H2 to H5 (Figure 26), fold into a globular, helical core. Notably, murine and human Eps8 C-terminal actin binding domains are nearly identical predicting that they adopt a similar fold. Structural atomic modelling using the Phyre software (Protein Homology/analogy Recognition Engine) confirmed this prediction (Figure 33, right). Conversely, the absence of experimental structural information on the first α-helix of Eps8 and Eps8L2 prevented modelling the folding of this helix with respect to the globular core. This region of Eps8 appears connected to the core helical bundle by an unstructured and presumably flexible linker of 20 residues (Figure 26). This latter notion is supported by the observation that in the more closely related ESP8 and EPS8L2 NMR structures (PDB ids 2E8M, 1WWU), the linker is in a disordered state and not part of the compact core. We also performed a limited proteolysis experiment in order to identify regions of the protein that are resistant to digestion, meaning that they adopt a compact conformation. Limited proteolysis of Eps8 (648-821) resulted in the generation of a fragment encompassing the proteolytic-resistant, helical globular core, which is, thus, connected by an exposed, cleavable linker to H1 (Figure 34), confirming the hypothesis derived from the structure.

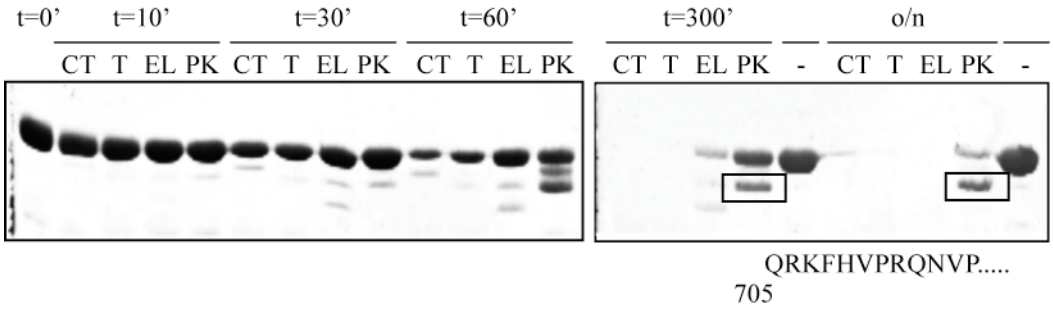

Figure 34: Limited proteolysis analysis of the C-terminal Eps8 fragment

Limited proteolysis of the C-terminal Eps8 fragment shows a major band of degradation.

Eps8 (648-821) (0.5 mg/ml) was digested with chymotrypsin (CT), trypsin (T), Elastase (EL) and proteinase K (PK) at the dilution 1/10000 in the buffer (50 mM Tris pH 7.5; 50 mM NaCl; 1 mM DTT) for the indicated time at room temperature. Digestion was terminated by the addition of phenylmethylsulfonyl fluoride (1 mM). Aliquots of the protelytic peptides were resolved by SDS-PAGE and stained with Coomassie Blue. The proteolytic-resistant fragments, indicated by boxes, were subjected to N-terminal sequencing. The resulting amino acid sequence is reported at the bottom.

8.7 The Eps8 actin binding domain wraps around actin filaments

Next we decided to investigate how Eps8 could bind actin filaments. To answer this question we adopted a combination of electron microscopy, three-dimensional image reconstruction and modelling. We performed EM experiments using actin filaments and Eps8. In order to visualize Eps8 bound on the filaments we used a fragment of the protein that span residue 535 until the end of the protein thus encompassing not only the C-terminal actin binding region, but also the SH3 domain of Eps8. The presence of this additional portion of the protein did not interfered with our structural analysis. Additionally, it had been already previously demonstrated that this fragment possessed the same biochemical characteristics of the C-terminal region of Eps8, and moreover that the SH3 domain itself could not bind actin [50]. Eps8 bound on the filaments was clearly visible in the EM images (Figure 35A). By subtracting the density of the undecorated filaments from the one in the presence of Eps8 we were able to obtain the extra density due to the presence of Eps8 on the filaments (depicted in red, Figure 35A). The difference density partitions into two main regions (Figure 35B). One part forms a big lobe that contacts three actin subunits; one subunit is mainly contacted at the back of subdomain 1 and 2 (grey subunit), one on the back of subdomain 3 (blue subunit) and one on the top of subdomain 4 (yellow subunit). The second region is located on the hydrophobic pocket present between subdomain 1 and 3 of the actin monomer. The third small density finally connects the other two contacting a region between the subdomains 3 and 4 of the actin monomer. We next docked into these densities our structural model for the C-terminal region of Eps8 (see material and methods section).

In the first density we could accommodate the structure corresponding to the H2-H5 lobe, while the H1 helix could be placed in the density that contacts the cleft between subdomain 1 and 3 on the actin monomer, in agreement with our biochemical predictions. In the

absence of structural information on this H1 helix, the H1 model and its interaction with actin were taken from the ciboulot crystal structure (PDB code 1sqk) [81] due to the already described similarity between the two proteins (Figure 29). Finally the linker connecting H1 and H2 could be docked into the third density that contact the region between subdomain 3 and 4 of the actin monomer. We could also observe an extra density region (showed by the arrow in Figure 35B), which accounted for the additional part of the protein that was not directly contacting the filament.

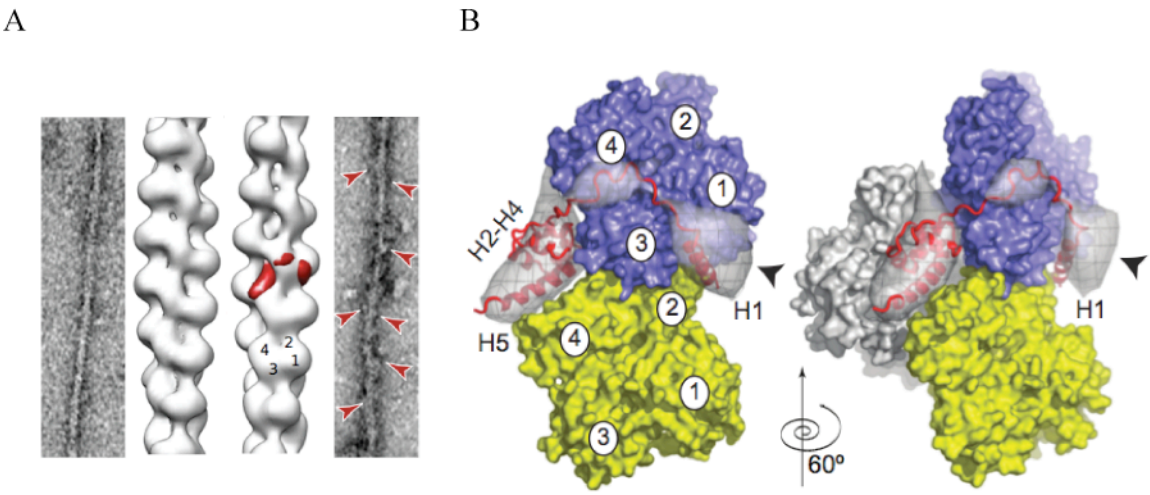

Figure 35: Three-dimensional reconstruction of Eps8 (535-821) bound to actin filaments

A. Three-dimensional reconstruction of Eps8 (535-821) bound to actin filaments by EM.

A reconstruction of undecorated actin filaments is shown for reference on the left, the reconstruction of actin filaments with bound Eps8 is shown on the right. The four actin subdomains are marked on one actin subunit on the filament reconstruction. The difference map corresponding to actin-bound Eps8 (535-821) is highlighted in red. Representative images of undecorated actin (left) and actin decorated with Eps8 (535-821) (right) are also shown. Some of the more obvious attached Eps8 (535-821) particles are marked by red arrowheads.

B. Difference map generated by subtracting the undecorated actin filament reconstruction from the reconstruction of the Eps8 (535-821) bound to actin filaments (grey transparent surface).

For clarity, only one asymmetric unit along the filament is shown. Two views, related by a 60º counter clockwise rotation around the filament axis, are shown. The pointed end is to the top of the figure. Three actin subunits (blue, yellow and light grey surfaces) are shown for reference. Subdomains 1-4 are labelled on the actin subunits. The difference density partitions into two main regions. At lower contour levels, these parts are connected by a bridge of density. The docked model of Eps8 (648-821) is shown in red cartoon representation.

This structural reconstruction is also in agreement with our mass spectrometry data (Figure 32D); the residues crosslinked in the mass spectrometry analysis are indeed in juxtaposition in our model.

We could also observe a change in the twist of the filament upon Eps8 binding, going from 2.14 to 2.16 subunits per turn. This indicates that Eps8 binding interferes with the contact between adjacent actin subunits within the filament.

We thus obtained structural information regarding the way of binding of the C-terminal region of Eps8 on the filaments, showing that the H2-H5 lobe and the H1 helix represent the 2 major surfaces of interaction between the two proteins, with the H1 binding the hydrophobic cleft between subdomain 1 and 3 as predicted by the biochemical analysis. This reconstruction suggested once more that the H1 helix is critical in mediating the capping activity of the protein blocking the further addition of actin monomers to the filament.

8.8 Eps8 capping and bundling activities can be biochemically dissected

Looking at Eps8 bound on actin filaments by EM we detected two major interaction surfaces, connected via a flexible linker. One of these surfaces is represented by the H1 helix of the C-terminal region of the protein, and contacts actin between subdomain 1 and 3, in the cleft that is exposed at the plus end of filaments. The other surface is composed by the H2-H5 lobe, and contacts the actin filament mainly on the side, interacting with 3 different monomers.

Eps8 can either cap barbed ends or crosslink actin filaments. The distinct topological distribution of the two surfaces of Eps8 on actin suggests the possibility that each of them may be specifically involved in mediating either capping or bundling. Indeed, filament capping is generally achieved by preventing the further addition of new monomers at the

end of the filaments, while in order to bundle actin proteins should contact the side of adjacent filaments crosslinking them together. Due to the incapability of the H1 helix alone to cap and bind actin, we also reasoned that the interaction mediated by the linker may primarily stabilize the binding of both the H1 and the lateral lobe, rather than directly participating in blocking monomer association.

We tested this hypothesis by generating mutants that selectively and specifically compromise one of the surfaces of interaction between Eps8 and actin. To this end, we; i) generated a mutant in the linker region (R706A, F708A, hereon refereed as linker mutant), which might weaken both protein functions as it may serve to stabilize the binding of Eps8 C-terminus around filament ends; ii) generated a double mutant (V689D, L693D, herein referred to as H1 or Δcapping mutant) in which we substituted two hydrophobic residues with two charged amino acids in order to destroy the non polar side of the amphipathic helix that is predicted to bind the hydrophobic actin cleft; iii) we identified within the H2-H5 lobe a motif (LNKDE, aa 757-761) that resembles the F-actin binding site of the Villin head piece domain (herein refereed to as Villin-like motif) [9]. Within this motif we mutated two residues that had been described as critical in mediating the interaction between actin filament and Villin, generating a mutant L757A-K759A, that we called Villin-like or Δbundling mutant. Finally, as a control, we also generated a double mutant in H1 and in the Villin like motif, that we called ΔcappingΔbundling mutant. We engineered these mutants in the contest of the C-terminal region of Eps8 (aa 648-821) fused to a GST moiety. This latter strategy was prompted by the observation that the crosslinking activity of the Eps8 C-terminal region is dependent on the presence of GST, which drives the formation of dimers (see below). Accordingly, we detected bundling of actin filaments only when Eps8 C-terminal fragments were fused to GST, (Figure 36) using low speed cosedimentation assays.

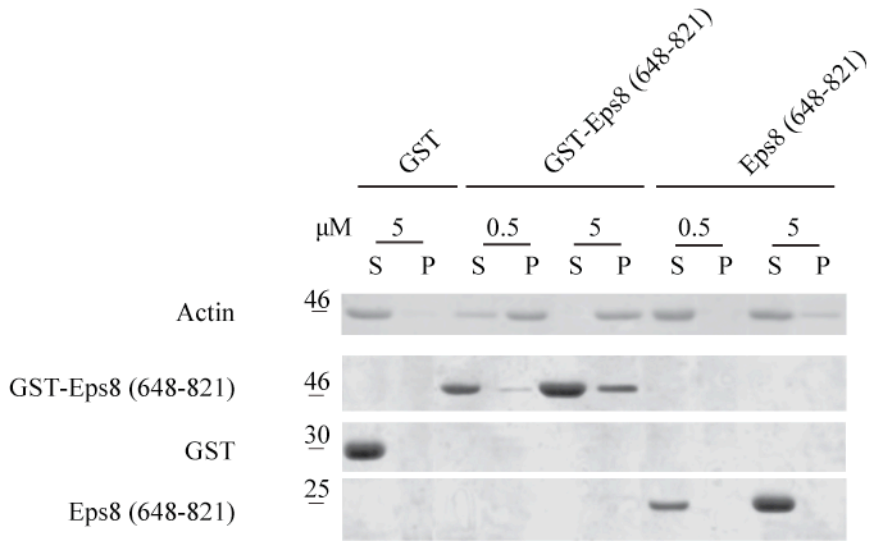

Figure 36: Dimerization drives Eps8 (648-821) bundling activity

The F-actin bundling ability of GST-Eps8-WT or Eps8-WT GST cleaved was determined by low speed co-sedimentation assays. F-actin (1 μM) was incubated either alone or in the presence of the indicated concentrations of GST, as control, or GST-fused Eps8 (648-821) or Eps8 (648-821) cleaved from the GST moiety. The mix was subjected to centrifugation at 10000 xg for 30 min. Aliquots of the pellet (P) and supernatants (S) were analyzed by immunoblotting.

We obtained similar results also employing a fluorescent-based *in vitro* assay of actin bundling. To this end, we incubated Eps8 (648-821) either cleaved from or fused to GST, together with F-actin. We then stained the filaments using rhodaminated-phalloidin to reveal the presence of bundles. Only GST-fused Eps8 caused the formation of prominent actin bundles (Figure 37). One possible explanation of these results is suggested by the fact that the GST moiety is a dimer [92], which might be necessary to enable two molecules of Eps8 to bind, and subsequently crosslink two adjacent actin filaments. We performed a hydrodynamic analysis in order to calculate the exact molecular weight of the GST fused Eps8 and thus to assess if the GST constructs behaved really like dimers.

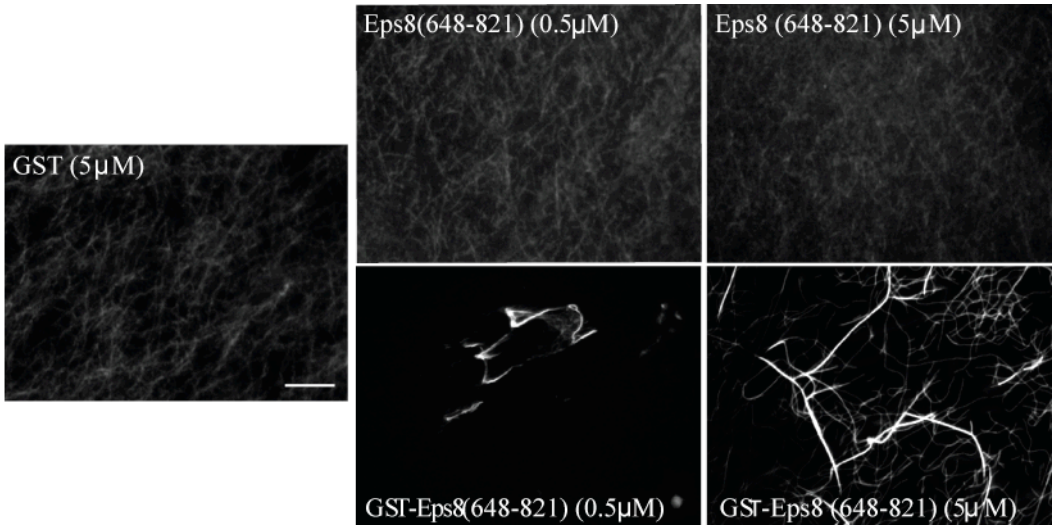

Figure 37: Dimerization drives Eps8 (648-821) bundling activity

F-actin (1 µM) was incubated with either 5 µM of GST, as control, or with the indicated concentrations of Eps8 (648-821) cleaved from the GST moiety or GST-fused Eps8 (648-821). Actin filaments were labelled with rhodamine-phalloidin and imaged using a fluorescence microscope. Data are representative fields acquired with a 100X magnification. Three independent experiments per condition were performed, all yielding similar results. Bar is 1 µM.

We first performed a gel filtration analysis of the GST-Eps8 (648-821) to calculate its Stokes radius, using markers of known stokes radii as standards to create a calibration curve. The GST Eps8 (648-821) calculated stokes radius was 59.44Å (Figure 38).

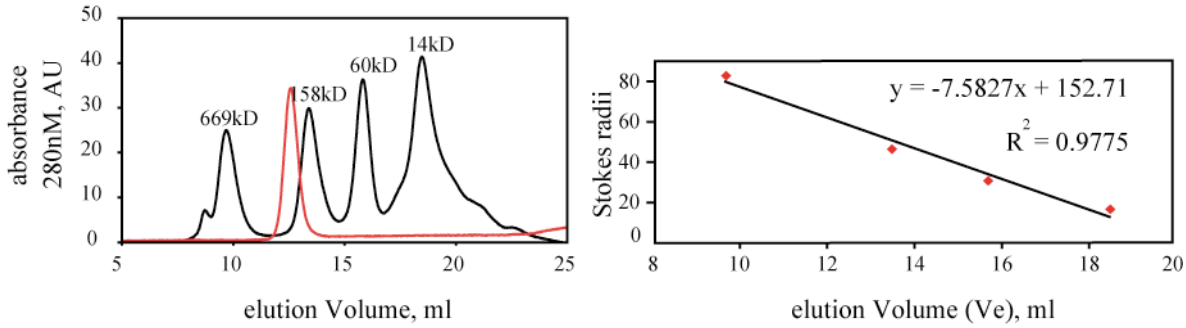

Figure 38: Gel filtration analysis of GST Eps8 (648-821)

Determination of the stoke radius of GST Eps8 (648-821) by gel filtration analysis.

Right panel: Superdex 200 elution profile of GST-Eps8 (648-821) and of markers of known Stoke radius. *Left panel:* elution volumes of the markers (bovine thyroglobulin, rabbit aldolase, hen egg albumin, and ribonuclease A) were plotted against their known Stokes radii to generate a calibration curve (R^2 = 0.9775) from which the Stokes radius of GST-Eps8 (648-821) was determined.

Next we determined the sedimentation behaviour of GST-Eps8 (648-821) using a glycerol density gradient. We determined a sedimentation coefficient of 4 Svedberg (Figure 39).

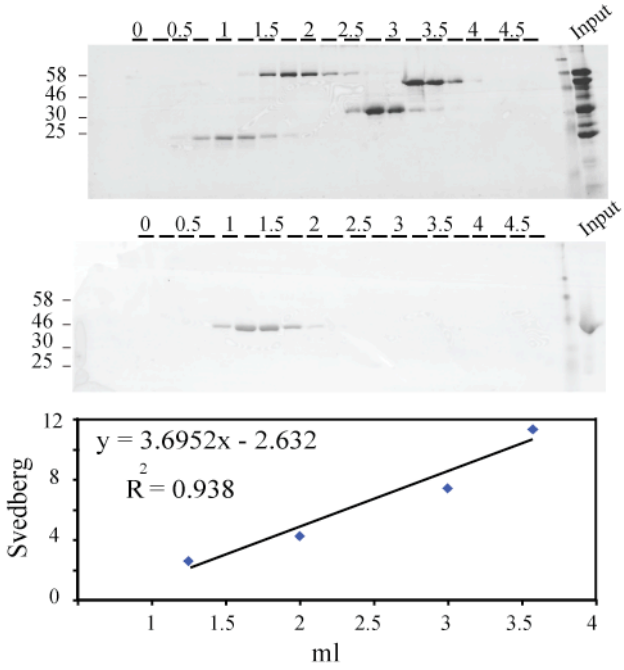

Figure 39: Glycerol density gradient of GST Eps8 (648-821)

Determination of the Svedberg coefficient of GST Eps8 (648-821).

Top panels: Glycerol (10-40%) gradient sedimentation of markers of defined Svedberg coefficient and of GST-Eps8 (648-821). Coomassie blue staining of aliquots of gradient fractions resolved by SDS-PAGE is shown. Samples were loaded directly onto 5-ml 10–40% glycerol gradient (gradient buffer = 100 mM Tris-HCl, pH 8, 500 mM NaCl, 1 mM dithiothreitol, 1 mM EDTA). Centrifugation was protracted for 13 h at 55,000 rpm on a Beckman SW41Ti swinging bucket rotor at 4 °C. The gradient was fractionated in 250-µl fractions. *Bottom graph:* Sedimentation volume of the markers (Bovine Pancreas Chymotrypsinogen, albumine, aldolase and catalase) were plotted against their known Svedberg coefficient (2,58S, 4,22S, 7,4S and 11,4S respectively) to generate a calibration curve from which the Svedberg coefficient (**s**) of GST-Eps8 (648-821) was determined.

With these values we used the Siegel and Monty equation (see the material and methods section) to calculate the molecular mass of the protein. We obtained a value of 97.4 kD, in excellent agreement with the predicted dimeric nature of the protein (the molecular weight of the monomeric GST Eps8 (648-821) would be 47.8 kD.

Next, we tested the capping activity of our mutants with respect to the Wt Eps8 using pyrenyl labelled actin and spectrin actin seeds in a fluorimetric assay (Figure 40). The linker mutant displayed a decreased, but still significant capping activity (Kcap = 180nM with respect to the WT Kcap = 7nM) (Figure 40A). The H1 mutant, instead, showed only a residual ability to decrease actin polymerization from the plus ends, with a significant reduction in the binding affinity that was in the submicromolar range (Kcap = 700nM with respect to the WT Kcap = 6.5nM) (Figure 40B). The Villin mutant had a capping activity similar to the WT protein, with only a slight decrease in its Kcap (Kcap =20nM with respect to the WT Kd = 4nM) (Figure 40C). Finally, the double mutant, as expected, was a very poor capper (Kcap = 4μM with respect to the WT Kcap = 16nM) (Figure 40D).

Collectively, these results reinforced the notion that the H1 helix is critical in mediating the capping activity of the Eps8 C-terminal domain. The slightly diminished capping activity of the linker mutant and, to a minor extent, of the villin mutant, are consistent with a role for these two surfaces in the stabilization of Eps8 at the plus end.

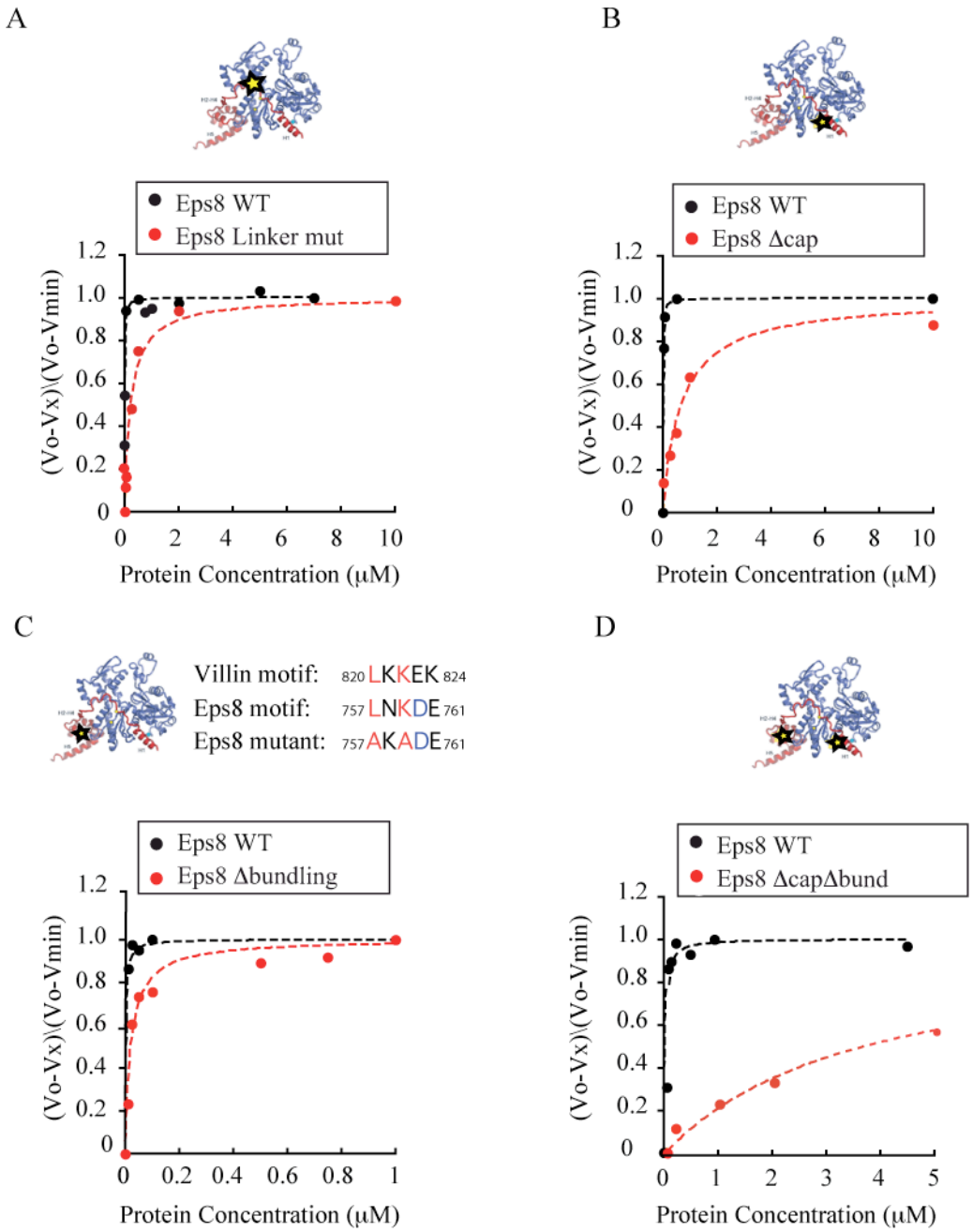

Figure 40: Eps8 capping activity requires an intact H1 helix and H1-to-H2 linker region

A. The barbed end capping activity of Eps8 requires an intact H1-to-H2 Linker region.

The rates of elongation from barbed ends using spectrin-actin seeds and 2 μM of G-actin (10% pyrenyl-labeled) in the presence of increasing concentrations Eps8 (648-821)-R706A-F708A-(Eps8-Linker mutant) (red line) with respect to Eps8 (648-821)(Eps8-WT) (black line) are shown. Rates are normalized taking as 100 % the rate of elongation from barbed ends measured in the absence of Eps8-WT. Symbols indicate data; line indicates fitted binding curves for a complex with 1:1 stoichiometry. The kinetic constant (Kcap) of barbed end inhibition for Eps8- Linker mutant = 180 nM; Eps8-WT = 9 nM. *On the top* the position of the critical, mutated residues of the H1-to-H2 Linker in the modelled complex Eps8 (648-821):G-actin are indicated by a star.

B. The barbed end capping activity of Eps8 requires an intact H1 amphipathic helix.

The rates of elongation from barbed ends using spectrin-actin seeds in the presence of increasing concentrations of Eps8-WT (black line) or Eps8 (648-821)-V689D -L693D (Eps8-Δcap) (red line) are shown. The Kcap of the Eps8-Δcap = 700 nM. *On the top* the position of the critical, mutated residues of the H1 in the modelled complex Eps8 (648-821):G-actin are indicated by a star.

C. The capping activity of Eps8 (648-821) is not mediated by a Villin-like motif in the globular, helical domain.

The rates of elongation from barbed ends in the presence of increasing concentrations of Eps8 (648-821)-L757A-K759A (Eps8-Δbund) (red line) with respect to Eps8-WT (black line), are shown (Kcap of Eps8-Δbund = 20 nM*). On the top*, the critical, mutated residues in the Villin-like motif of Eps8 (648-821) are indicated in red, their position in the modelled complex Eps8 (648-821):G-actin is indicated by a star.

D. Actin capping activity of Eps8 (648-821) is impaired by a mutation in the helix H1 and in the Villin-like motif (Eps8-ΔcapΔbund), whose position within the complex Eps8 (648-821):G-actin is shown on top.

We then tested the bundling activity of our mutants in low speed co-sedimentation assays. The linker mutant showed only a marginal reduction in the capacity of the protein to mediate bundling of actin filaments (Figure 41A). The H1 mutant was as efficient as the WT protein (Figure 41B), while the Villin mutant was no longer able to bundle actin filaments even at high micromolar concentrations, thus confirming the importance of this latter motif in mediating Eps8 crosslinking of actin filaments (Figure 41C). As expected, the double mutant ΔcappingΔbundling was also impaired in bundling actin filaments (Figure 41D).

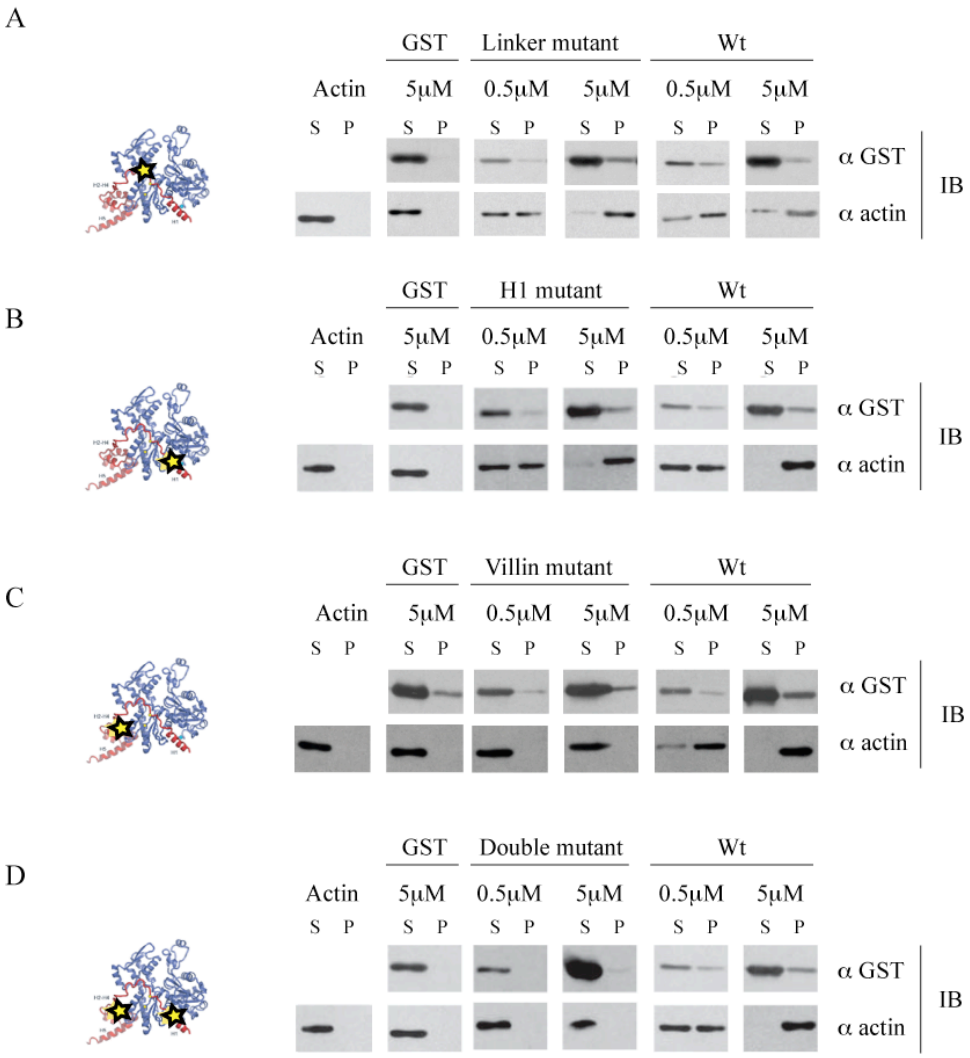

Figure 41: Eps8 bundling activity is mediated by a Villin – like motif in the globular domain

A. The bundling activity of Eps8 doesn't require an intact H1-to-H2 Linker (Linker mutant) region. *Left*, the position of critical, mutated residues of the H1-to-H2 Linker in the modelled complex Eps8 (648-821):G-actin are indicated by a star. *Right*, The F-actin bundling ability GST-fused Eps8-WT or Eps8-Linker mutant was determined by co-sedimentation assays. F-actin (1 μM) was incubated either alone or in the presence of the indicated concentrations of GST, as control, or GST-fused WT or mutated Eps8 (648-821). The mix was subjected to centrifugation at 10000 xg for 30 min. Aliquots of pellets (P) and supernatants (S) were analyzed by immunoblotting with the antibodies indicated on the right.

B. The bundling activity of Eps8 doesn't require an intact H1 amphipathic helix.

Left, the position of critical, mutated residues of the H1 in the modelled complex Eps8(648-821):G-actin are indicated by a star. *Right*, The F-actin bundling ability of the indicated Eps8-Δcap was determined as described in A.

C. The bundling activity of Eps8 (648-821) is mediated by a Villin-like motif in the globular, helical domain. *Left*, the critical, mutated residues in the Villin-like motif of Eps8 (648-821) are indicated in red, their position in the modelled complex Eps8(648-821):G-actin is indicated by a star. *Right*, the F-actin bundling ability of GST-Eps8-Δbund was determined as in A.

D. Actin bundling activity of Eps8 (648-821) is impaired by a mutation in the helix H1 and in the Villin-like motif (Eps8-ΔcapΔbund), whose position within the complex Eps8 (648-821):G-actin is shown on the left.

We obtained similar results also by analyzing the bundling activity of our mutants by fluorescence staining of the filaments with rodhaminated phalloidin (Figure 42).

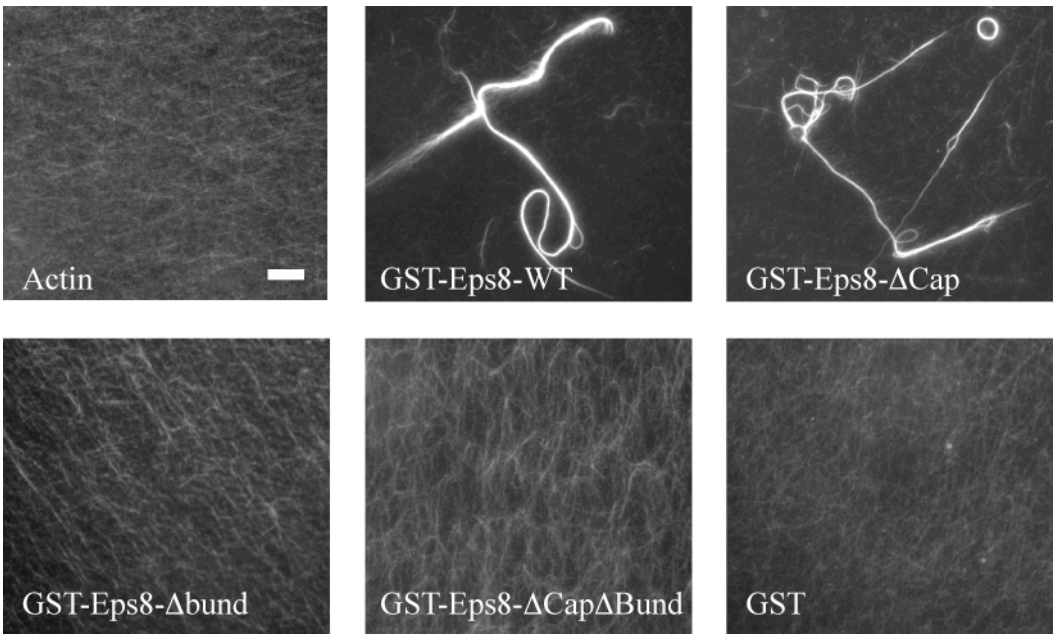

Figure 42: The Eps8 Villin-like motif is responsible for Eps8 bundling activity
Immunofluorescence visualization of actin bundles induced by wild type and GST-Eps8(648-821) mutants. F-actin (1 μM) was incubated either alone (Actin) or together with 5 μM of GST, as control, or with Eps8-WT or the indicated Eps8 mutants fused to GST. Actin filaments were labelled with rhodamine-phalloidin and imaged using a fluorescence microscope. Data are representative fields of view acquired at 100X magnification. For each condition three independent experiments were performed yielding similar results. Bar represents 5 μM.

Since aggregation of partially misfolded protein could lead to artificial bundling of actin, caused by an aspecific binding to filaments of the aggregated proteins, we tested the proper folding and the stability of our mutants using a set of hydrodynamic biochemical assays. Using size exclusion chromatography, WT and mutant proteins displayed identical elution profiles both when kept at 4°C and after exposure for 1 hour at room temperature, suggesting that the proteins are properly folded, stable and do not obviously aggregate (Figure 43).

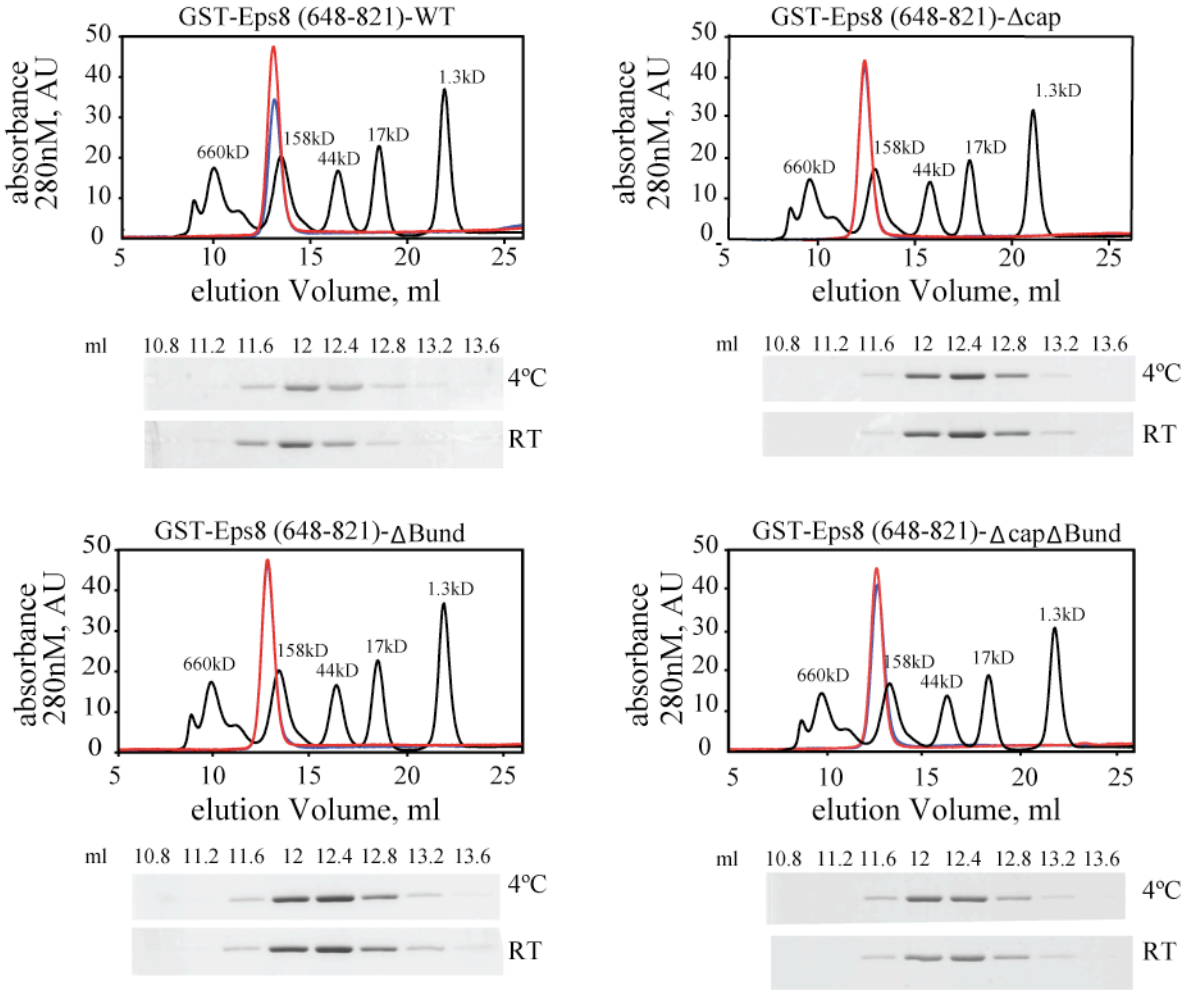

Figure 43: Hydrodynamic analysis of wild type and GST-Eps8 (648-821) mutants

The Eps8 mutants do not aggregate both at 4°C and at room temperature.

Size exclusion chromatography (SEC) of the purified Eps8 (648-821) wild type and of the various indicated mutants fused to GST was performed on a Superdex200 10/30 column. The elution profile of markers of defined molecular weight is reported along the profile of the various Eps8 (648-821) proteins detected by measuring the absorbance at 280nm wavelength. Comassie blue staining of aliquots of eluted fractions resolved by SDS-PAGE are shown below the elution profile. SEC was performed after incubation of the samples for 1h at room temperature (Red line and RT) or at 4ºC (blue line) with identical results.

8.9 Eps8 capping and bundling properties correlate with a specific cellular localization of the protein

Using a mutagenesis approach we next generated mutants selectively deprived either of their capping (Δcapping mutant) or bundling (Δbundling mutant) activity in the context of full length Eps8 and engineered them into eukaryotic expression vectors in order to assess whether these distinct actin related functions were responsible for the cellular localization of Eps8. Full length Eps8 localizes in correspondence to specific cytoskeletical structures. The wt protein is mainly localized at the cellular leading edge, both along the lamellipodia tip as well as on filopodia and microspikes. Notably, actin filaments within the lamellipodia form a meshwork of differentially angled filaments oriented with their plus ends towards the cell membrane. Filaments barbed ends are thus concentrated at the lamellipodia tip, correlating with the restricted localization of several capping proteins. Filopodia and microspikes are instead formed by bundles of actin filaments crosslinked together with their tip occupied by a large protein assembly, the tip complex, that is though to exclude capping proteins [93].

We analyzed the cellular localization of the protein in MEF (mouse embryonic fibroblasts) cells derived from Eps8 KO mice, and thus not expressing the endogenous protein and stably expressing GFP Eps8, either WT or carrying the different mutations (Figure 44).

In order to better visualize the lamellipodium, that in this cell line is usually very thin, we performed a spreading experiment. Cells were tripsinized, incubated 30 minutes with warm medium and replated on fibronectin-coated cover-slips. Cells were then fixed after 30 minutes, while they were still attaching to the plate. As expected Eps8 localized both at the lamellipodia tip and on microspikes. The Δcapping mutant retained the microspikes localization, but showed a broader distribution within the entire lamellipodium. The Δbundling mutant, on the contrary, retained the specific restricted localization on the lamellipodia tip, but completely lost the microspikes localization. With the double mutant,

we had a diffused localization, without correlation to any specific cytoskeletical structure. Thus, different Eps8 biochemical activities appear responsible of its localization into specific actin structures.

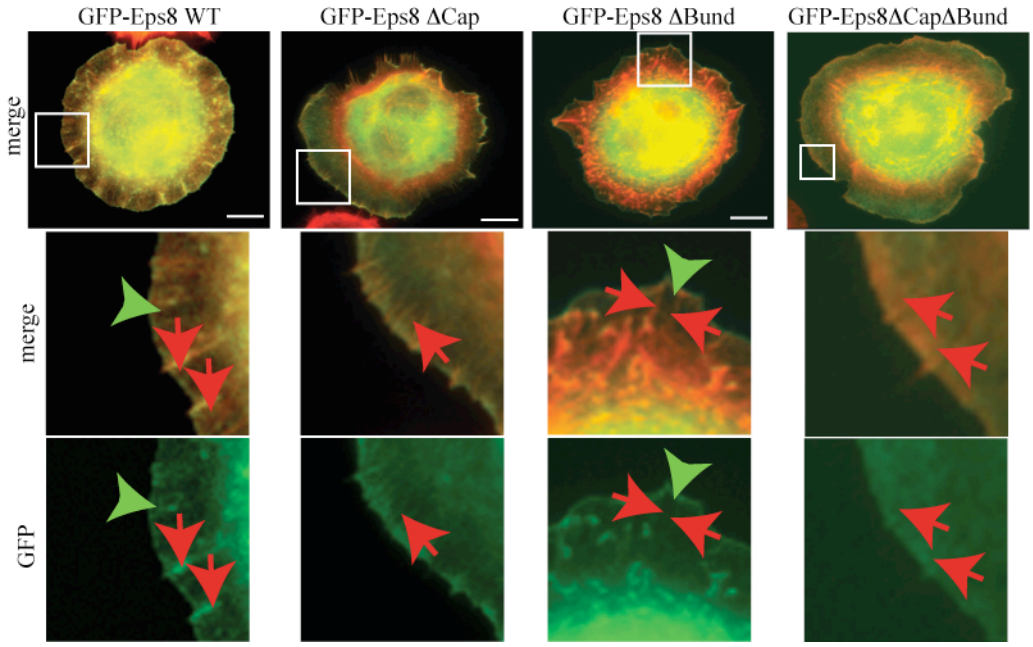

Figure 44: Differential requirement of Eps8 actin activities in architecturally diverse actin-based processes

Eps8 -/- mouse embryo fibroblasts (MEFs) expressing GFP or GFP-Eps8 (full length) or the indicated GFP-Eps8 mutants were trypsinized, incubated with warm complete medium before plating them on Fibronectin-coated cover slips. After 30 min cells were fixed and counterstained with phalloidin to detect F-actin (red) and the respective GFP-tagged protein (Green). Representative merged images are shown. Magnified images corresponding to the boxed insets on top panels are shown as merge (Middle panels) or GFP (lower panels), to evidence the localization of Eps8 and the various Eps8 mutants. Red arrows points to microspikes, Green arrowheads indicate the leading edges of lamellipodia. Bar represents 10 μm.

We confirmed our results also in another cell line. We used B16-F1 mouse melanoma cells, which possess very large and flat lamellipodia and thus allow a better discrimination between subtle differences in the cellular localization of the proteins.

In this cell line, we could confirm the requirement of Eps8 capping activity for its proper localization at the lamellipodia tip. The H1 mutant, in fact, assumed a very diffuse distribution within the whole lamellipodium, loosing the restricted localization at the tip (Figure 45). We also confirmed that the bundling activity of Eps8 is required to localize the protein on microspikes; the Δbundling mutant was indeed completely excluded from these cytoskeletical structures (Figure 45). The double mutant, finally, showed a very diffuse distribution like in MEF (Figure 45).

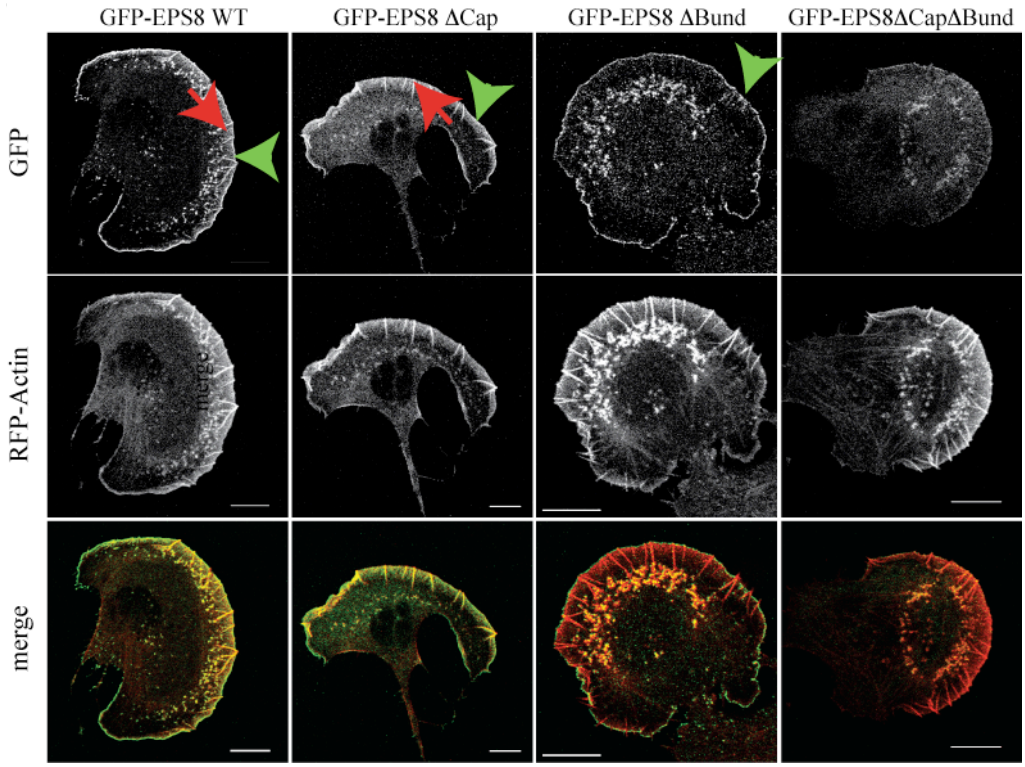

Figure 45: Differential requirement of Eps8 activities in architecturally diverse actin-based structures in B16 melanoma cells

Mouse melanoma B16-F1 cells transfected with GFP-Eps8 WT or the indicated mutants together with mCherry-actin were plated on laminin-coated cover slips and monitored by live-cell confocal microscopy. Stills visualizing GFP constructs (top panels) or mCherry-actin (middle panels) or both as merged images (bottom panels) are shown. Red arrows points to microspikes, green arrowheads indicate lamellipodia. Bars: 10 μM.

We also looked at the dynamics of Eps8 WT and of the different mutants in these cellular structures by Fluorescence Recovery After Photobleaching (FRAP) analysis.

Because of the restricted localization of the Eps8 Δbundling mutant in the lamellipodium we performed the FRAP experiment by bleaching a region encompassing the lamellipodium tip to analyze the behaviour of this mutant (Figure 46 left and see also movies 1 and 2 in the Supplementary material). We measured a significant difference between the time of recovery of the wt protein (Eps8wt T 1\2 = 9.2 sec) and of the Δbundling mutant (Eps8 Δbundling T1\2 = 1.9 sec) (Figure 46 right).

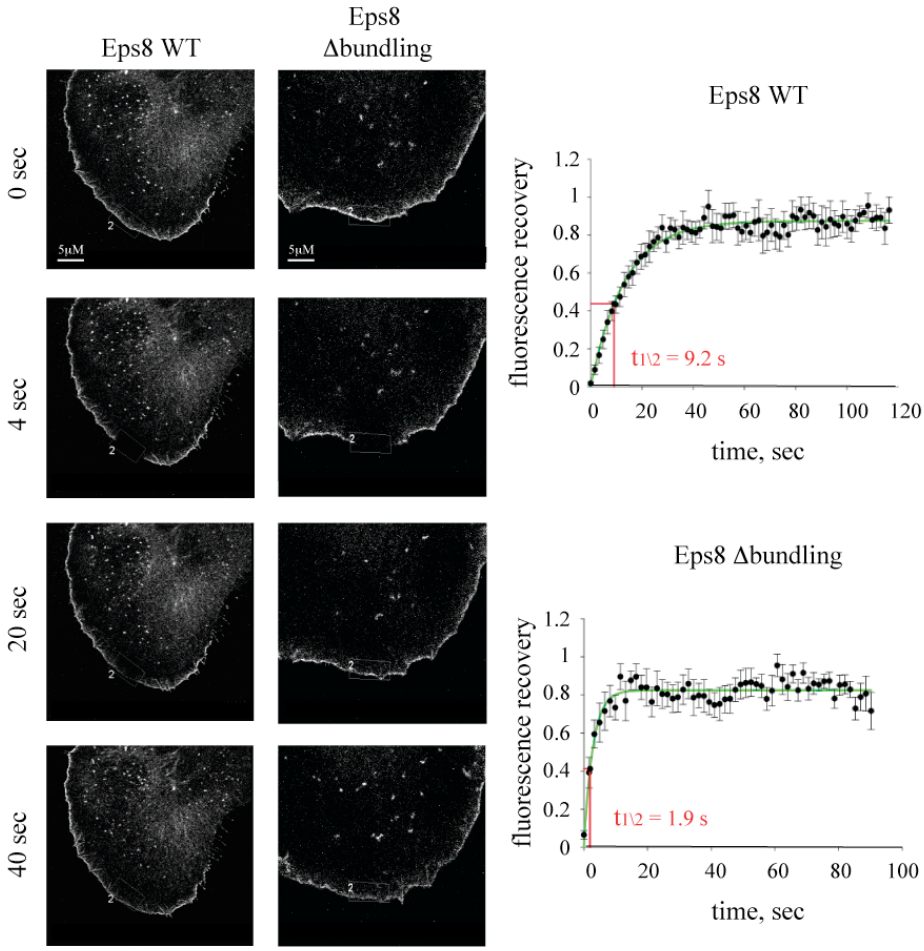

Figure 46: Eps8 dynamics at the cellular leading edge

Eps8 Δbundling mutant shows a less stable association to the filaments ends.

Left: FRAP experiment on B16-F1 melanoma cells expressing GFP Eps8 either WT or Δbundling. Still images of a FRAP experiment at the reported time points are shown (see movies 1 and 2 in the supplementary material). The four second time point corresponds to the bleaching of the cell. The bleached area is indicated in a white rectangle.

Right: the percentage of the fluorescence recovery is plotted over time. Data are means and s.e.m. of five different movies. Half-time of fluorescence recovery ($t_{1/2}$) was calculated from best linear fit (green curve).

This result suggests a less stable association of the mutant at the ends of actin filaments, indicating a possible role of the H2-H5 lobe in the protein stabilization at the plus ends.

The H1 mutant showed, instead, a very broad distribution within the lamellipodium. We thus performed the FRAP experiment on microspikes. We took two other regions in order to calculate the background signal coming from both the cover slip and the cellular body (Figure 47 left and see also movies 3-4 in the Supplementary material). We could not score any differences in the dynamic of Eps8 wt or of the Δcapping mutant on microspikes, indicating a dispensable role of the H1 helix in the binding of Eps8 on the filaments side (Figure 47 right).

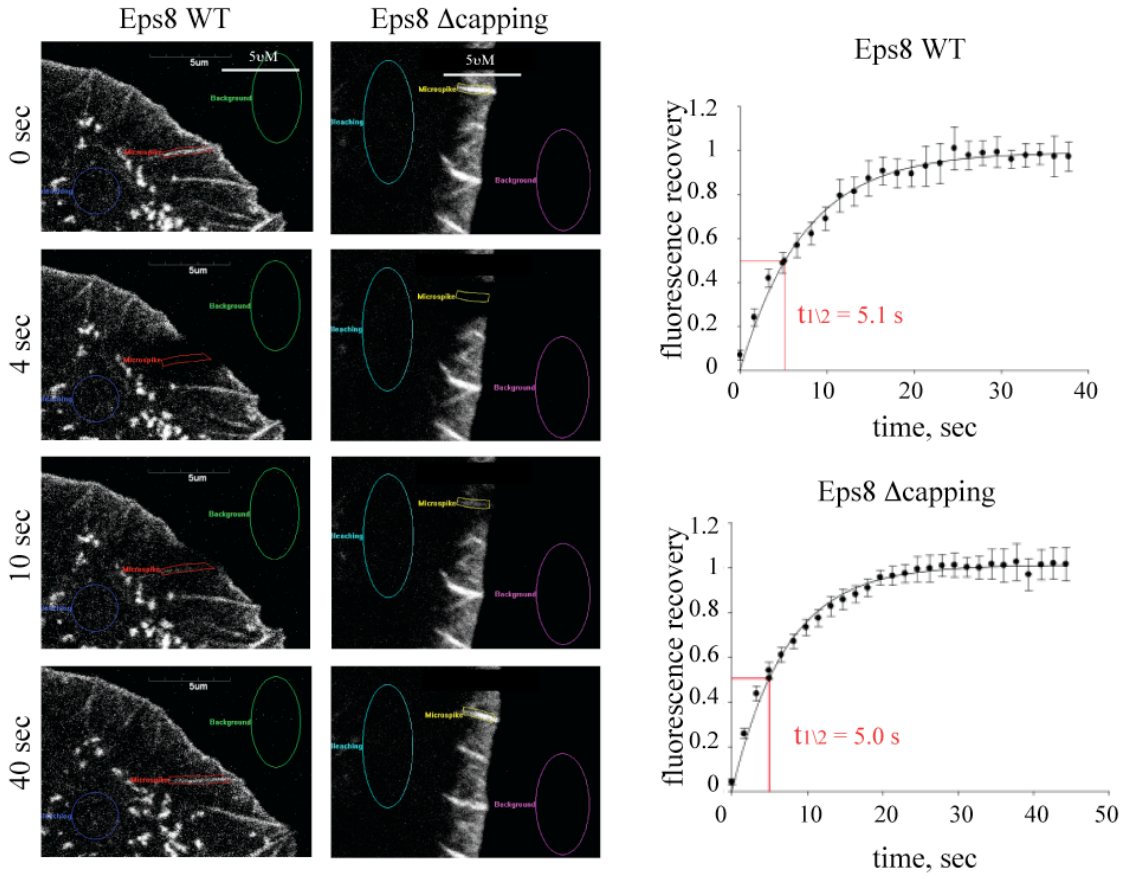

Figure 47: Eps8 dynamics on microspikes

Eps8 Δcapping mutant shows the same dynamic of the wt protein on microspikes.

Left: FRAP experiment on B16-F1 melanoma cells expressing GFP Eps8 either WT or Δcapping.

Still images of a FRAP experiment at the reported time points are shown (see movies 3 and 4 in the Supplementary material). Four second corresponds to the bleaching of the cell. The bleached area is indicated in a yellow or red rectangle. The areas taken as background are also indicated. Right: the percentage of the fluorescence recovery is plotted over time. Data are means and s.e.m. of five different movies. Half-time of fluorescence recovery ($t_{1/2}$) was calculated from best linear fit (black curve).

8.10 Eps8 capping activity mediates the sustaining of actin based motility

The availability of mutants selectively deprived of one of Eps8 biochemical activities prompted us to investigate whether these two distinct biochemical properties are linked to specific cellular functions. It is well established in the literature that capping activity is required to sustain actin treadmilling and thus processes such as actin based motility. Reconstitution of actin based motility *in vitro* can be achieved using functionalized beads, coated with the Arp2/3 activator N-WASP, and a minimal set of purified proteins, among which a capping protein is essential [24]. We tested our mutants in order to test weather the capping activity of Eps8 was the only function required to sustain actin treadmilling and if our mutants behaved consistently with the previous biochemical assays. As expected, the wt protein was able to reconstitute the treadmilling leading to beads movement in the absence of other capping proteins. The Δbundling mutant was also able to induce beads movement, even if at slightly higher concentrations, possibly reflecting its decreased, but still significant, ability to cap actin filaments. The Δcapping and the double ΔcappingΔbundling mutants were, instead, completed unable to sustain beads movement, even when tested at very high concentrations (up to 10 μM) (Figure 48 and see movies from 5 to 10 in the Supplemental Material).

We also tested the H1-H2 and the H2-H5 fragments behaviour and confirmed that the region encompassing the first two helices of the domain is the only one retaining the protein capping activity. H1-H2, but not H2-H5, was in fact still able to sustain the treadmilling and the beads actin based motility (Figure 48 and see movies 11-12 in the Supplementary Material).

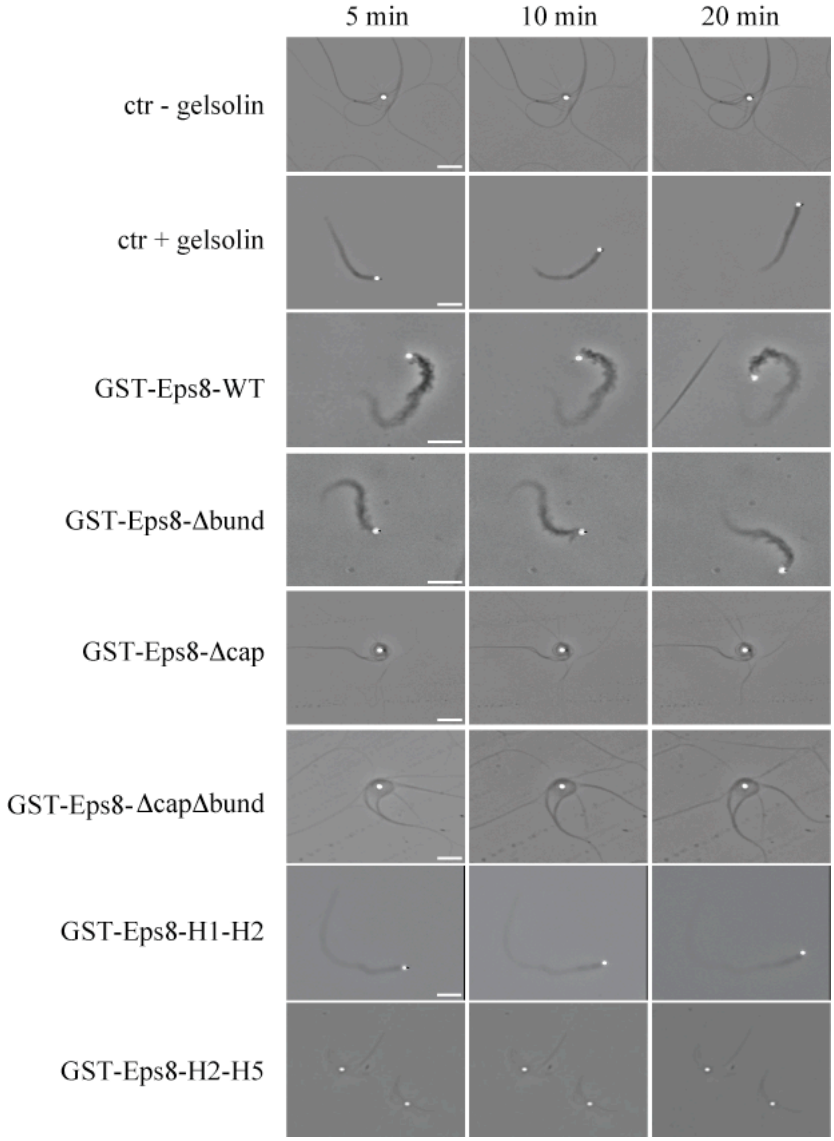

Figure 48: The Eps8 capping, but not its bundling activity, is required to reconstitute actin-based motility in biomimetic motility assays

N-WASP coated beads (2μM) were mixed with a biomimetic motility medium in the absence of any capping protein or in the presence of 50 nM of Gelsolin, or 150nM of GST-fused Eps8 (648-821), or 500 nM of Eps8-Δbund mutant, or 10μM of Eps8-Δcap mutant, or 10μM of Eps8-ΔcapΔbund mutant or 2 μM H1-H2 or 10 μM H2-H5 fragments. Reactions were incubated for 30-to-60 min before starting imaging recording. In the picture images taken at the indicated time points from 20 minutes movies are shown (see also movies from 5 to 12 in the Supplementary Material). Bars, 5 μm.

We next investigated whether we could confirm these findings also in a cellular system. We transfected MEF cells ko for Eps8 with GFP Eps8, either wt or carrying the different mutations, together with cherrylifeact, to visualize actin filaments, and Phosphatidylinositol 5-Kinase (PI5K). PI5K over-expression induces the formation of 4,5-bisphosphate (PIP2) enriched vesicles, whose propulsion is sustained by the actin treadmilling with the formation of a clearly visible actin comet tail. This system mimics cellular propulsion of pathogens such as *L.monocytogenes* or *Shigella*, whose optimal motility has been already reported to be dependent on Eps8 [50].

We first checked by immunofluorescence Eps8 localization on these comets. We could not score major differences within wt and mutants localization, with the exception of the double mutant ΔcappingΔbundling that as expected showed a very diffuse distribution loosing a clear localization on the actin comet tails (Figure 49A). We next performed time-lapse analysis to calculate comets velocity when the different proteins were expressed. Manual tracking of at least 30 comets per condition was performed and the vesicle propulsion rate was calculated. We scored a diminishing of the vesicle velocity when GFP, Eps8 Δcapping or Eps8 ΔcappingΔbundling mutants were expressed. The Δbundling mutant showed at the contrary a propulsion rate similar to the wt protein (Figure 49B and see movies from 13 to 17 in the Supplemental Material).

We thus confirmed that Eps8 capping activity is required for optimal actin based motility both *in vitro* and in a cellular system.

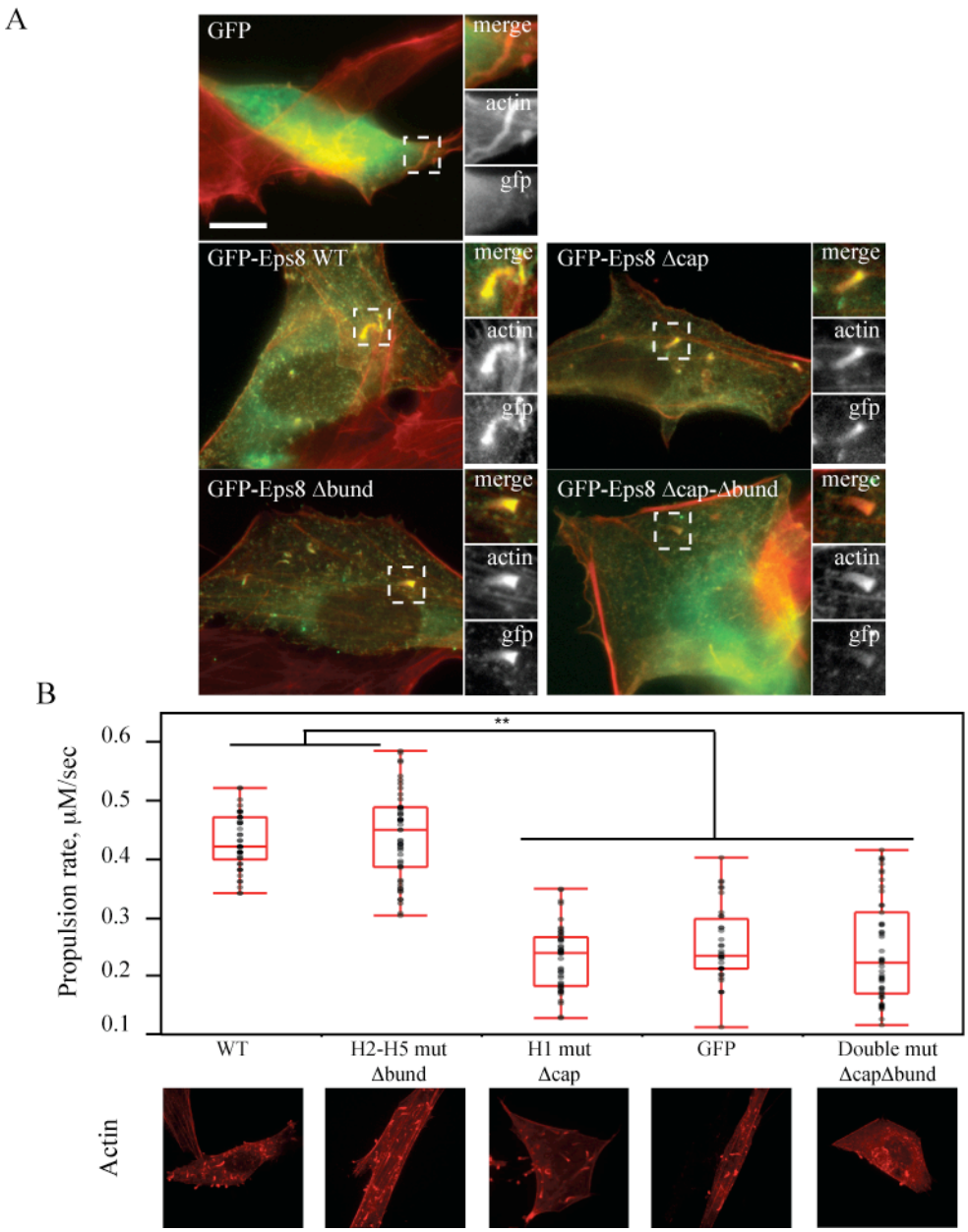

Figure 49: Requirement of Eps8 capping activity for optimal rocketing velocity of PIP2-rich endomembranes

A. Localization of Eps8 FL either WT or carrying the different mutations on actin comet tails.

eps8-null MEFs co-microinjected with Myc–Phosphaditylinositol 4,5 kinase [PI(4,5)K], lifeact-cherry (a kind gift from Roland Wedlich-Soldner) [94] and the indicated Eps8 mutants fused to GFP or GFP alone, as control, were processed for epifluorescence. Bar, is 10 μm.

B. Tracking of the velocity of rocketing endomembranes.

The same cells were subjected to video microscopy. The first frame of each representative movie (see also movies from 13 to 17 in the Supplemental Material) is show to visualize Cherry-lifeact. The velocity of rocketing endomembranes was determined by manually tracking individual vesicles in at least 5-10 different cells using imageJ software. Data are shown as whisker plots, the median, quartiles and highest and lowest values are indicated; ** indicates *HSD (*honestly significant difference), alpha-value < 0.05, Turkey-Kramer HSD test.

8.11 Eps8 bundling activity is required for proper intestinal morphogenesis *in vivo*

Next, we set out to identify biological processes in which the bundling, but not the capping, activity of Eps8 is involved. To this end, we utilized as model system the nematode *Caernorabdtitis Elegans*, which express one single Eps8 hortologue that displays a significant level of colinearity and identity to mammalian Eps8, encompassing the critical residues for the capping and bundling activity, respectively (Figure 50).

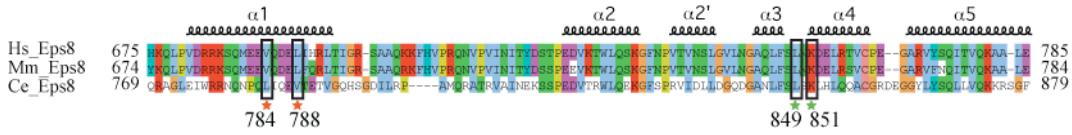

Figure 50: EPS-8 in *C. elegans*

The critical residues mediating barbed end and side binding of EPS8 are conserved in the nematode homologue of EPS8 (Ce-EPS8). Sequence Alignment of the C-terminal region of human (Hs), mouse (Mm) and C. elegans (Ce) Eps8. The organization into 5 α-helices is indicated on top. Red and green stars indicate the conserved amino acids required to mediate capping and bundling, respectively. Amino acids positions are shown on right and left.

It has been previously demonstrated that deletion of the eps8-A gene in *C.elegans* leads to larval lethality, due to intestinal dysfunctions caused by an altered microvilli morphology [51]. Two splice EPS-8 isoforms are expressed in *C.elegans*, a long one (EPS-8A) and a short one (EPS-8B) that lacks the C-terminal region, including the determinants responsible for the interaction with actin. Importantly, only the intestinal expression of EPS-8A rescues both the lethality and the intestinal defects, thus indicating that the function of Eps8 is linked to its C-terminal region [51]. It is relevant to underline that at the time these findings were obtained only the capping activity of Eps8 was known, thus a precise correlation between Eps8 biochemical activities and the *in vivo* observed phenotype had not been performed. Microvilli, however, are made of parallel bundles of

actin filaments crosslinked together, suggesting that their proper formation requires a bundling activity, which may be provided by Eps8. To test this possibility, we first engineered the corresponding Δcapping, Δbundling and the double ΔcapΔbund mutants in the context of the *C.elegans* Eps-8A C-terminal region (aa 714-917) that recapitulates the actin binding properties of full length Ce-EPS-8A and tested their biochemical actin related activities. Capping activity was tested using pyrenyl actin and spectrin actin seeds. Similarly to mammalian Eps8, mutations in the Ce-Eps-8A H1 helix, but not in the Villin motif of the H2-H5 lobe, led to a significant decrease of the capping activity of the protein. The double mutant displayed an even reduced capping activity (Figure 51).

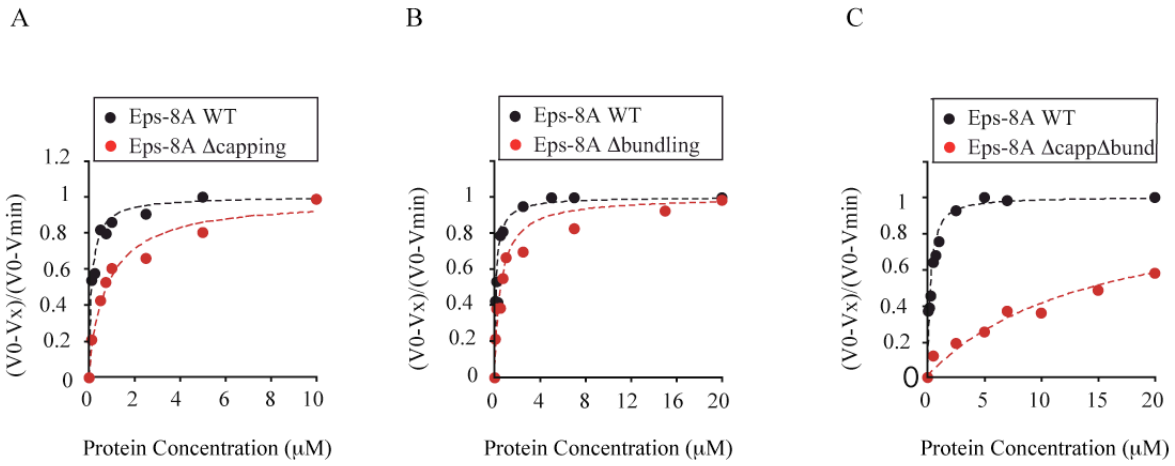

Figure 51: Analysis of the capping activity of the nematode EPS-8A mutants

The capping activity of the *C.e.* mutants reflects the one of their mammalian counterparts.

The barbed end capping activity of the indicated mutants fused to GST (A, Δcap; B, Δbund; C, ΔcapΔbund) is shown. The mutants were engineered in the context of a C-terminal fragment of Ce-EPS-8A (aa 714-917, WT in all panels) that recapitulates the actin binding properties of full length Ce-EPS-8A. Rates of elongation from plus ends using spectrin-actin seeds and 2 μM of G-actin (10% pyrenyl-labeled) in the presence of increasing concentrations of the indicated constructs are shown. Rates are normalized taking as 100 % the rate of elongation from barbed ends measured in the absence of Ce-EPS-8A-WT. The kinetic constants (Kcap) of barbed end inhibition were: WT, 108 nM; Δcap, 980 nM; Δbund, 205 nM; ΔcapΔbund, > 4000 nM.

To test the mutants bundling activity we used a low speed co-sedimentation assay.

The WT EPS-8A showed a detectable bundling activity, comparable with the mammalian protein. This bundling capacity was retained by the Δcapping, but not by the Δbundling or by the double ΔcapΔbund mutant (Figure 52).

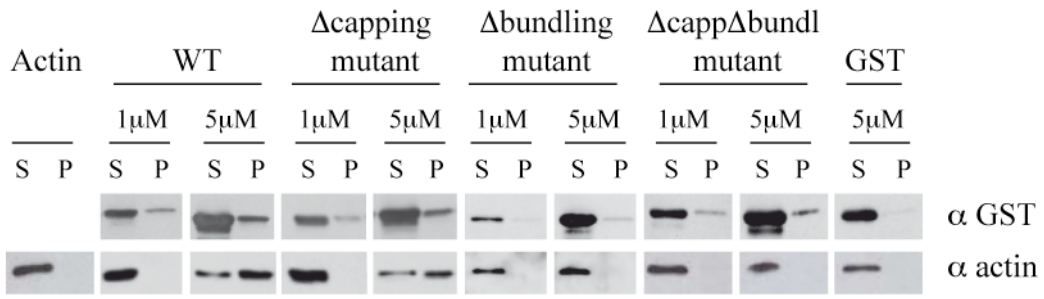

Figure 52: Analysis of the bundling activity of the nematode EPS-8A mutants

The bundling activity of the *C.e.* mutants reflects the one of their mammalian counterparts.

The F-actin bundling activity of the indicated mutants fused to GST is shown. The mutants were engineered in the context of a C-terminal fragment of Ce-EPS-8A (aa 714-917, WT in all panels) that recapitulates the actin binding properties of full length Ce-EPS-8A. The F-actin bundling ability of the indicated constructs was determined by co-sedimentation assays. F-actin (1 μM) was incubated either alone or in the presence of the indicated constructs. The mix was subjected to low-speed centrifugation for 30 minutes. Aliquots of pellets (P) and supernatants (S) were analyzed by IB, as shown.

We then generated heterozygous *eps-8* transgenic lines expressing either EPS-8A mutant or WT. The constructs were fused to GFP in order to visualize them by fluorescence and were expressed under control of a specific gut promoter in order to restrict their localization in the intestine. EPS-8 constructs were injected into the *eps-8(by 160)* deletion mutant strain, [51]. All the proteins were correctly targeted to the intestine (Figure 53).

The morphology of the EPS-8 WT and EPS-8 Δcapping expressing worms looked normal, comparable to a wild type *C.elegans* strain (Figure 53).

On the contrary, the worms expressing the Δbundling or the double ΔcappingΔbundling mutants had the same intestinal morphological defects as the *eps-8(by 160)* strain, showing

constipation and/or paleness, with the presence of clumped and more refractile gut granules.

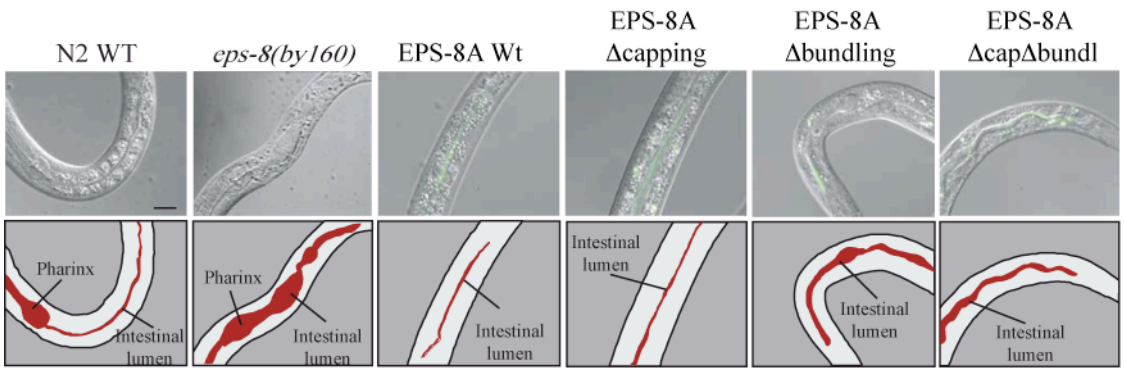

Figure 53: morphological analysis of the intestine of *C.e.* strains expressing EPS-8A WT or mutant proteins

The intestinal expression of EPS-8A bundling deficient mutants cause morphogenetic defects in the nematode gut.

Photomicrographs depicting intestinal morphology of wild-type (WT), *eps-8(by160)* and *eps-8(by160)* expressing EPS-8 WT or mutant proteins (Δcap, Δbund, and ΔcapΔbund) under a gut specific promoter. Fusion of the EPS-8 constructs to GFP allowed their visualization in epifluorescence. Merges of Normaski and epifluoresence photomicrographs are shown (proteins are in green). To facilitate visualization of the gut phenotype, cartoon panels are depicted underneath each merged image. The intestinal lumen is also indicated. Bar, 10 μm. Worms are oriented with the head pointing down or to the left.

Importantly, analysis of the intestine at higher magnification by confocal microscopy revealed that Ce-EPS-8A likewise all the mutants generated not only properly localized to the intestine, but were specifically targeted to the apical brush border (Figure 54).

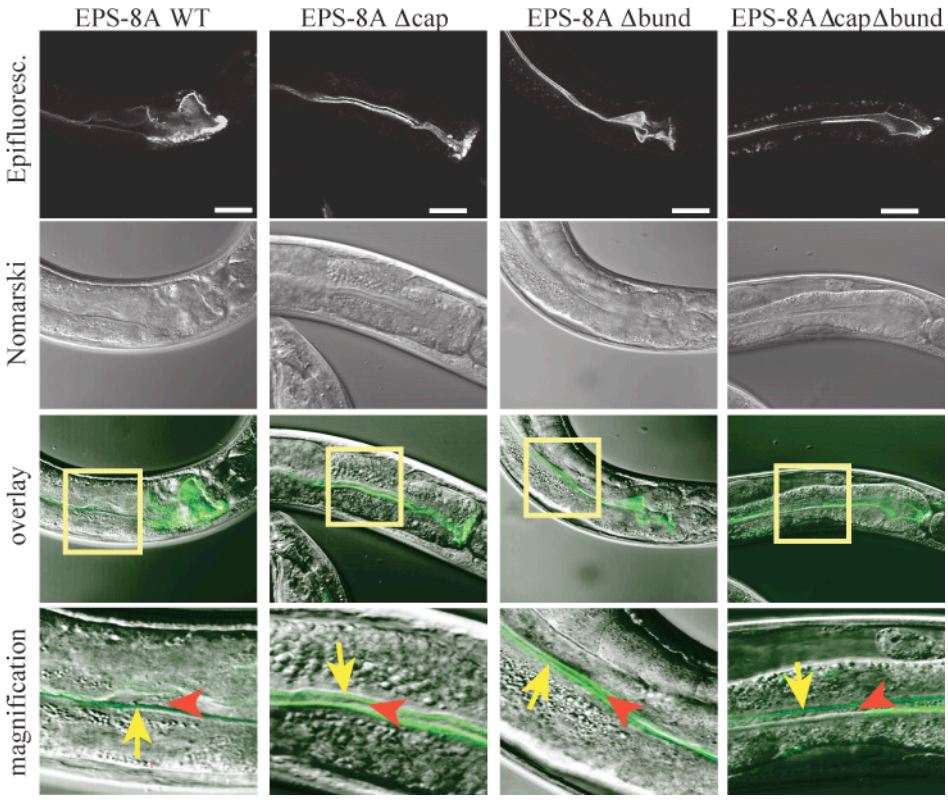

Figure 54: CeEPS8::GFP WT and mutant proteins expressed in the intestine display an apical-restricted localization

Localization study of CeEPS8::GFP WT and mutant proteins.

Photomicrographs depicting intestinal morphology of *eps-8(by160)* heterozygous worms expressing EPS-8 WT or (Δcap, Δbund, and ΔcapΔbund) under a gut specific promoter, *opt-2*. Fusion of the EPS-8 constructs to GFP allowed their visualization in epifluorescence to evidence their restricted gut expression (upper panels). Nomarski, epifluoresence, overlays of epifluorescence over Nomarski photomicrographs are also shown (proteins are in green). Overlays of magnified boxed areas are shown at the bottom. Red arrowheads indicate the intestinal lumen. Yellow arrows point to the brush apical intestinal border. Worms are oriented with the head pointing down or to the right. Bar, 10 μm.

To further strengthen this latter finding, we compared the pattern of expression of EPS-8A with that of DLG-1::RFP transgene, that encodes for Discs, large homolog-1 (DLG-1), an intestinal brush border apical marker. WT EPS-8A or the various mutants were invariably localized on the luminal intestinal surface, apical, with respect to DLG-1, thus confirming our localization analysis (Figure 55).

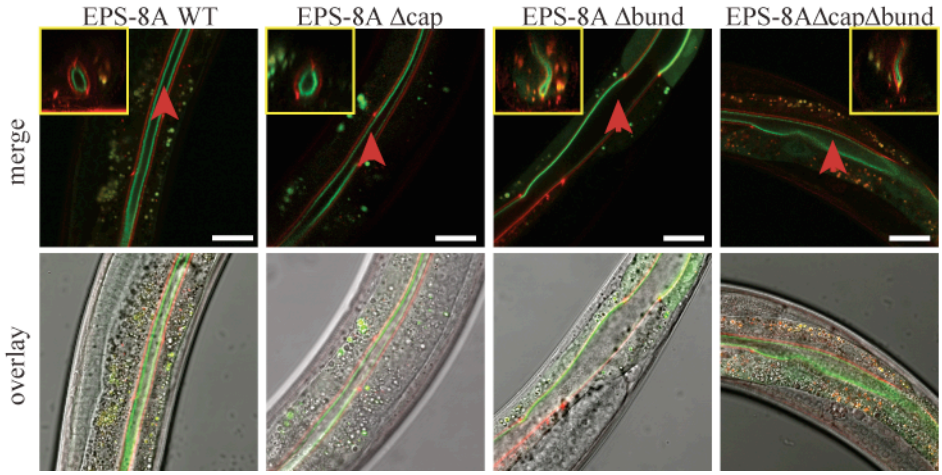

Figure 55: Specific localization of CeEPS8::GFP WT and mutant proteins along the brush border

Localization study of CeEPS8::GFP WT and mutant in the intestine.

Photomicrographs depicting the apical localization of GFP::EPS-8 WT or mutant proteins (Δcap, Δbund, and ΔcapΔbund) arrays under a gut specific promoter, *opt-2*, in *DLG-1::RFP* transgene expressing worms. Intestinal sections in the merged epifluorescence green and red channels (top) and overlays of epifluorescence channels over Nomarski (bottom) photomicrographs are shown. Yellow boxed insets are transversal Z sections of nematode intestines to visualize the more luminal localization of WT EPS8::GFP and mutant proteins with respect to DLG-1::RFP. Red arrowheads indicate the intestinal lumen. Bar,10 μm.

We finally performed a rescue experiment analyzing the survival of the progeny of heterozygous *eps-8* mutants expressing the different arrays. Lethality of the F1 *eps-8* homozygous worms was rescued by the EPS-8A Δcap mutant but not by the EPS-8A Δbundling or by the double mutant EPS-8A ΔcappΔbundling one (table 1).

Thus we demonstrated that the bundling, but not the capping activity of EPS-8 is responsible for the proper intestinal morphology in *C.elegans*, reflecting its requirement in the architectural organization of actin in this tissue.

Genotype	Overexpressed Array	Rescue of Lethality[1]	Intestinal defects (n)[2]
Wild-type N2	none		0% (21)
eps-8(by160)	none		79% (28)
eps-8(by160)	*Ex[opt-2::EPS-8A::GFP]*	YES	28% (18)
eps-8(by160)	*Ex[opt-2::EPS-8A::Δcap::GFP]*	YES	30% (30)
eps-8(by160)	*Ex[opt-2::EPS-8A::Δbund::GFP]*	NO	70% (20)
eps-8(by160)	*Ex[opt-2::EPS-8A Δcap Δbund::GFP]*	NO	73% (22)

table 1: Summary of the rescue of lethality and intestinal morphogenetic defects by the expression of CeEPS-8 mutants

[1]Rescue of lethality was tested in two different transgenic lines for each construct. At least one hundred GFP positive L1 larvae (F1), from heterozygous *eps-8* animals (F0), were individually plated and allowed to grow and self fertilize. Rescued homozygous *eps-8* mutants were recognized by loss of the genetic balancing markers (*unc-26*, *dpy-4*) and positivity for GFP expression. Confirmation for homozygosity for the mutated *eps-8* allele was obtained by PCR [51]. Alternatively, the entire progeny (ranging from 30 to 120 F1 animals) of at least three heterozygous adults was individually plated and allowed to grow and self fertilize. Rescue of lethality analysis was performed as described above.

[2] Intestinal alterations in homozygous *eps-8(by160)* mutant worms are characterized by constipation and/or paleness, with the presence of clumped and more refractile gut granules. Rescue of this phenotype was scored in live L1/L2 larvae under a microscope with Nomarski optics and epifluorescence. For the analysis of the gut phenotype in *eps-8(by160)* opt-2:EPS-8AΔbund, and *eps-8(by160)* opt-2:EPS-8A-ΔbundΔcap, homozygous larvae were identified by growth retardation respective to siblings in a synchronous F1 progeny from heterozygous worms. The % of worms displaying intestinal defects is shown. In parentheses, the number of analyzed animals is reported.

9. DISCUSSION

This work investigates the structural and molecular bases of the barbed end capping and crosslinking activities of Eps8.

Through EM, biochemical, cellular and mutagenesis studies we have elucidated the mechanism through which Eps8 binds both the side and the filament ends, exerting its bundling and capping activity respectively (Figure 56).

We have shown how distinct portions within the C-terminal region of Eps8 contribute to actin binding. Eps8 contains two actin-binding surfaces linked by an unstructured loop (Figure 56A). The first region, H1, displays secondary structure similar to a WH2 domain and is crucial for capping, whereas the second surface, composed of four alpha helices organized into a globular core (H2-H5), is crucial for bundling. The long flexible linker between the two regions contributes to the stabilization of the Eps8:actin interaction on the filament side and allows the amphipathic helix H1 to plug into the actin hydrophobic binding pocket at barbed ends, acting as a lock that increases the binding affinity of Eps8 actin binding domain from 10^6 to 10^9 M^{-1}, as typically observed for cappers (Figure 56B-C). CP, for instance, adopts a similar mechanism whereby full capping activity is achieved when a flexible domain swings into the hydrophobic pocket, locking barbed ends [20, 43]. Thus, the capping activity of Eps8 appears to be determined by a clamp mechanism by which the extended C-terminal Eps8 domain fasten around the barbed end actin unit blocking further filament elongation. Within this context, both the side binding of the globular core and the end binding mediated by H1 are spatially coordinated by the linker that contributes to the high affinity interaction of Eps8 to filaments ends (accounting also for the slightly reduced affinity for barbed ends of the bundling-deficient mutants). The flexibility of the linker ensures also a bimodal topological arrangement of Eps8 with respect to either the side or the barbed end of the filaments, reflecting its bundling or capping activities, respectively. These two latter functions of Eps8 can, indeed, be dissected and consistently exert distinct roles in diverse actin-based processes.

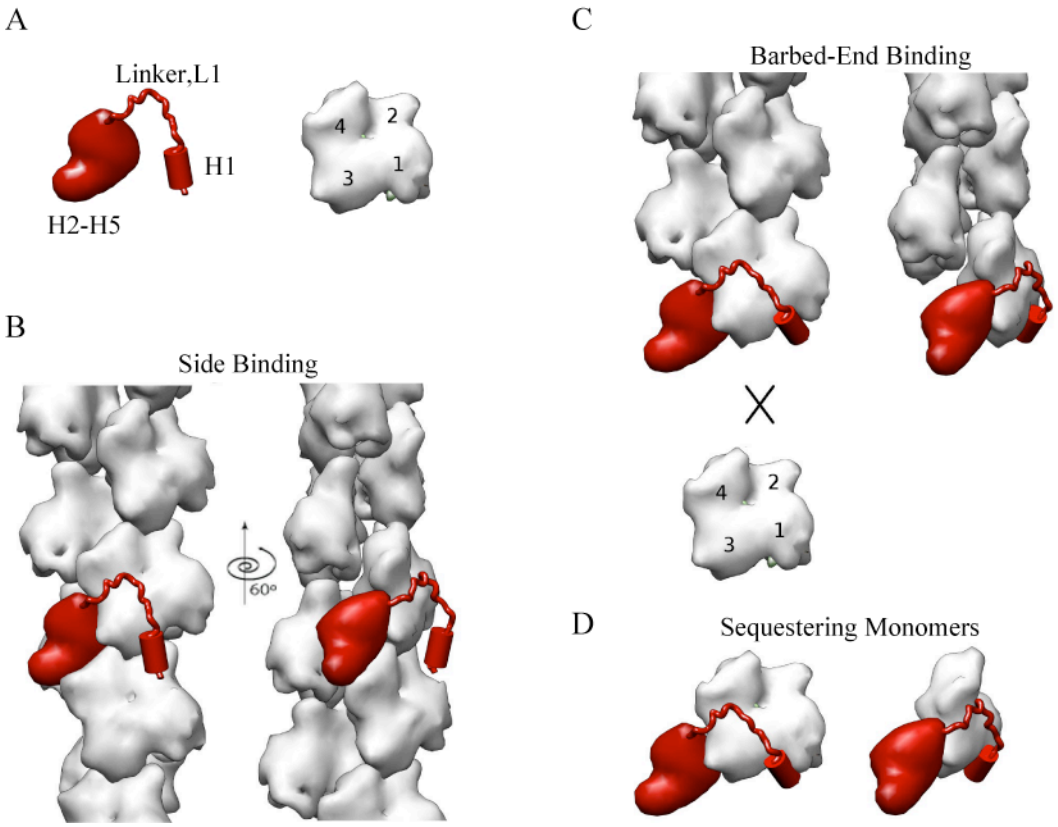

Figure 56: A schematic model for the binding modes of Eps8 to actin

A. A cartoon representation of Eps8 actin binding regions and monomeric actin. The N-terminal amphipathic helix, H1, the connecting linker, L1, and the globular helical core, H2-H5, of Eps8 are indicated. Monomeric actin is oriented with its barbed end downwards. Actin subdomains are numbered from 1 to 4.

B. The binding of Eps8 C-terminal region to the side of actin filaments is mainly mediated by the globular helical bundle (H2-H5). The helical bundle (H2-H5) positions in the long grove of the filament, contacting three actin subunits. The amphipathic helix (H1) does not contribute significantly. The H1 binding site may not be fully exposed in filamentous actin.

C. At the barbed ends, the H1 binding site is fully accessible and H1 can bind within the hydrophobic pocket blocking further addition of monomeric actin.

D. A similar arrangement as seen at the barbed end is presumably occurring on monomeric actin, accounting for the sequestering activity of Eps8.

In B-D, two views, related by a 60º counter clockwise rotation around the filament axis, are shown.

9.1 Eps8 H1 helix is crucial for the capping activity of the protein

We have shown through several and diverse approaches that the H1 actin-binding surface of Eps8 is critical for capping. Several lines of evidences indicate that this helix behaves as a WH2 domain.

The WH2 domain is a motif that is emerging as a common actin binding surface shared by several classes of ABPs, including Ciboulot and WASP homology domain-2 (WH2)-related proteins such as Thymosin β–4. It consists in a short α helix, with few exposed hydrophobic side chains, which binds in a hydrophobic cleft between actin subdomains 1 and 3 [82].

Firstly, we showed through competition binding studies that an Eps8 fragment encompassing the entire five terminal α-helices (Eps8 648-821) or the isolated H1-H2, but not H5, can displace the WH2 domain-containing proteins, Ciboulot and Thymosin β-4, as well as ADF/Cofilin, from actin, indicating a common surface of interaction on the actin monomer. Binding of all these proteins to the hydrophobic pocket on the actin monomer is well established. Secondly, a mass spectrometry analysis of chemically cross-linked peptides of the Eps8:actin complex revealed that the residues K675 and K683 on H1 are in close proximity with the K375 of actin, which is located in the hydrophobic cleft on subdomain 1. Additionally, helical wheel analysis confirmed that H1 forms an amphipathic helix, which displays the same "signature" of conserved hydrophobic residues as the helix of the WH2 domain.

Finally and most importantly, the relevance of the hydrophobic contacts of the amphipathic helix H1 for Eps8 capping activity is demonstrated by the observations that a mutant in these residues, both in mammalian Eps8 and in the nematode Eps-8A, has a significantly reduced capping activity *in vitro* with respect to wild type, and fails to support actin-based motility.

Strikingly there is no sequence similarity between WH2 domains of the different actin binding proteins, indicating that the actin cleft is very adaptable, being able to accommodate interactions with a wide range of unrelated ABPs with the sole requirement of possessing patches of ordered hydrophobic residues. Moreover it has been demonstrated that this cleft is able to accommodate protein-protein interactions either at its front or back halves, or throughout its entire length [82]. This latter feature is important since it renders the cleft accessible for binding to interacting proteins not only when it is exposed on the last actin unit of a protomer, but also when actin monomers are linked to form the helical filament, where part of the surface is occupied by the contact between monomers. The flexibility of the actin cleft in accommodating interactors has already been demonstrated for Thymosin β-4, which tightly binds G-actin up to a certain concentration threshold, upon which it becomes incorporated in the filament [95]. Binding of Thymosin β-4 to F-actin changes the twist of actin from 2.16 to 2.14 subunits per turn, interfering with some inter-subunit contacts in the filament [96]. Notably, in our EM analysis we show the same change in the filament twist to occur upon Eps8 binding, which further suggests a similar mode of interaction.

The WH2 domain is a common motif of several nucleating promoting factors, such as WASP, N-WASP or Spire, Cordonbleau and Leiomodin families, which by binding on more monomeric actin units or on the Arp2/3 complex promote filament nucleation [26]. Eps8 amphipatic helix, despite structural similarity, cannot support nucleation even at high concentrations, tightly capping, instead, filaments barbed ends. One of the biochemical reasons preventing Eps8 to switch from capping to nucleation, may be found in the finding that Eps8 associates with equal affinity to ATP or ADP bound actin. Thus, at variance with respect to NPFs, which show a higher affinity for ATP-bound actin and detach from the filament after ATP hydrolysis, Eps8 after binding tightly to filament ends remains associated to the ends with relative low k_{off}, ultimately blocking further filament assembly.

9.2 The H2-H5 helical globular lobe is responsible for Eps8 bundling activity

The globular lobe, composed of H2-H5 helices, represents the second distinct binding site of Eps8 and is primarily responsible for the bundling activity the protein. Indeed, the isolated H2-H5 domain of Eps8 is sufficient to bind and bundle F-actin. Moreover, mutations in key conserved residues within this domain completely abrogate Eps8 bundling activity, both in the mouse and in the *C.elegans* nematode, while leaving unaffected the ability of the domain to cap filament ends. In the 3D reconstruction the H2-H5 lobe appears to slot in between three actin subunits of the filament, with the major contacts with the subdomain 3 of the actin subunit that has the H1 bound and with the subdomain 4 of the actin subunit below. This is significantly different from other F-actin binding proteins, such as Fimbrin and Vinculin, which share common actin interacting surfaces, associating along the filament between subdomains 1 and 2 of two adjacent actin protomers [97, 98]. These structural differences may underline functional specificity since Fimbrin and Vinculin organize actin into higher order cross-linked, stable structures, whereas Eps8-actin assemblies are likely more dynamics. Conversely, the helical lobe of Eps8 binds actin filament mainly through a critical stretch of amino acids (LNKDE), which resembles those identified in the headpiece of Villin (LKKEK) [99] and in a variety of other actin-binding proteins homologous to the Villin headpiece [100]. Interestingly, EM reconstructions show Villin as well as Demantin headpiece to bind in a similar location on F-actin as the H2-H5 lobe of Eps8 [101].

Bundling proteins usually promote filament bundling through a bivalent interaction with F-actin, contacting at least two actin filaments in order to crosslink them together. Accordingly, bundling proteins either posses two distinct actin binding sites or acquire them through dimerization when they posses a single surface of interaction [5]. Alternatively, since actin filaments are poly-electrolytes, proteins rich in basic residues

can, by associating to the side of actin filaments, neutralize the repulsive charges of the actin polymer driving bundling [102, 103]. In the case of Eps8 this latter hypothesis appears unlikely since the minimal, isolated C-terminal region (aa 648-821), cleaved from GST, displays no bundling activity. Conversely we showed that the GST–tagged C-terminal region dimerizes and possesses bundling activity. In the context of the full-length protein, moreover, the bundling activity of Eps8 is enhanced by association of Eps8 with IRSp53, which has been demonstrated to dimerize through its IMD domain. Thus we propose that Eps8 crosslinks actin filaments by forming homo- or hetero-dimers, in this latter case, presumably together with IRSp53, which was previously shown not only to bind tightly to Eps8 but also to form dimers [73].

9.3 The flexible linker between H1-H2 connects the two Eps8 actin binding surfaces

The H1 helix and the H2-H5 lobe are separated by a linker, which winds around subdomain 3 and accommodates toward the cleft between subdomains 3 and 4 of actin, physically connecting the capping with the bundling surfaces, and accounting for the extra density observed in the 3D reconstruction of Eps8 bound to the filament. This arrangement is also consistent with the actin:Eps8 crosslinking experiments, indicating a juxtaposition between the residue K707 of the linker and the Lysine K330 of subdomain 3 of actin. We can thus position the linker just in front of the cleft between subdomains 3 and 4 (Figure 56C).

The presence of flexible linkers interconnecting actin-binding domains is a common occurrence in capping proteins. However, the orientation of the Eps8 linker and its contacts with actin are somehow unique. For instance, in Gelsolin, the G1 and G2 repeats are separated by a linker segment, which extends upwards and away from G1, along the face of actin, in a direction that enables positioning G2 along the same long-pitch helical strand

of the actin bound to G1 [104, 105]. Similar overall architectural organization with respect to actin has also been proposed for Twinfilin C and for the N-terminal ADF domain [48]. In the case of the Eps8 capping domain, the H1 helix, like the G1 and WH2 domains, plugs into the hydrophobic cleft between subdomains 1 and 3 of the barbed end of actin. Remarkably, however, the peptide linker, extending from the H1 amphipathic helix, adopts a significantly different orientation that enables positioning the globular lobe (H2-H5) in a cleft formed by the adjacent actin unit of the second protofilament. This mode of binding predicts that residues in the linker between H1 and H2 are critical for its orientation, and suggests that their mutation may switch the architectural organization and position of the H2-H5 lobe to resemble that of Gelsolin G1-G2 repeat bound to actin. A possibility that warrants further investigation.

9.4 Correlating Eps8 dual functions and actin-binding modes from *in vitro* to *in vivo*

In this work, we have provided evidence that two segregated actin binding domains confer Eps8 with bimodal functionality; capping and bundling. We had previously shown in the laboratory that this dual function is regulated in the context of the full-length protein by activation of different effectors (IRSp53, and Abi1 [50, 73]). Our data further support the notion that this bimodal functionality in the context of one single protein can be dissected and exert independent, cell- and tissue-specific roles.

The bundling, but not the capping function of Eps8 appears essential for the proper structural organization of gut microvilli, which are composed of parallel, highly cross-linked actin filaments. Importantly, the role of Eps8 in the intestine is conserved also in mice, where Eps8 genetic removal disrupts intestinal morphology leading to reduced fat absorption, calorie restriction and improved metabolic status [106]. Filament side binding and bundling of Eps8 are also critical to direct the protein to microspikes. This is

consistent with the role of Eps8 (together with IRSp53 [73]) in filopodia formation and also suggests that Eps8 through its crosslinking properties may be generally implicated in the regulation of highly dynamic structures composed of parallel actin bundles.

The capping activity, instead, is required to reconstitute actin-based rocketing motility *in vitro* and for optimal velocity of intracellular pathogens [50] or PIP2-rich endomembranes *in vivo;* to restrict localization of Eps8 to the leading edge of the cell in migratory cells; and to control the number of axonal filopodia in primary hippocampal neurons [107]. In these latter cells, Eps8 acts, like capping protein CP [108], by negatively regulating, through barbed end binding, the filament lengths of the actin network from which filopodia then arise.

Finally, the role of Eps8 as a bifunctional actin remodeller further suggests that this protein by controlling various actin-based protrusions regulates optimal cell locomotion both in physiological and in pathological contexts, such as during tumour development. In keeping with this latter possibility, Eps8 has been reported to be unregulated in a variety of tumour types and to be specifically required for optimal cell migration and invasion in a subset of metastatic oral squamous carcinoma cells [56, 109]. Whether the capping or bundling activities are critical for Eps8 to exert this pro-invasive functions remains to be tested. However, the availability of Eps8 mutants specifically impaired in either one or the other of its actin-related functions will be instrumental in addressing this issue and certainly worth to be investigated.

9.5 Perspectives

The sum of our results provides a molecular framework to account for the role of Eps8 as a key regulator of the actin cytoskeleton underneath membrane protrusion. Eps8 can regulate both the rate of filament elongation and the cytoskeletal architecture trough its capping and bundling activities, respectively. These two distinct Eps8 functions are regulated by diverse protein:protein interactions whereby the binding to Abi1, mediated by the SH3 domain of Eps8, triggers the capping activity, while the association with IRSp53 promotes actin crosslinking. Thus, the dynamic interplay between different Eps8-based complexes is likely to be critical for the generation of different actin-based migratory structures. Within this context, Eps8 and its interacting partners represent components of a larger network of signalling proteins whose activities and modes of regulation remain largely ill-defined. For instance, IRSp53 in addition to associate tightly with Eps8 can form mutually exclusive complexes with VASP family members [110], which possess anticapping and crosslinking properties. Additionally, IRSp53 is a direct effector of Cdc42 and Rac, which are critical regulators of actin remodelling and can bind and deform the plasma membrane contributing to generate protrusions. Consistently, IRSp53 and its interactors (namely Eps8/Abi1 complex and VASP) are all present at the cellular leading edge, raising the issues as to how they are organized into a dynamic, spatially and temporally controlled network, capable of generating the formation of diverse cellular protrusions.

Our present and future aim is to investigate how this “minimal protein network” is regulated in order to establish the basic principles and mechanisms of its action. We will then enrich, in stepwise mode, the levels of complexity of the system by adding further layers of proteins and lipid interactions and regulation with the ultimate goal to built a dynamic map of the network responsible for the generation of actin-based cellular protrusions.

In order to achieve these goals we plan to combine *in vitro in vivo* approaches.

An *in vitro* system will be used to reconstitute, using purified proteins, the minimal protein network with the specific goal to define the contribution of Eps8 and its interacting proteins (IRSp53, VASP and Abi-1) in coupling membrane deformation and actin cytoskeleton remodelling. An *in vivo* approach will be then implemented in order to define the exact dynamics of all these proteins at the cellular leading edge.

These approaches should set the stage defining the dynamic parameters of Eps8 and of its actin related functions at the leading edge with respect to actin and a number of actin binding proteins [111].

10. REFERENCES

1. Fletcher, D.A. and R.D. Mullins, *Cell mechanics and the cytoskeleton.* Nature, 2010. **463**(7280): p. 485-92.
2. Mattila, P.K. and P. Lappalainen, *Filopodia: molecular architecture and cellular functions.* Nat Rev Mol Cell Biol, 2008. **9**(6): p. 446-54.
3. Hall, A., *Rho GTPases and the actin cytoskeleton.* Science, 1998. **279**(5350): p. 509-14.
4. Disanza, A., et al., *Actin polymerization machinery: the finish line of signaling networks, the starting point of cellular movement.* Cell Mol Life Sci, 2005. **62**(9): p. 955-70.
5. Revenu, C., et al., *The co-workers of actin filaments: from cell structures to signals.* Nat Rev Mol Cell Biol, 2004. **5**(8): p. 635-46.
6. Chhabra, E.S. and H.N. Higgs, *The many faces of actin: matching assembly factors with cellular structures.* Nat Cell Biol, 2007. **9**(10): p. 1110-21.
7. Small, J.V., et al., *The lamellipodium: where motility begins.* Trends Cell Biol, 2002. **12**(3): p. 112-20.
8. George, S.P., et al., *Dimerization and actin-bundling properties of villin and its role in the assembly of epithelial cell brush borders.* J Biol Chem, 2007. **282**(36): p. 26528-41.
9. Khurana, S. and S.P. George, *Regulation of cell structure and function by actin-binding proteins: villin's perspective.* FEBS Lett, 2008. **582**(14): p. 2128-39.
10. Kabsch, W., et al., *Atomic structure of the actin:DNase I complex.* Nature, 1990. **347**(6288): p. 37-44.
11. Chik, J.K., U. Lindberg, and C.E. Schutt, *The structure of an open state of beta-actin at 2.65 A resolution.* J Mol Biol, 1996. **263**(4): p. 607-23.
12. Burtnick, L.D., R.C. Robinson, and S. Choe, *Structure and function of gelsolin.* Results Probl Cell Differ, 2001. **32**: p. 201-11.
13. Otterbein, L.R., et al., *Crystal structures of the vitamin D-binding protein and its complex with actin: structural basis of the actin-scavenger system.* Proc Natl Acad Sci U S A, 2002. **99**(12): p. 8003-8.
14. Irobi, E., et al., *Structural basis of actin sequestration by thymosin-beta4: implications for WH2 proteins.* EMBO J, 2004. **23**(18): p. 3599-608.
15. Otterbein, L.R., P. Graceffa, and R. Dominguez, *The crystal structure of uncomplexed actin in the ADP state.* Science, 2001. **293**(5530): p. 708-11.
16. Aguda, A.H., L.D. Burtnick, and R.C. Robinson, *The state of the filament.* EMBO Rep, 2005. **6**(3): p. 220-6.
17. Holmes, K.C., et al., *Atomic model of the actin filament.* Nature, 1990. **347**(6288): p. 44-9.
18. Oda, T., et al., *The nature of the globular- to fibrous-actin transition.* Nature, 2009. **457**(7228): p. 441-5.
19. Holmes, K.C., *Structural biology: actin in a twist.* Nature, 2009. **457**(7228): p. 389-90.
20. Wear, M.A. and J.A. Cooper, *Capping protein: new insights into mechanism and regulation.* Trends Biochem Sci, 2004. **29**(8): p. 418-28.
21. Carlier, M.F. and D. Pantaloni, *Control of actin dynamics in cell motility.* J Mol Biol, 1997. **269**(4): p. 459-67.
22. Pantaloni, D., C. Le Clainche, and M.F. Carlier, *Mechanism of actin-based motility.* Science, 2001. **292**(5521): p. 1502-6.
23. Loisel, T.P., et al., *Reconstitution of actin-based motility of Listeria and Shigella using pure proteins.* Nature, 1999. **401**(6753): p. 613-6.
24. Bernheim-Groswasser, A., et al., *The dynamics of actin-based motility depend on surface parameters.* Nature, 2002. **417**(6886): p. 308-11.

25. Wiesner, S., et al., *A biomimetic motility assay provides insight into the mechanism of actin-based motility.* J Cell Biol, 2003. **160**(3): p. 387-98.
26. Campellone, K.G. and M.D. Welch, *A nucleator arms race: cellular control of actin assembly.* Nat Rev Mol Cell Biol, 2010. **11**(4): p. 237-51.
27. Carlier, M.F., *Control of actin dynamics.* Curr Opin Cell Biol, 1998. **10**(1): p. 45-51.
28. Kurisu, S. and T. Takenawa, *The WASP and WAVE family proteins.* Genome Biol, 2009. **10**(6): p. 226.
29. Coutts, A.S., L. Weston, and N.B. La Thangue, *A transcription co-factor integrates cell adhesion and motility with the p53 response.* Proc Natl Acad Sci U S A, 2009. **106**(47): p. 19872-7.
30. Zuchero, J.B., et al., *p53-cofactor JMY is a multifunctional actin nucleation factor.* Nat Cell Biol, 2009. **11**(4): p. 451-9.
31. Chesarone, M.A., A.G. DuPage, and B.L. Goode, *Unleashing formins to remodel the actin and microtubule cytoskeletons.* Nat Rev Mol Cell Biol, 2010. **11**(1): p. 62-74.
32. Chereau, D., et al., *Actin-bound structures of Wiskott-Aldrich syndrome protein (WASP)-homology domain 2 and the implications for filament assembly.* Proc Natl Acad Sci U S A, 2005. **102**(46): p. 16644-9.
33. Bosch, M., et al., *Analysis of the function of Spire in actin assembly and its synergy with formin and profilin.* Mol Cell, 2007. **28**(4): p. 555-68.
34. Quinlan, M.E., et al., *Regulatory interactions between two actin nucleators, Spire and Cappuccino.* J Cell Biol, 2007. **179**(1): p. 117-28.
35. Carlier, M.F., et al., *Actin depolymerizing factor (ADF/cofilin) enhances the rate of filament turnover: implication in actin-based motility.* J Cell Biol, 1997. **136**(6): p. 1307-22.
36. Didry, D., M.F. Carlier, and D. Pantaloni, *Synergy between actin depolymerizing factor/cofilin and profilin in increasing actin filament turnover.* J Biol Chem, 1998. **273**(40): p. 25602-11.
37. Witke, W., *The role of profilin complexes in cell motility and other cellular processes.* Trends Cell Biol, 2004. **14**(8): p. 461-9.
38. Yang, C., et al., *Profilin enhances Cdc42-induced nucleation of actin polymerization.* J Cell Biol, 2000. **150**(5): p. 1001-12.
39. Witke, W., et al., *In mouse brain profilin I and profilin II associate with regulators of the endocytic pathway and actin assembly.* EMBO J, 1998. **17**(4): p. 967-76.
40. Huff, T., et al., *beta-Thymosins, small acidic peptides with multiple functions.* Int J Biochem Cell Biol, 2001. **33**(3): p. 205-20.
41. Domanski, M., et al., *Coupling of folding and binding of thymosin beta4 upon interaction with monomeric actin monitored by nuclear magnetic resonance.* J Biol Chem, 2004. **279**(22): p. 23637-45.
42. Akin, O. and R.D. Mullins, *Capping protein increases the rate of actin-based motility by promoting filament nucleation by the Arp2/3 complex.* Cell, 2008. **133**(5): p. 841-51.
43. Narita, A., et al., *Structural basis of actin filament capping at the barbed-end: a cryo-electron microscopy study.* EMBO J, 2006. **25**(23): p. 5626-33.
44. Yin, H.L. and T.P. Stossel, *Control of cytoplasmic actin gel-sol transformation by gelsolin, a calcium-dependent regulatory protein.* Nature, 1979. **281**(5732): p. 583-6.
45. McGough, A.M., et al., *The gelsolin family of actin regulatory proteins: modular structures, versatile functions.* FEBS Lett, 2003. **552**(2-3): p. 75-81.
46. Choe, H., et al., *The calcium activation of gelsolin: insights from the 3A structure of the G4-G6/actin complex.* J Mol Biol, 2002. **324**(4): p. 691-702.

47. Burtnick, L.D., et al., *Structure of the N-terminal half of gelsolin bound to actin: roles in severing, apoptosis and FAF.* EMBO J, 2004. **23**(14): p. 2713-22.
48. Paavilainen, V.O., et al., *Structural basis and evolutionary origin of actin filament capping by twinfilin.* Proc Natl Acad Sci U S A, 2007. **104**(9): p. 3113-8.
49. Helfer, E., et al., *Mammalian twinfilin sequesters ADP-G-actin and caps filament barbed ends: implications in motility.* EMBO J, 2006. **25**(6): p. 1184-95.
50. Disanza, A., et al., *Eps8 controls actin-based motility by capping the barbed ends of actin filaments.* Nat Cell Biol, 2004. **6**(12): p. 1180-8.
51. Croce, A., et al., *A novel actin barbed-end-capping activity in EPS-8 regulates apical morphogenesis in intestinal cells of Caenorhabditis elegans.* Nat Cell Biol, 2004. **6**(12): p. 1173-9.
52. Tocchetti, A., et al., *In silico analysis of the EPS8 gene family: genomic organization, expression profile, and protein structure.* Genomics, 2003. **81**(2): p. 234-44.
53. Fazioli, F., et al., *Eps8, a substrate for the epidermal growth factor receptor kinase, enhances EGF-dependent mitogenic signals.* EMBO J, 1993. **12**(10): p. 3799-808.
54. Di Fiore, P.P. and G. Scita, *Eps8 in the midst of GTPases.* Int J Biochem Cell Biol, 2002. **34**(10): p. 1178-83.
55. Calderwood, D.A., et al., *Integrin beta cytoplasmic domain interactions with phosphotyrosine-binding domains: a structural prototype for diversity in integrin signaling.* Proc Natl Acad Sci U S A, 2003. **100**(5): p. 2272-7.
56. Yap, L.F., et al., *Upregulation of Eps8 in oral squamous cell carcinoma promotes cell migration and invasion through integrin-dependent Rac1 activation.* Oncogene, 2009. **28**(27): p. 2524-34.
57. Maa, M.C., et al., *Eps8 facilitates cellular growth and motility of colon cancer cells by increasing the expression and activity of focal adhesion kinase.* J Biol Chem, 2007. **282**(27): p. 19399-409.
58. Mayer, B.J. and M.J. Eck, *SH3 domains. Minding your p's and q's.* Curr Biol, 1995. **5**(4): p. 364-7.
59. Kishan, K.V., et al., *Effect of pH and salt bridges on structural assembly: molecular structures of the monomer and intertwined dimer of the Eps8 SH3 domain.* Protein Sci, 2001. **10**(5): p. 1046-55.
60. Scita, G., et al., *EPS8 and E3B1 transduce signals from Ras to Rac.* Nature, 1999. **401**(6750): p. 290-3.
61. Innocenti, M., et al., *Phosphoinositide 3-kinase activates Rac by entering in a complex with Eps8, Abi1, and Sos-1.* J Cell Biol, 2003. **160**(1): p. 17-23.
62. Zerial, M. and H. McBride, *Rab proteins as membrane organizers.* Nat Rev Mol Cell Biol, 2001. **2**(2): p. 107-17.
63. Scita, G., et al., *An effector region in Eps8 is responsible for the activation of the Rac-specific GEF activity of Sos-1 and for the proper localization of the Rac-based actin-polymerizing machine.* J Cell Biol, 2001. **154**(5): p. 1031-44.
64. Haas, A.K., et al., *A GTPase-activating protein controls Rab5 function in endocytic trafficking.* Nat Cell Biol, 2005. **7**(9): p. 887-93.
65. Lanzetti, L., et al., *The Eps8 protein coordinates EGF receptor signalling through Rac and trafficking through Rab5.* Nature, 2000. **408**(6810): p. 374-7.
66. Lanzetti, L., et al., *Rab5 is a signalling GTPase involved in actin remodelling by receptor tyrosine kinases.* Nature, 2004. **429**(6989): p. 309-14.
67. Swanson, J.A. and C. Watts, *Macropinocytosis.* Trends Cell Biol, 1995. **5**(11): p. 424-8.
68. Suetsugu, S., et al., *Differential roles of WAVE1 and WAVE2 in dorsal and peripheral ruffle formation for fibroblast cell migration.* Dev Cell, 2003. **5**(4): p. 595-609.

69. Palamidessi, A., et al., *Endocytic trafficking of Rac is required for the spatial restriction of signaling in cell migration.* Cell, 2008. **134**(1): p. 135-47.
70. Buccione, R., J.D. Orth, and M.A. McNiven, *Foot and mouth: podosomes, invadopodia and circular dorsal ruffles.* Nat Rev Mol Cell Biol, 2004. **5**(8): p. 647-57.
71. Innocenti, M., et al., *Abi1 regulates the activity of N-WASP and WAVE in distinct actin-based processes.* Nat Cell Biol, 2005. **7**(10): p. 969-76.
72. Bogdan, S. and C. Klambt, *Kette regulates actin dynamics and genetically interacts with Wave and Wasp.* Development, 2003. **130**(18): p. 4427-37.
73. Disanza, A., et al., *Regulation of cell shape by Cdc42 is mediated by the synergic actin-bundling activity of the Eps8-IRSp53 complex.* Nat Cell Biol, 2006. **8**(12): p. 1337-47.
74. Yamagishi, A., et al., *A novel actin bundling/filopodium-forming domain conserved in insulin receptor tyrosine kinase substrate p53 and missing in metastasis protein.* J Biol Chem, 2004. **279**(15): p. 14929-36.
75. Schafer, D.A. and T.A. Schroer, *Actin-related proteins.* Annu Rev Cell Dev Biol, 1999. **15**: p. 341-63.
76. Tseng, Y., et al., *How actin crosslinking and bundling proteins cooperate to generate an enhanced cell mechanical response.* Biochem Biophys Res Commun, 2005. **334**(1): p. 183-92.
77. Volkmann, N., et al., *The structural basis of myosin V processive movement as revealed by electron cryomicroscopy.* Mol Cell, 2005. **19**(5): p. 595-605.
78. Egelman, E.H., *A robust algorithm for the reconstruction of helical filaments using single-particle methods.* Ultramicroscopy, 2000. **85**(4): p. 225-34.
79. Volkmann, N. and D. Hanein, *Quantitative fitting of atomic models into observed densities derived by electron microscopy.* J Struct Biol, 1999. **125**(2-3): p. 176-84.
80. Volkmann, N. and D. Hanein, *Docking of atomic models into reconstructions from electron microscopy.* Meth Enzym, 2003. **374**: p. 204-225.
81. Hertzog, M., et al., *The beta-thymosin/WH2 domain; structural basis for the switch from inhibition to promotion of actin assembly.* Cell, 2004. **117**(5): p. 611-23.
82. Dominguez, R., *Actin-binding proteins--a unifying hypothesis.* Trends Biochem Sci, 2004. **29**(11): p. 572-8.
83. DeLano, W.L., *The PyMOL molecular graphics system*. 2002, Palo Alto, CA, USA: DeLano Scientific.
84. Murshudov, G.N., A.A. Vagin, and E.J. Dodson, *Refinement of Macromolecular Structures by the Maximum-Likelihood Method.* Acta Cryst., 1997. **D53**: p. 240-255.
85. Pettersen, E.F., et al., *UCSF Chimera--a visualization system for exploratory research and analysis.* J Comput Chem, 2004. **25**(13): p. 1605-12.
86. Paavilainen, V.O., et al., *Regulation of cytoskeletal dynamics by actin-monomer-binding proteins.* Trends Cell Biol, 2004. **14**(7): p. 386-94.
87. Vartiainen, M.K., et al., *Mammals have two twinfilin isoforms whose subcellular localizations and tissue distributions are differentially regulated.* J Biol Chem, 2003. **278**(36): p. 34347-55.
88. Tellam, R.L., *Gelsolin inhibits nucleotide exchange from actin.* Biochemistry, 1986. **25**(19): p. 5799-804.
89. Hertzog, M., et al., *Control of actin dynamics by proteins made of beta-thymosin repeats: the actobindin family.* J Biol Chem, 2002. **277**(17): p. 14786-92.
90. Paunola, E., P.K. Mattila, and P. Lappalainen, *WH2 domain: a small, versatile adapter for actin monomers.* FEBS Lett, 2002. **513**(1): p. 92-7.
91. Offenhauser, N., et al., *The eps8 family of proteins links growth factor stimulation to actin reorganization generating functional redundancy in the Ras/Rac pathway.* Mol Biol Cell, 2004. **15**(1): p. 91-8.

92. Hengen, P.N., *Methods and reagents. Purification of GST fusion proteins.* Trends Biochem Sci, 1996. **21**(10): p. 400-1.
93. Faix, J., et al., *Filopodia: Complex models for simple rods.* Int J Biochem Cell Biol, 2009. **41**(8-9): p. 1656-64.
94. Riedl, J., et al., *Lifeact: a versatile marker to visualize F-actin.* Nat Methods, 2008. **5**(7): p. 605-7.
95. Carlier, M.F., et al., *Tbeta 4 is not a simple G-actin sequestering protein and interacts with F-actin at high concentration.* J Biol Chem, 1996. **271**(16): p. 9231-9.
96. Ballweber, E., et al., *Polymerisation of chemically cross-linked actin:thymosin beta(4) complex to filamentous actin: alteration in helical parameters and visualisation of thymosin beta(4) binding on F-actin.* J Mol Biol, 2002. **315**(4): p. 613-25.
97. Hanein, D., et al., *An atomic model of fimbrin binding to F-actin and its implications for filament crosslinking and regulation.* Nat Struct Biol, 1998. **5**(9): p. 787-92.
98. Janssen, M.E., et al., *Three-dimensional structure of vinculin bound to actin filaments.* Mol Cell, 2006. **21**(2): p. 271-81.
99. Friederich, E., et al., *An actin-binding site containing a conserved motif of charged amino acid residues is essential for the morphogenic effect of villin.* Cell, 1992. **70**(1): p. 81-92.
100. Yamamoto, M., et al., *Identification of multiple actin-binding sites in cofilin-phosphatase Slingshot-1L.* FEBS Lett, 2006. **580**(7): p. 1789-94.
101. Chen, J.Z., et al., *Low-resolution structure refinement in electron microscopy.* J Struct Biol, 2003. **144**(1-2): p. 144-51.
102. Tang, J.X. and P.A. Janmey, *The polyelectrolyte nature of F-actin and the mechanism of actin bundle formation.* J Biol Chem, 1996. **271**(15): p. 8556-63.
103. Tang, J.X. and P.A. Janmey, *Two distinct mechanisms of actin bundle formation.* Biol Bull, 1998. **194**(3): p. 406-8.
104. Irobi, E., et al., *From the first to the second domain of gelsolin: a common path on the surface of actin?* FEBS Lett, 2003. **552**(2-3): p. 86-90.
105. McGough, A., W. Chiu, and M. Way, *Determination of the gelsolin binding site on F-actin: implications for severing and capping.* Biophys J, 1998. **74**(2 Pt 1): p. 764-72.
106. Tocchetti, A., et al., *Loss of the actin remodeler Eps8 causes intestinal defects and improved metabolic status in mice.* PLoS One, 2010. **5**(3): p. e9468.
107. Menna, E., et al., *Eps8 regulates axonal filopodia in hippocampal neurons in response to brain-derived neurotrophic factor (BDNF).* PLoS Biol, 2009. **7**(6): p. e1000138.
108. Mejillano, M.R., et al., *Lamellipodial versus filopodial mode of the actin nanomachinery: pivotal role of the filament barbed end.* Cell, 2004. **118**(3): p. 363-73.
109. Wang, H., et al., *Role for EPS8 in squamous carcinogenesis.* Carcinogenesis, 2009. **30**(1): p. 165-74.
110. Krugmann, S., et al., *Cdc42 induces filopodia by promoting the formation of an IRSp53:Mena complex.* Curr Biol, 2001. **11**(21): p. 1645-55.
111. Lai, F.P., et al., *Arp2/3 complex interactions and actin network turnover in lamellipodia.* EMBO J, 2008. **27**(7): p. 982-92.

11. SUPPLEMENTRY MATERIAL

Movies 1-2: FRAP experiments on BL16-F1 melanoma cells expressing GFP Eps8 either WT (movie 1) or Δbundling (movie 2).

Movies have been performed as indicated in Figure 46 and in the Material and Method section 7.5.4.

Movies 3-4: FRAP experiments on BL16-F1 melanoma cells expressing GFP Eps8 either WT (movie 3) or Δcapping (movie 4).

Movies have been performed as indicated in Figure 47 and in the Material and Method section 7.5.4.

Movies 5-12: Time-lapse phase contrast microscopy of *in vitro* actin based motility assays performed as described in Figure 48.

Video represents a time period of 20 minutes.

The movies are performed:

Movie 5: in the absence of capping proteins.

Movie 6: in the presence of the capping protein Gelsolin.

Movie 7: in the presence of wild type Eps8 (648-821).

Movie 8: in the presence of EPS8-Δbundling mutant.

Movie 9:in the presence of EPS8-Δcapping mutant.

Movie 10: in the presence of EPS8-Δcap Δbund mutant.

Movie 11: in the presence of H1–H2.

Movie 12: in the presence of H2–H5.

Movies 13-17: Time-lapse fluorescent microscopy of PIP2-rich vesicles performed as described in Figure 49.

Only the dynamic of lifeact-cherry is shown to facilitate the visualization of rocketing vesicles. Frames were taken every 3.3 to 7.1 s for a total time period of 5 min using a Spinning Disk confocal microscope Ultra VIEW VoX, Perkin Elmer 100× objective, 1.49 N.A, Nikon TiEclipse.

The movies were performed by expressing PI4,5K together with:

Movie 13: EPS8(648–821) (Eps8-WT).

Movie 14: EPS8-Δbundling.

Movie 15: Eps8-Δcapping.

Movie 16: GFP.

Movie 17: EPS8-Δcap Δbund.